

REPORT DOCUMENTATION PAGE			Form Approved OMB No. 074-0188	
Public reporting burden for this collection of information is estimated to average 1 hour per response, including the time for reviewing instructions, searching existing data sources, gathering and maintaining the data needed, and completing and reviewing this collection of information. Send comments regarding this burden estimate or any other aspect of this collection of information, including suggestions for reducing this burden to Washington Headquarters Services, Directorate for Information Operations and Reports, 1215 Jefferson Davis Highway, Suite 1204, Arlington, VA 22202-4302, and to the Office of Management and Budget, Paperwork Reduction Project (0704-0188), Washington, DC 20503				
1. AGENCY USE ONLY (Leave blank)		2. REPORT DATE 1997	3. REPORT TYPE AND DATES COVERED Ph.D. Thesis	
4. TITLE AND SUBTITLE  Pyrolysis and Oxidation Kinetics of Anisole and Phenol			5. FUNDING NUMBERS  DOE DE-FG02-86ER13554	
6. AUTHOR(S)  Melissa S. Pecullan				
7. PERFORMING ORGANIZATION NAME(S) AND ADDRESS(ES)  Princeton University Dept. of Mechanical & Aerospace Engineering			8. PERFORMING ORGANIZATION REPORT NUMBER  2097-T	
9. SPONSORING / MONITORING AGENCY NAME(S) AND ADDRESS(ES)  SERDP 901 North Stuart St. Suite 303 Arlington, VA 22203			10. SPONSORING / MONITORING AGENCY REPORT NUMBER  N/A	
11. SUPPLEMENTARY NOTES This work was supported in part by DOE under Grant No. DE-FG02-86ER13554. The United States Government has a royalty-free license throughout the world in all copyrightable material contained herein. All other rights are reserved by the copyright owner.				
12a. DISTRIBUTION / AVAILABILITY STATEMENT  Approved for public release: distribution is unlimited			12b. DISTRIBUTION CODE A	
13. ABSTRACT (Maximum 200 Words)  This thesis recounts an investigation of the high-temperature chemistry of the phenoxy radical and its parent phenol through the acquisition of reaction intermediate data from experiments performed in a turbulent flow reactor. Anisole, a chemical source of phenoxy at high temperature, and phenol were employed as reactor fuels at reaction temperatures near 1000 and 1170 K, respectively. Oxidation experiments were performed at fuel lean, stoichiometric, and fuel rich conditions. Pyrolysis experiments were also undertaken to provide bench mark data for comparison with oxidation data.				
14. SUBJECT TERMS  Anisole, Phenol, Pyrolysis, Oxidation, SERDP			15. NUMBER OF PAGES 198	
			16. PRICE CODE N/A	
17. SECURITY CLASSIFICATION OF REPORT  unclass.	18. SECURITY CLASSIFICATION OF THIS PAGE  unclass.	19. SECURITY CLASSIFICATION OF ABSTRACT  unclass.	20. LIMITATION OF ABSTRACT  UL	

NSN 7540-01-280-5500

Standard Form 298 (Rev. 2-89)  
Prescribed by ANSI Std. Z39-18  
298-102

DTIC QUALITY INSPECTED 1

19980710 024

# Princeton University

---



Department of  
Mechanical and  
Aerospace Engineering

PYROLYSIS AND OXIDATION KINETICS  
OF ANISOLE AND PHENOL

MELISSA S. PECULLAN

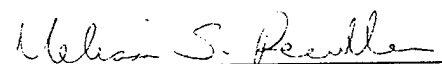
A DISSERTATION  
PRESENTED TO THE FACULTY  
OF PRINCETON UNIVERSITY  
IN CANDIDACY FOR THE DEGREE  
OF DOCTOR OF PHILOSOPHY

RECOMMENDED FOR ACCEPTANCE  
BY THE DEPARTMENT OF  
MECHANICAL AND AEROSPACE ENGINEERING

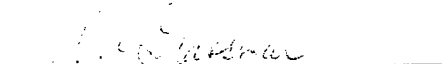
JUNE, 1997


PYROLYSIS AND OXIDATION KINETICS  
OF ANISOLE AND PHENOL

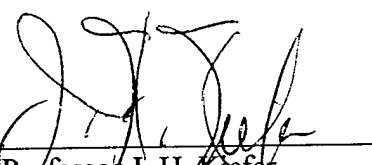
Prepared by:

  
Melissa S. Pecullan

Approved by:

  
Professor I. Glassman  
Dissertation Advisor

  
Professor M. J. Wornat  
Dissertation Reader

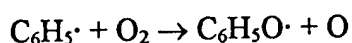
  
Professor J. H. Kiefer  
Dissertation Reader

© COPYRIGHT BY MELISSA S. PECULLAN, 1997. ALL RIGHTS RESERVED.

## ABSTRACT

---

Acknowledging the importance of aromatic constituents in practical hydrocarbon fuels, the Princeton Fuels Combustion Laboratory initiated a research effort in the late 1970s to study the oxidation chemistry of aromatic compounds. One of the seminal results was the identification of the chain branching reaction:



as a primary step in aromatics combustion. It became apparent as kinetic models evolved that a deeper understanding of phenoxy reaction kinetics was necessary.

This thesis recounts an investigation of the high-temperature chemistry of the phenoxy radical and its parent phenol through the acquisition of reaction intermediate data from experiments performed in a turbulent flow reactor. Anisole, a chemical source of phenoxy at high temperature, and phenol were employed as reactor fuels at reaction temperatures near 1000 and 1170 K, respectively. Oxidation experiments were performed at fuel lean, stoichiometric, and fuel rich conditions. Pyrolysis experiments were also undertaken to provide bench mark data for comparison with oxidation data.

Anisole pyrolysis experiments confirmed that at flow reactor temperatures its thermal decomposition proceeds exclusively via homolysis of the O-CH<sub>3</sub> bond. The anisole decay was also observed to be first-order in the presence of oxygen. Moreover,

the distribution of reaction intermediates was virtually independent of equivalence ratio. Phenol, cresols, methylcyclopentadiene, and CO were major products. Minor species included benzene, cyclopentadiene, ethane, and methane. Trace yields of ethene, toluene, and naphthalenes were observed under all conditions; trace  $C_2$ – $C_4$  species including acetylene, allene, and 1,3-butadiene were observed only in the oxidation experiments. Oxidation occurs preferentially through intermediate methylcyclopentadiene.

A multichannel reaction scheme is proposed involving the formation of a chemically activated adduct from phenoxy and methyl. The complex reacts to form primarily cresols and methylcyclopentadiene + CO either directly or subsequent to stabilization. A kinetic model for anisole pyrolysis was developed to predict the disappearance of anisole and the production of reaction intermediates. Excellent agreement is obtained between experimental data and model predictions of anisole, CO, methylcyclopentadiene, and total phenolics.

For the phenol experiments, new equipment was developed to permit solid fuel melting and delivery to the existing flow reactor evaporator system. CO, cyclopentadiene, and benzene were major pyrolysis reaction intermediates. CO yield was found to exceed that of  $C_5H_6$ . Trace methane and methylcyclopentadiene were observed and suggest that some fraction of the observed benzene is derived from the cyclopentadienyl radical rather than from phenol directly. This may explain in part the disparity between the CO and  $C_5H_6$  data.

High-temperature phenol oxidation data has been acquired and, to the author's knowledge, is the first and only data of its kind. Major species included cyclopentadiene,

carbon monoxide, carbon dioxide, acetylene, benzene, 1,3-butadiene, ethene, and methane. Minor species were allene, methylacetylene, propene, ethane, methylcyclopentadiene, and naphthalene.

Overall, the results of this study indicate that recombination reactions play a significant role in the high-temperature chemistry of phenoxy and cyclopentadienyl, resonance stabilized radicals. Reactions of this type will hinder the conversion to  $\text{CO}_2$  of hydrocarbon fuels which contain aromatics.



## ACKNOWLEDGMENTS

The list of people who have contributed to my personal and professional growth during my time at Princeton is long and varied. Many have given generously of their time and expertise but more importantly of themselves.

I came to Princeton initially to join the Center for Energy and Environmental Studies (CEES). After a stimulating semester at the Center, I decided to pursue a more traditional program of engineering research in the Fuels Combustion Laboratory. I am grateful to Prof. Rob Socolow, the Center's director, for his support of that decision and for his assistance in finding a new advisor. I am pleased to have had the opportunity later on to serve as Rob's teaching assistant.

I chose to work with Profs. Irv Glassman and Ken Brezinsky because of their obvious enthusiasm for their work and concern for their students. I would like to thank Prof. Glassman for his continuing guidance. I feel fortunate to have been the beneficiary of his wisdom and inspiration over the past four years. But I am perhaps most grateful to him for his confidence in my abilities. I am equally grateful to Prof. Brezinsky for his boundless patience and for his contribution to this research. Ken was always willing to make time for me in order to discuss the myriad experimental and modeling difficulties

encountered in this work. Ken also lent an ear to more personal career concerns, and his encouragement in that regard is greatly appreciated.

I would like to acknowledge Prof. Judy Wornat and Prof. John Kiefer of the University of Illinois at Chicago for their careful reading of this dissertation and their many constructive remarks. I would also like to thank Prof. Fred Dryer who was gracious enough to make available his computational facilities for the modeling portion of this work.

The technical assistance of Joe Sivo was invaluable to this project. To an inexperienced experimentalist, the flow reactor can be an imposing device. It is only through Joe's patience and unflappable good humor that I was able to overcome my initial apprehension in the lab. I would also like to acknowledge the technical support of Yolanda Stein in the general maintenance of the gas chromatograph system and for taking time from her own research for so many emergency repairs. The administrative support of Betty Adam is also gratefully acknowledged.

This summer I took a short leave from Princeton to collaborate on a project at Sandia National Laboratory in Livermore, California aimed at the development of a novel technology for the clean destruction of hazardous wastes. I would like to thank Dr. Steve Rice at the Combustion Research Facility for affording me that opportunity.

My associations and friendships with other graduate students and post-docs have been an important part of my Princeton experience both within and outside of the laboratory. I would like to thank the entire APFR group and, in particular, Bob Butler for answering my innumerable questions about organic chemistry. I would also like to thank

Scott Davis and Dr. Hai Wang for many helpful discussions about kinetics. Outside of the lab, I'd like to thank "the girls"—Cindy Gooch, Courtney Cahill, and Kristina Richardson—for much laughter and spirited conversation. Thanks also to Ken and Karen Southerland for their friendship and for putting up with two housemates when they had bargained for just one.

I would like to acknowledge my parents, Taube and Michael. Throughout the course of this work and always they have been my most steadfast supporters. Words are not really sufficient to thank them for twenty-six years of unconditional love and understanding. I'd also like to recognize my brother Scott for being a wonderful sibling and an even better friend. I am grateful for the opportunity we've had this year to once again be a part of each other's daily lives.

Finally, I'd like to thank Joe Fielding for his love and friendship. These are the most precious things I will take with me from Princeton.

---

This work was supported by the Department of Energy, Office of Basic Energy Sciences, Division of Chemical Sciences under contract number DE-FG02-86ER13554 and by the DoD/DOE/EPA Strategic Environmental Research and Development Program (SERDP).

This dissertation carries the number 2097-T in the records of the Department of Mechanical and Aerospace Engineering.

## TABLE OF CONTENTS

---

ABSTRACT.....	iii
ACKNOWLEDGMENTS .....	vi
TABLE OF CONTENTS .....	ix
LIST OF TABLES .....	xi
LIST OF FIGURES .....	xii
CHAPTER 1. INTRODUCTION .....	1
1.1 MOTIVATION .....	2
1.2 LOW-, INTERMEDIATE-, AND HIGH-TEMPERATURE CHEMISTRY REGIMES .....	5
1.3 PRIOR WORK ON HIGH-TEMPERATURE BENZENE OXIDATION.....	9
1.4 PRIOR WORK ON ANISOLE PYROLYSIS.....	13
1.5 PRIOR WORK ON PHENOL PYROLYSIS.....	16
1.6 STRUCTURE OF THESIS.....	20
CHAPTER 2. EXPERIMENTAL TECHNIQUE.....	25
2.1 THE PRINCETON ATMOSPHERIC PRESSURE FLOW REACTOR .....	26
2.2 CALCULATION OF REACTION TIME.....	35
2.3 EFFECTS OF DIFFUSION ON KINETICS.....	42
2.4 EFFECTS OF MIXING AND TURBULENCE ON KINETICS .....	46
2.5 HYDROCARBON, OXIDIZER, AND CARRIER PURITIES .....	48

2.6 SUMMARY .....	49
<b>CHAPTER 3. ANISOLE PYROLYSIS AND OXIDATION: EXPERIMENTAL RESULTS .....</b>	<b>58</b>
3.1 EXPERIMENTAL RESULTS.....	59
3.2 SUMMARY .....	69
<b>CHAPTER 4. ANISOLE PYROLYSIS AND OXIDATION: KINETIC MODELING .....</b>	<b>81</b>
4.1 PYROLYSIS MODEL DEVELOPMENT .....	81
4.2 PYROLYSIS MODELING RESULTS.....	100
4.3 PYROLYSIS SUMMARY .....	110
4.4 OXIDATION MODEL DEVELOPMENT.....	112
4.5 OXIDATION SUMMARY .....	117
<b>CHAPTER 5. PHENOL PYROLYSIS AND OXIDATION.....</b>	<b>144</b>
5.1 PYROLYSIS .....	145
5.2 OXIDATION.....	149
5.3 SUMMARY .....	152
<b>CHAPTER 6. SUMMARY AND RECOMMENDATIONS.....</b>	<b>168</b>
6.1 THE PYROLYSIS AND OXIDATION OF ANISOLE.....	168
6.2 THE PYROLYSIS AND OXIDATION OF PHENOL.....	171
6.3 RECOMMENDATIONS .....	172
6.4 FINAL REMARKS.....	174
<b>REFERENCES .....</b>	<b>175</b>

## LIST OF TABLES

---

Table 3.1:	Experimental conditions for anisole experiments.....	59
Table 3.2:	Pressure and temperature conditions for measurement of rate constant for $C_6H_5O-CH_3$ bond homolysis .....	61
Table 3.3:	R-H bond strengths for anisole reaction intermediates.....	66
Table 4.1:	Anisole pyrolysis mechanism .....	119
Table 4.2:	High pressure limit rate parameters for QRRK analysis of $C_6H_5O\cdot + CH_3$ ..	89
Table 4.3:	Vibrational frequencies of $(H)(CH_3)C_6H_4O$ .....	90
Table 4.4:	Molecular parameters for $(H)(CH_3)C_6H_4O$ and $N_2$ bath gas .....	92
Table 4.5:	Apparent reaction rate constants calculated via QRRK analysis .....	93
Table 4.6:	Comparison of observed $\Delta H_f$ with PM3 predictions for species similar to $CH_3C_5H_5$ .....	96
Table 4.7:	Summary of PM3 calculations.....	96
Table 4.8:	Rate constants for formation of $C_6H_6$ from $CH_3C_5H_4\cdot$ .....	97
Table 4.9:	Thermodynamic properties for select species .....	123
Table 4.10:	Experimental conditions for anisole pyrolysis experiments in 5 and 10 cm reactor test sections .....	108
Table 5.1:	Experimental conditions for phenol experiments .....	144

## LIST OF FIGURES

---

Figure 1.1:	Temperature as a function of pressure for a constant ratio R of the rates of $H+O_2=OH+O$ and $H+O_2+M=HO_2+M$ .....	22
Figure 1.2:	Select aromatic and aliphatic species relevant to the high-temperature oxidation of anisole and phenol.....	23
Figure 1.3:	Benzene oxidation mechanism.....	24
Figure 2.1:	Schematic of the Princeton Atmospheric Pressure Flow Reactor .....	50
Figure 2.2:	Schematic of fuel preparation and delivery system.....	51
Figure 2.3:	Schematic of gas sample collection system.....	52
Figure 2.4:	Representative species, total carbon, and temperature profiles from the oxidation of anisole near 1000 K.....	53
Figure 2.5:	Major reaction intermediate profiles from duplicate anisole experiments...	54
Figure 2.6:	Major reaction intermediate profiles from duplicate phenol experiments ...	55
Figure 2.7:	Anisole pyrolysis model (Table 4.1) prediction of fuel decay and carbon monoxide for T=998, 1003, and 1008 K .....	56
Figure 2.8:	Anisole pyrolysis model (Table 4.1) prediction of cresol and methylcyclopentadiene for T=998, 1003, and 1008 K.....	57
Figure 3.1:	Comparison of experimental anisole data with first-order anisole decay profiles derived from reported rate constants (T=1003 K).....	71
Figure 3.2:	First-order anisole decay profiles from the pyrolysis and oxidation of anisole near 1000 K.....	72
Figure 3.3:	Phenol and cresol profiles from the pyrolysis and oxidation of anisole near 1000 K .....	73

Figure 3.4:	Formation of <i>o</i> - and <i>p</i> -cresols illustrated by consideration of the phenoxy radical as a hybrid of three resonance structures.....	74
Figure 3.5:	Methane, ethane, and ethene profiles from the pyrolysis and oxidation of anisole near 1000 K.....	75
Figure 3.6:	Cyclopentadiene, benzene, and naphthalene profiles from the pyrolysis and oxidation of anisole near 1000 K.....	76
Figure 3.7:	Methylcyclopentadiene profiles from the pyrolysis and oxidation of anisole near 1000 K.....	77
Figure 3.8:	Carbon monoxide profiles from the pyrolysis and oxidation of anisole near 1000 K.....	78
Figure 3.9:	Acetylene, C <sub>3</sub> (allene + propene + methylacetylene), and 1,3-butadiene profiles from the oxidation of anisole near 1000 K.....	79
Figure 3.10:	Comparison of carbon monoxide and sum of C <sub>5</sub> H <sub>5</sub> moieties = C <sub>5</sub> H <sub>6</sub> , + CH <sub>3</sub> C <sub>5</sub> H <sub>5</sub> + C <sub>6</sub> H <sub>6</sub> + C <sub>6</sub> H <sub>5</sub> CH <sub>3</sub> + 2 × (C <sub>10</sub> H <sub>8</sub> + C <sub>10</sub> H <sub>10</sub> ) from the pyrolysis of anisole at 1003 K.....	80
Figure 4.1:	Potential energy diagram for C <sub>6</sub> H <sub>5</sub> O· + CH <sub>3</sub> as evaluated by QRRK.....	124
Figure 4.2:	Direct formation of 5-CH <sub>3</sub> C <sub>5</sub> H <sub>5</sub> via (a) C <sub>5</sub> H <sub>5</sub> -CH <sub>3</sub> recombination or (b) decomposition of (H)(CH <sub>3</sub> )C <sub>6</sub> H <sub>4</sub> O and (c) subsequent formation of the 1- and 2- isomers by sigmatropic rearrangement(s).....	125
Figure 4.3:	Potential energy diagram for H + C <sub>6</sub> H <sub>6</sub> addition as evaluated by QRRK.	126
Figure 4.4:	Comparison of anisole pyrolysis data (T=1003 K) with model predictions of carbon monoxide and anisole.....	127
Figure 4.5:	Comparison of anisole pyrolysis data (T=1003 K) with model predictions of methylcyclopentadiene.....	128
Figure 4.6:	Comparison of anisole pyrolysis data (T=1003 K) with model predictions of benzene, cyclopentadiene, cyclopentadienyl radical, and naphthalene.....	129
Figure 4.7:	Comparison of anisole pyrolysis data (T=1003 K) with model predictions of total phenolics (C <sub>6</sub> H <sub>5</sub> OH + CH <sub>3</sub> C <sub>6</sub> H <sub>4</sub> OH).....	130
Figure 4.8:	Comparison of anisole pyrolysis data (T=1003 K) with model predictions of phenol and cresols.....	131



Figure 4.9:	Comparison of anisole pyrolysis data (T=1003 K) with model predictions of methane and ethane .....	132
Figure 4.10:	Comparison of species profiles from anisole pyrolysis in 5 and 10 cm diameter test sections.....	133
Figure 4.11:	Flux diagram at 15 ms for anisole pyrolysis model (Table 4.1).....	134
Figure 4.12:	Comparison of reaction fluxes for direct and indirect formation of cresol and methylcyclopentadiene.....	135
Figure 4.13:	Flux of 1- and 2-methylcyclopentadiene through isomerization and abstraction reactions .....	136
Figure 4.14:	Formation of $\text{CH}_3\text{C}_5\text{H}_4\cdot$ radical from 5-, 1-, or 2- $\text{CH}_3\text{C}_5\text{H}_5$ .....	137
Figure 4.15:	Addition of $\text{HO}_2$ to $\text{CH}_3\text{C}_5\text{H}_4\cdot$ at the (a) 2 and (b) 3 sites.....	138
Figure 4.16:	(a) Addition of O to $\text{CH}_3\text{C}_5\text{H}_4\cdot$ at the 2 site..... (b) Addition of O to $\text{CH}_3\text{C}_5\text{H}_4\cdot$ at the 3 site.....	139 140
Figure 4.17:	Subsequent reactions of the 1,3-pentadien-4-yl and 2-methyl-1,3-butadien-1-yl radicals .....	141
Figure 4.18:	Addition of H to (a) 1- and (b) 2-methylcyclopentadiene.....	142
Figure 4.19:	Addition of H to (a) 1- and (b) 2-methylcyclopentadien-one.....	143
Figure 5.1:	Fuel decay profile from the pyrolysis of phenol at 1173 K .....	155
Figure 5.2:	Carbon monoxide, cyclopentadiene, and benzene profiles from the pyrolysis of phenol at 1173 K .....	156
Figure 5.3:	Methane and acetylene profiles from the pyrolysis of phenol at 1173 K ..	157
Figure 5.4:	Comparison of carbon monoxide and sum of $\text{C}_5\text{H}_5\cdot$ derivatives from the pyrolysis of phenol at 1173 K .....	158
Figure 5.5:	Fuel decay profiles from the oxidation of phenol at 1169 K .....	159
Figure 5.6:	Cyclopentadiene profiles from the oxidation of phenol at 1169 K .....	160
Figure 5.7:	Acetylene profiles from the oxidation of phenol at 1169 K .....	161

Figure 5.8:	1,3-Butadiene profiles from the oxidation of phenol at 1169 K.....	162
Figure 5.9:	Methane profiles from the oxidation of phenol at 1169 K.....	163
Figure 5.10:	C <sub>3</sub> profiles for the oxidation of phenol at 1169 K .....	164
Figure 5.11:	Benzene profiles from the oxidation of phenol at 1169 K .....	165
Figure 5.12:	Carbon monoxide and carbon dioxide profiles from the oxidation of phenol at 1169 K .....	166
Figure 5.13:	Naphthalene profiles from the oxidation of phenol at 1169 K .....	167

## CHAPTER 1. INTRODUCTION

---

Recognizing the importance of aromatic fuel constituents with respect to energy and environmental considerations, the Fuels Combustion Laboratory launched over 15 years ago an ongoing study of the high-temperature oxidation of aromatic hydrocarbons. Since its inception, this research program has contributed to the development of chemical kinetic models essential to the analysis of actual combustion systems. The present investigation of anisole and phenol kinetics is the latest contribution to this continuing research effort. The experimental portion of this work has involved the acquisition of reaction intermediate measurements from the Princeton Atmospheric Pressure Flow Reactor (APFR). As in other flow reactor studies, detailed kinetic modeling has been employed for validation of the mechanistic interpretation of species data.

Earlier APFR studies of aromatic species including benzene, toluene, and other alkylbenzenes have revealed the common importance of the early reaction intermediate phenoxy ( $\text{C}_6\text{H}_5\text{O}\cdot$ ) and its unimolecular decomposition product cyclopentadienyl ( $\text{C}_5\text{H}_5\cdot$ ). Specifically, the formation and destruction of the phenoxy radical is the dominant route by which the aromatic ring is converted to aliphatic fragments. Efforts to model APFR data [Emdee et al., 1992, Butler, 1992] as well as the flow reactor [Arends et al., 1993] and flame data [Lindstedt and Skevis, 1994; Zhang and McKinnon, 1995; Davis et al., 1996]

of other laboratories have indicated a need for further investigation of the fates of these two radicals. The present study of anisole and phenol, employed as sources of the phenoxy radical, represents an endeavor to gain a heightened understanding of the chemistry of  $C_6H_5O\cdot$  and  $C_5H_5\cdot$  and thus the chemistry of all aromatics.

### 1.1 MOTIVATION

Aromatic hydrocarbons have been exploited as a means of boosting octane rating of automotive fuel blends since the discontinuation of tetraalkyllead (TAL) gasoline additives. Organic lead compounds in gasoline are known to reduce the susceptibility of the fuel to "knock" or premature ignition of the fuel-air mixture during the engine's compression stroke [Heywood, 1988]. However, these additives were found to contribute to both organic (vapor-phase TALs) and inorganic (particulate) lead pollution. Prior to the enactment of legislation requiring all new cars to use lead-free gasoline, vehicular emission was by far the leading contributor to total lead emissions in this country [US Environmental Protection Agency, 1977]. By law, in the United States all cars of 1975 or later model year are required to use unleaded gasoline. The shift to lead-free gasoline was motivated in part by concern over the toxicity of lead itself but was also essential to prevent poisoning of the new exhaust catalysts required for those cars to meet EPA emission standards for carbon monoxide and unburned hydrocarbons [Heywood, 1988]. While high octane, lead-free gasoline may be readily produced by capitalizing on the known knock resistance of aromatics, this approach is not without liability. The exceptional chemical stability which lends these species their desirable knock properties

also implicates them as a source of unburned hydrocarbon emissions. Indeed aromatics have been found to constitute a significant portion, approximately 30% by weight, of the organic fraction of automobile exhaust [Nelson and Quigley, 1984]. Nevertheless, in 1990 the industry average gasoline contained 34% aromatics by volume including 1.7 vol% benzene [Mayotte et al., 1994], a known carcinogen [US Environmental Protection Agency, 1981].

Emissions of benzene, classified as a toxic air contaminant, have been correlated to both fuel benzene content and the total aromatics content of the fuel [Mayotte et al., 1994]. This result is not unexpected as benzene is a major reaction intermediate present during the oxidation of alkylbenzenes such as toluene [Venkat et al., 1982], ethylbenzene [ibid.], and the xylenes [Emdee et al., 1990, 1991] which are commonly found in gasoline. Flame studies suggest that benzene is also derived in the engine combustion process from smaller, nonaromatic hydrocarbons [Frenklach and Warnatz, 1987; Harris et al., 1988; Westmoreland et al., 1989]. Therefore, while the EPA has proposed reformulated gasolines with aromatic contents as low as 21.7 vol% [Mayotte et al., 1994] these species will continue to influence engine chemistry and the nature of tailpipe emissions.

Finally, the presence of aromatics in practical fuels has ramifications with regard to soot formation. The first step in the overall model of soot formation is the synthesis of the first aromatic ring from aliphatic fragments. The production of soot particles then proceeds via a multistep sequence which begins with the addition of hydrocarbon fragments to the aromatic ring and subsequent cyclization to form the initial PAH or polycyclic aromatic hydrocarbon. Planar PAH growth and particle nucleation, the

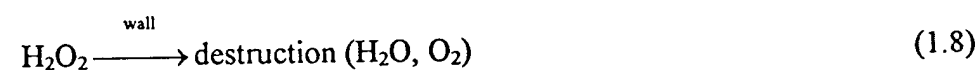
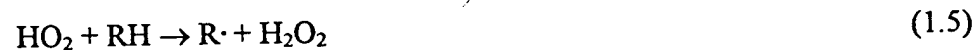
coalescence of PAHs into three-dimensional clusters, follow. In the case of an initially aromatic fuel, the direct condensation of intact aromatic rings becomes an important, additional reaction pathway in the mechanism of PAH growth [Scully and Davies, 1965; Graham et al., 1975; Frenklach and Wang, 1991]. In fact, condensation reactions have been found to dominate the initial stages of PAH growth in the high-temperature pyrolysis of benzene [Frenklach et al., 1988]. Therefore, aromatic constituents may be expected to enhance the sooting tendency of a fuel. The correlation between fuel aromatics content and sooting tendency has obvious implications regarding particulate emission from automobiles. In addition there are impacts for jet engines. JP-4 and JP-5 jet fuels may contain up to 25% aromatics by volume [Goodger, 1995] since a substantial aromatics content is desirable to achieve a high fuel energy density. The presence of soot, however, enhances flame radiation and in turn the heat loading on the combustor liner resulting in a shortening of engine life [ibid.].

In summary, it is evident that a knowledge of the oxidation chemistry of aromatic species will be useful in the optimization of practical combustion devices whose effective operation relies in part upon the fuel's aromatic content. Kinetic modeling of species data acquired from flow reactor experiments like those reported in this thesis is a systematic approach to elucidating the chemistry responsible for soot and other undesirable tailpipe emissions. The ability to predict—with the goal, ultimately, to control—the chemistry of aromatics is an essential task in the evolution of cleaner practical fuels and combustion systems.

## 1.2 LOW-, INTERMEDIATE-, AND HIGH-TEMPERATURE CHEMISTRY REGIMES

In forthcoming discussions it will be necessary to distinguish between the three temperature regimes listed above. Therefore, before proceeding, a brief description of the kinetic phenomena associated with each will be given.

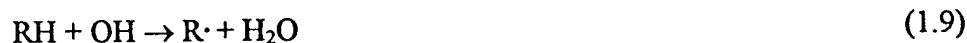
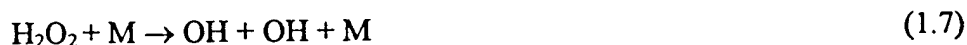
Below about 700 K, peroxy ( $\text{HO}_2$ ) and organic peroxy radicals ( $\text{ROO}\cdot$ ) typically play a significant role in the oxidation chemistry of hydrocarbons as demonstrated by the general, simplified mechanism below [Dryer, 1991]:



Reaction 1.1, the initiation reaction, is generally quite endothermic ( $E_a \approx 45\text{--}55$  kcal for alkanes) and thus slow. Reactions 1.2 and 1.3 are the two essential types of propagation reactions at low temperature. It should be noted that thermal decompositions of  $\text{R}\cdot$  are usually highly endothermic and are important only above approximately 750 K, beyond the low-temperature regime. The organic peroxy radical  $\text{ROO}\cdot$  formed in reaction 1.2 may abstract H from the initial fuel molecule (1.4) or another hydrogen donor to form the hydroperoxide  $\text{ROOH}$ . The rate of formation of  $\text{ROOH}$  is dependent upon the

competition for  $R\cdot$  between reactions 1.2 and 1.3. Reaction 1.3 yields a stable olefin.  $ROO\cdot$  will form the hydroperoxide but can also decompose to yield aldehydes and ketones. Destruction of the initial reactant is accomplished primarily via attack by  $ROO\cdot$  (1.4),  $HO_2$  (1.5), or  $OH$  formed in reaction 1.6. At low temperature, the decomposition of hydrogen peroxide (1.7) is slow, and the fate of  $H_2O_2$  is termination (e.g. at the reactor wall) forming water and oxygen (1.8).

As temperature is increased, reactions 1.3 and 1.5 play a more significant role resulting in an accelerated production of  $H_2O_2$ . And hydrogen peroxide decomposition (1.7) becomes more significant. Furthermore, the formation of organic peroxy radicals (1.2) is rapidly reversible above about 500 K [Benson, 1982]. Thus, the decomposition of  $ROO\cdot$  is important at intermediate temperatures. As a result of the shift with temperature of relative reaction importance,  $HO_2$  and  $OH$  become the primary chain-propagating radicals in the intermediate-temperature regime ( $\sim 700$ – $1000$  K at 1 atm). And, the dominant oxidation mechanism becomes:



Finally, at temperatures above about 800 K, thermal decomposition of  $R\cdot$  via  $\beta$ -scission processes becomes prevalent, competing with olefin formation (1.3). Unimolecular H loss from  $R\cdot$  is disfavored with respect to  $\beta$ -scission pathways due to the relative strengths of C–H and C–C bonds. Only radicals which do not possess a  $\beta$ -scission site (e.g. ethyl,



isopropyl, t-butyl) will tend to eliminate H. H atoms so formed will in this temperature regime yield HO<sub>2</sub> via reaction 1.10:



The boundary between low/intermediate- and high-temperature chemistry is usually defined by the temperature and pressure conditions at which the rates of reactions 1.10 and 1.11:



are equal [Dryer, 1991]. High-temperature chemistry is then characterized by the dominance of reaction 1.11 over reaction 1.10 and thus by radical reactions involving H, OH, and O which are much faster than analogous reactions of HO<sub>2</sub>. At atmospheric pressure this transition takes place below 1000 K, i.e. at 985 K [Yetter et al., 1991], and thus the flow reactor experiments reported in this thesis (1000–1170 K) may be classified as high-temperature. However, for the conditions studied here, the rate of reaction 1.11 is still less than an order of magnitude greater than that of reaction 1.10 (Figure 1.1). Thus the HO<sub>2</sub> chemistry must be given consideration in reaction modeling.

As discussed by Brezinsky [1986], the oxidation of benzene and alkylated aromatics involves certain reaction features without analogues in the oxidation of aliphatics. For example, the ring is a site for electrophilic addition reactions which compete with H abstraction from the aromatic nucleus or side chain. Therefore, it is worthwhile to characterize the temperature regimes of chemistry with regard to aromatics in particular. At high enough temperatures, the partially oxidized ring thermally decomposes via reaction 1.12:



[Colussi et al., 1977] resulting in a loss of aromaticity. It is useful then to use the temperature at which this reaction pathway becomes significant (on the time scales relevant to flames, typically ~milliseconds) as a means of defining the high-temperature chemistry regime. To further illustrate the distinction between the temperature regimes of chemistry as they pertain specifically to aromatics, a brief review of the low-temperature chemistry follows.

The low-temperature (673–738 K) oxidation of toluene was outlined by Barnard and Ibberson [1965]. Abstraction of a methyl side chain H by  $\text{O}_2$  was the suggested initiation step. Addition of  $\text{O}_2$  to the resulting benzyl radical was postulated to yield benzylperoxy. Multiple decomposition paths exist for the benzylperoxy radical which ultimately yield either phenoxy or phenyl radicals. The authors suggested that oxidation of the aromatic ring was accomplished by a bridging of  $\text{O}_2$  across the benzylperoxy nucleus. Decomposition of the resulting bridged structure was thought to be the final step in the destruction of the aromatic ring. It is worthwhile to note that once again organic peroxy radicals are seen to play a significant role in low-temperature hydrocarbon chemistry. Norrish and Taylor [1956] described the low-temperature oxidation of benzene. Their mechanism shares many of the salient features of the toluene mechanism of Barnard and Ibberson. Organic peroxy radicals were thought to play an essential role as precursors to the formation of bridged  $\text{O}_2$  structures whose ultimate decomposition marked the loss of aromaticity.

As stated previously, the lifetimes of hydrocarbon peroxy species are considerably shortened at higher temperatures. Furthermore, the formation of bridged  $O_2$  structures at high temperature is doubtful and has been questioned even at low temperature [Benson, 1965]. The loss of aromaticity at high temperature proceeds instead through the formation and destruction of the phenoxy radical,  $C_6H_5O\cdot$ . Reaction 1.12 has an activation energy of approximately 44 kcal/mol [Lin and Lin, 1986a; Frank et al., 1994] and is fast only at temperatures greater than about 1000 K. This represents another important demarcation between the low/intermediate- and high-temperature regimes of hydrocarbon chemistry.

### 1.3 PRIOR WORK ON HIGH-TEMPERATURE BENZENE OXIDATION

The oxidation of benzene, the simplest of the aromatic molecules, is a logical starting point in the development of a comprehensive mechanism for the combustion chemistry of aromatic compounds. A survey of prior work on benzene will serve to place the present study of anisole and phenol in its proper context.

First, a review of the molecular structure of benzene is appropriate. Figure 1.2 depicts the structures of benzene and other species, both aromatic and aliphatic, which are discussed in this thesis. Benzene is a planar, hexagonal molecule ( $C_6H_6$ ) with a carbon atom situated at each of the six vertices. Each carbon atom is  $sp^2$ -hybridized leaving an unhybridized  $2p_z$  orbital on each carbon atom, perpendicular to the plane of the benzene ring. Six  $\pi$  molecular orbitals are formed due to the interaction of the six  $2p_z$  atomic orbitals. A special property of these molecular orbitals is that they are delocalized, i.e.

electrons residing in any of these orbitals are free to move around the entire ring. The benzene molecule is therefore sometimes represented by a circle inscribed in a hexagon to indicate that the  $\pi$  electron densities are evenly distributed. It is this delocalized  $\pi$  electron structure which gives the aromatic nucleus its unusual chemical stability [Chang, 1988].

Benzene and toluene, the simplest alkylbenzene, were the subjects of the earliest attempts to model in detail the high-temperature combustion chemistry of aromatics. In a 1981 paper, Bittner and Howard reported the mole fraction profiles of fifty-one species measured using a molecular beam mass spectrometer system in a near-sooting premixed benzene/oxygen/argon flame. The authors reported unexpectedly low phenyl radical mole fractions and noted that unimolecular decomposition of phenyl is not fast enough to account for their observation. Large mole fractions of phenol observed early in the flame were said to suggest that O atom attack on phenyl may be a major path. It was postulated that multiple collisions of phenol might then yield either of two  $C_5H_6$  species that were observed, cyclopentadiene and an open-chain compound. Nevertheless, conclusive evidence of a predominant route for ring fragmentation was not found.

The work of Euchner et al. [1981] and Venkat et al. [1982] revealed that at flow reactor conditions ( $T \sim 1200$  K) cyclopentadiene and phenol are important intermediates in the oxidation of benzene, toluene, and ethylbenzene. Species measurements were obtained via GC-FID (gas chromatography with flame-ionization detection), a technique which allows detection of stable species only. The presence of radicals was inferred from measurements of their parent compounds. GC measurements of phenol and cyclopentadiene, therefore, were indicative of the existence of phenoxy and

cyclopentadienyl in the flow reactor. In a lean benzene oxidation experiment, the cyclopentadiene peak (i.e. the point of maximum concentration) was observed to just follow that of phenol. The same observation was made in a lean toluene experiment with the phenol peak just following that of benzene. It was deduced that following removal of the side chain (or, in the case of benzene, abstraction of H) O is added to the ring by reaction of phenyl with O<sub>2</sub>. And, CO is expelled from the resulting phenoxy radical to yield C<sub>5</sub>H<sub>5</sub> which is oxidized to form ultimately C<sub>2</sub> and C<sub>4</sub> species.

In a review paper on aromatic hydrocarbon oxidation, Brezinsky [1986] qualitatively outlined a benzene oxidation mechanism (Figure 1.3) which became the basis for the detailed kinetic models of Bittker [1991] and Emdee [1991]. Emdee first modeled the benzene data of Lovell [1988] taken near 1100 K. It was found that the benzene decay profile was most sensitive to three reactions:



The H+O<sub>2</sub> branching reaction is essential to the development of the H<sub>2</sub>/O<sub>2</sub> radical pool, and almost any high-temperature oxidation system will be sensitive to its rate. The second two reactions determine the fate of the phenoxy radical. As noted by Emdee et al. [1992], the benzene fuel molecule must pass through phenoxy to reach final products and thus the fate of this radical is very important. Phenol, and presumably the fate of phenoxy, was predicted reasonably well by the benzene model. An extension of the benzene model to toluene was developed from Emdee's data for the oxidation of toluene near 1200 K. The

extended model was found to underpredict phenol. It was suspected that the temperature dependence of reaction 1.12 was in error since phenol prediction matched experiment well for the lower temperature benzene experiments. Nevertheless, Emdee's toluene results were consistent with previously proposed mechanisms for the oxidation of alkylbenzenes.

Lindstedt and Skevis [1994], in their endeavor to model the benzene flame data of Bittner and Howard [1981] and Hausmann et al. [1992], overpredicted phenoxy levels by a factor of 20. Zhang and McKinnon [1995] attempted to model the same data, overpredicting phenoxy concentration by two orders of magnitude. It was suspected by the authors that the huge discrepancy between their mechanism and the experimental result indicated either incorrect rate constants or missing mechanisms. They noted that removal from their mechanism of the three primary phenoxy production channels still did not provide agreement with experiment and concluded that the error must lie in the phenoxy consumption channels.

Finally, Davis et al. [1996] modified the benzene/toluene model of Emdee et al. (the EBG model) to improve its prediction of laminar flame speeds. Using the counterflow twin flame technique, Davis determined experimentally the stretch-corrected flame speeds of benzene/air and toluene/air mixtures over a large range of equivalence ratios at room temperature and atmospheric pressure. The laminar flame speed, a parameter which describes the propagation of a one-dimensional, planar, adiabatic, premixed flame, has been commonly used to partially validate kinetic mechanisms. The original EBG mechanism, which has been found to predict well the fuel decomposition and major intermediate species measured in the flow reactor oxidation of benzene and toluene,

underpredicts the flame speeds by about 10–15 cm/s. Through incorporation of a recently proposed rate constant for the  $C_6H_5+O_2$  reaction [Frank et al., 1994] and rate coefficient fall-off for a number of key radical/radical recombination reactions, the flame speed predictions were substantially improved while maintaining accurate prediction of the flow reactor experiments. A deficiency remained, however, in the model's ability to predict the lean flame speeds of benzene/air flames. Notably, sensitivity analysis revealed that the computed flame speed was sensitive to many reactions of phenol.

In summary, the high-temperature oxidation of benzene and toluene have been studied repeatedly with consensus regarding the importance, as initially proposed in this laboratory [Venkat et al., 1982], of the early reaction intermediate phenoxy. Yet, kinetic modeling of the combustion chemistry of these species has been plagued by an inability to predict successfully measurements of phenoxy and the parent species phenol. It has been recognized [Davis et al., 1996] that further experimental and theoretical studies of phenol oxidation will be necessary to arrive at a comprehensive mechanism for benzene combustion. As stated by Zhang and McKinnon [1995], the inadequacies of benzene models—in particular with regard to the phenoxy predictions—indicate an “urgent need” for more experimental data.

#### **1.4 PRIOR WORK ON ANISOLE PYROLYSIS**

It is evident from the preceding discussion that: 1) the phenoxy radical is a key intermediate in the high-temperature oxidation of aromatic species, and 2) further study, both experimental and modeling, is required in order to establish conclusively the

chemistry which governs the fate of this radical and thus the conversion of the aromatic ring to aliphatic fragments. In the present study, anisole is used as a chemical source of the phenoxy radical in high-temperature flow reactor experiments. But the thermal decomposition of anisole has been investigated before in varying degrees of detail, by an assortment of experimental techniques, and for a variety of motivations.

The focus of the earliest gas-phase studies [Paul and Back, 1975; Suryan et al., 1989] was determination of the rate constant for O-methyl bond homolysis. Over the temperature range 720–795 K, reaction 1.14:



was observed to be the principal course of anisole decay.

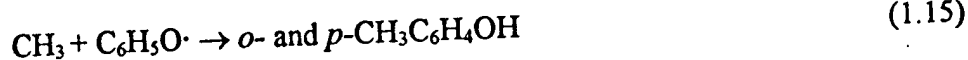
Lin and Lin [1985, 1986a] decomposed anisole in a shock tube over the temperature range 1000–1580 K (0.4–0.9 atm). Here anisole was exploited as a source of phenoxy radical in order to determine a rate constant for the unimolecular decomposition of phenoxy to CO and cyclopentadienyl radical (1.12). CO production was monitored by resonance absorption spectroscopy and was modeled initially on the basis of the two-step mechanism:



Implicit in this approach is the assumption that the system is free from any additional reactions which may consume phenoxy, thereby reducing the final concentration of CO. But at the longer residence times, CO concentration was found to plateau at a value less



than the initial concentration of anisole; even at 1311 K  $[\text{CO}]_{t=\infty}/[\text{C}_6\text{H}_5\text{OCH}_3]_0$  was less than unity,  $\approx 0.75$ . It was presumed that the occurrence of reaction 1.15:



was responsible for the deficiency in the oxygen mass balance. With the inclusion of reaction 1.16:



$k_{15}$  was modeled to fit the data, i.e. for each set of  $[\text{CO}]$  data  $k_{15}$  was varied to account for the "missing" oxygen. At the same time,  $k_{12}$  was adjusted to maintain agreement with the experimental CO profile. Though Lin and Lin were able to model their data, scatter was evident in the required values of  $k_{15}$  which ranged from  $(1-10) \times 10^{11} \text{ cc}\cdot\text{mol}^{-1}\cdot\text{s}^{-1}$ .

Mackie and coworkers [1989] noted that to establish the validity of Lin and Lin's measurement of  $k_{12}$  it is important to determine the extent to which reaction 1.15 influences the phenoxy kinetics. To determine the distribution of oxygen in the products, Mackie et al. studied the thermal decomposition of anisole in a perfectly stirred reactor (850–1000 K,  $16-120 \times 10^{-3} \text{ atm}$ ). Methane, ethane, methylcyclopentadiene, and benzene were among the non-oxygenated species detected. The majority of product oxygen was found to exist in cresols and phenol, rather than in CO. The validity of Lin and Lin's work was ultimately neither confirmed nor refuted since the observed yields of phenol could not be accounted for by homogeneous gas-phase abstraction reactions. Nevertheless, the kinetics of anisole decomposition proved to be more complex than is suggested by the 4-step mechanism discussed above.

Finally, Arends and coworkers [1993] produced a detailed model for the thermolysis of anisole in hydrogen at atmospheric pressure over the temperature range 793–1020 K. Again, the production of phenol could not be modeled strictly via homogeneous gas-phase reactions with physically meaningful rate constants.

Notably, no prior anisole oxidation studies have been reported. To further our understanding of the chemistry relevant to practical combustion systems (typically oxidation systems) an investigation of both the pyrolysis and oxidation of anisole was undertaken in this laboratory. At APFR conditions ( $T \sim 1000$  K), anisole decomposes readily to phenoxy and methyl radicals. The oxidation of anisole in the flow reactor—where the phenoxy radical is introduced into an oxidizing environment replete with aliphatic fragments—is then a simple model for practical combustion processes in which the fuel is a blend of aromatic and aliphatic constituents.

### 1.5 PRIOR WORK ON PHENOL PYROLYSIS

The use of pure phenol as a fuel in combustion experiments has been limited by certain practical considerations. Phenol is a room-temperature solid reactant and must be either mixed with a solvent or melted in its pure form for introduction into reactor evaporator systems. And, as will be further discussed in Chapter 2, accurate quantification of phenol yield by GC methods is difficult owing to the compound's polarity. Nevertheless, several studies of phenol pyrolysis have been reported and will be reviewed here.

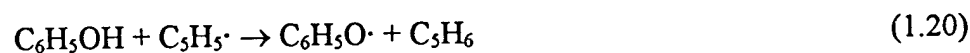
Cypres and Bettens [1974, 1975a] pyrolyzed phenol between 938 and 1138 K. Major products, measured after 2.5 seconds, were CO, benzene, naphthalene, hydrogen, water, and methane. Cyclopentadiene was among the minor products observed. On the basis of deuterium labeling experiments they concluded that, following isomerization of phenol to a cyclohexadienone intermediate, CO was formed via a molecular elimination reaction.

The first data depicting the evolution of phenol reaction intermediates with time were reported by Weckman et al. [1983]. Phenol was dissolved in benzene and pyrolyzed in an atmospheric pressure flow reactor at 1183 K. Intermediate cyclopentadiene, a major product, supported the existence of a CO elimination reaction of either phenol itself or the phenoxy radical. But the CO yield was found to grow at a rate approximately twice that of the  $C_5H_6$  yield. And it was determined that only 60% of the phenol disappearance was accounted for by the formation of CO. Thus it was concluded that another phenol decomposition pathway must exist which was postulated to involve the formation of benzene and water. Experimental verification was not possible as relatively small increases in benzene concentration were not perceptible with respect to the background solvent levels.

He et al. [1988] investigated the kinetics of hydrogen and hydroxyl radical attack on phenol in a single-pulse shock tube experiment (1000–1150 K, 2–2.5 atm). Gas mixtures of phenol and hexamethylethane (the H source) in argon were prepared as fuel feeds. Benzene was revealed to be a major product on the millisecond time scale and it

was concluded that hydrogen atoms react with phenol via both abstraction of the phenolic H and displacement of OH.

With the design of a device to melt phenol and deliver a metered flow of the hot liquid, Lovell et al. [1989] expanded upon the work of Euchner et al. [1981]. Pure phenol was pyrolyzed over a range of temperatures (1064–1162 K) and initial mole fractions (500–2016 ppm). As observed by Euchner, the CO yield was found to grow at a rate significantly greater than that of the  $C_3H_6$  yield for all experimental conditions. Accurate quantification of phenol was not achieved via GC analysis. The 7-step mechanism below was developed to account for CO, cyclopentadiene, and benzene:



Reactions 1.12, 1.13, and 1.17–19 had been reported previously in the archival literature [Lin and Lin, 1986; He et al., 1988]. These reactions together with reaction 1.20 predict nearly equal yields of CO and  $C_3H_5\cdot$ . In order to model the experimental data, it was necessary to add reaction 1.21 which removes  $C_3H_5\cdot$  from the system without an equivalent restriction of CO production. The observation of trace naphthalene and indene suggested that molecular weight growth reactions did occur, however the observed yields

of these two species were too small to constitute a major  $C_3H_5\cdot$  consumption route. It was postulated that a large oxygenated aromatic like that produced by reaction 1.21 might go undetected due to difficulties associated with the trapping and analysis of these species. Next, rate parameters for reactions 1.17, 1.20, and -1.13 were varied (within realistic limits) while literature rate values for reactions 1.17–19 and 1.12 were held fixed. This procedure allowed the CO and  $C_5H_6$  data to be reproduced. Benzene however was overpredicted.

Manion and Louw [1989] examined the pyrolysis of phenol in  $H_2$  at atmospheric pressure between 922 and 1175 K. Phenol was dissolved in water to produce a tractable liquid. At residence times of 3–4 seconds, primarily benzene and CO were observed accompanied by lesser amounts of cyclopentadiene and other hydrocarbons. CO formation was predicted well by a 5-step mechanism composed of reactions 1.12, -1.13, 1.17, -1.17, and 1.18. Rate data for reactions other than 1.12 were determined by thermodynamic estimations coupled with some assumptions regarding  $[C_6H_5O\cdot]$  and  $[H]$ . These rate parameters, while derived by sound methods, are not in agreement with those of either Lovell or He.

It is evident from the above discussion that while some relevant rate data do exist, further investigation is required in order to resolve the discrepancies between reported phenol pyrolysis mechanisms and to arrive at a model which is detailed and complete. Furthermore, until now no phenol oxidation studies have been reported. The present study of phenol oxidation serves to isolate a subset of benzene chemistry—from the phenoxy radical down to final products—which is still not conclusively defined and is

critical to the development of a comprehensive mechanism for the combustion of all aromatic species.

## 1.6 STRUCTURE OF THESIS

The remainder of this thesis recounts an investigation of the high-temperature pyrolysis and oxidation of anisole and phenol through the acquisition of experimental data, the qualitative mechanistic interpretation of data, and the development of a detailed kinetic model for comparison with experimental results.

The design and validation of the Princeton Atmospheric Pressure Flow Reactor have been described previously in some detail [Dryer, 1972; Euchner, 1980]. However, over the past few years, a number of changes and additions have been made to the APFR itself as well as to the standard analytical procedure. Therefore Chapter Two, *Experimental Technique*, will detail the reactor operation and sample analysis techniques with an emphasis on the recent modifications and their impacts.

Reaction intermediate data obtained from the flow reactor pyrolysis and oxidation of anisole near 1000 K are reported in Chapter Three, *Anisole Pyrolysis and Oxidation: Experimental Results*. As will be discussed, pyrolytic chemistry was found to dominate even under oxidative conditions. A kinetic modeling study is presented in Chapter Four, *Anisole Pyrolysis and Oxidation: Kinetic Modeling*. At the experimental conditions of this effort, most of the important reaction steps are pyrolytic. Thus the bulk of the detailed modeling effort was directed at reproducing the pyrolysis data. Chapter Four also

includes an extension of the pyrolysis mechanism to include the oxidative chemistry which becomes important later in the reaction sequence.

The greater part of this work was, as described above, devoted to an experimental and modeling study of anisole oxidation. As will be discussed in Chapter Two, the procurement and modification of a syringe pump required for the phenol experiments delayed the commencement of the phenol study. Therefore, the primary intent of the phenol study was the acquisition of experimental data over a range of equivalence ratios. Chapter Five, *Phenol Pyrolysis and Oxidation*, presents the reaction intermediate data obtained from flow reactor experiments near 1170 K without accompanying detailed modeling. It is hoped that these data will contribute to the modeling efforts of other investigators who have expressed a compelling need for them.

Chapter Six, *Summary and Recommendations*, will reiterate the salient findings of this study and outline the author's suggestions for future investigation.

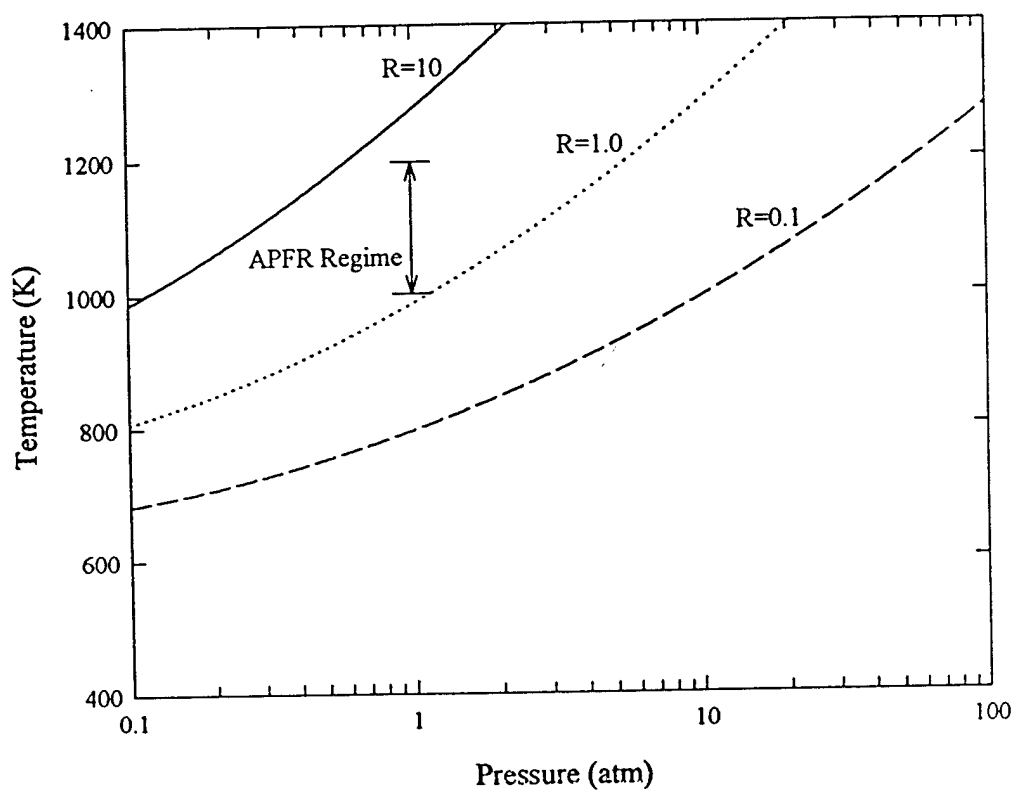


Figure 1.1: Temperature as a function of pressure for a constant ratio  $R$  of the rates of  $\text{H} + \text{O}_2 = \text{OH} + \text{O}$  and  $\text{H} + \text{O}_2 + \text{M} = \text{HO}_2 + \text{M}$ . Adapted from Dryer [1991].



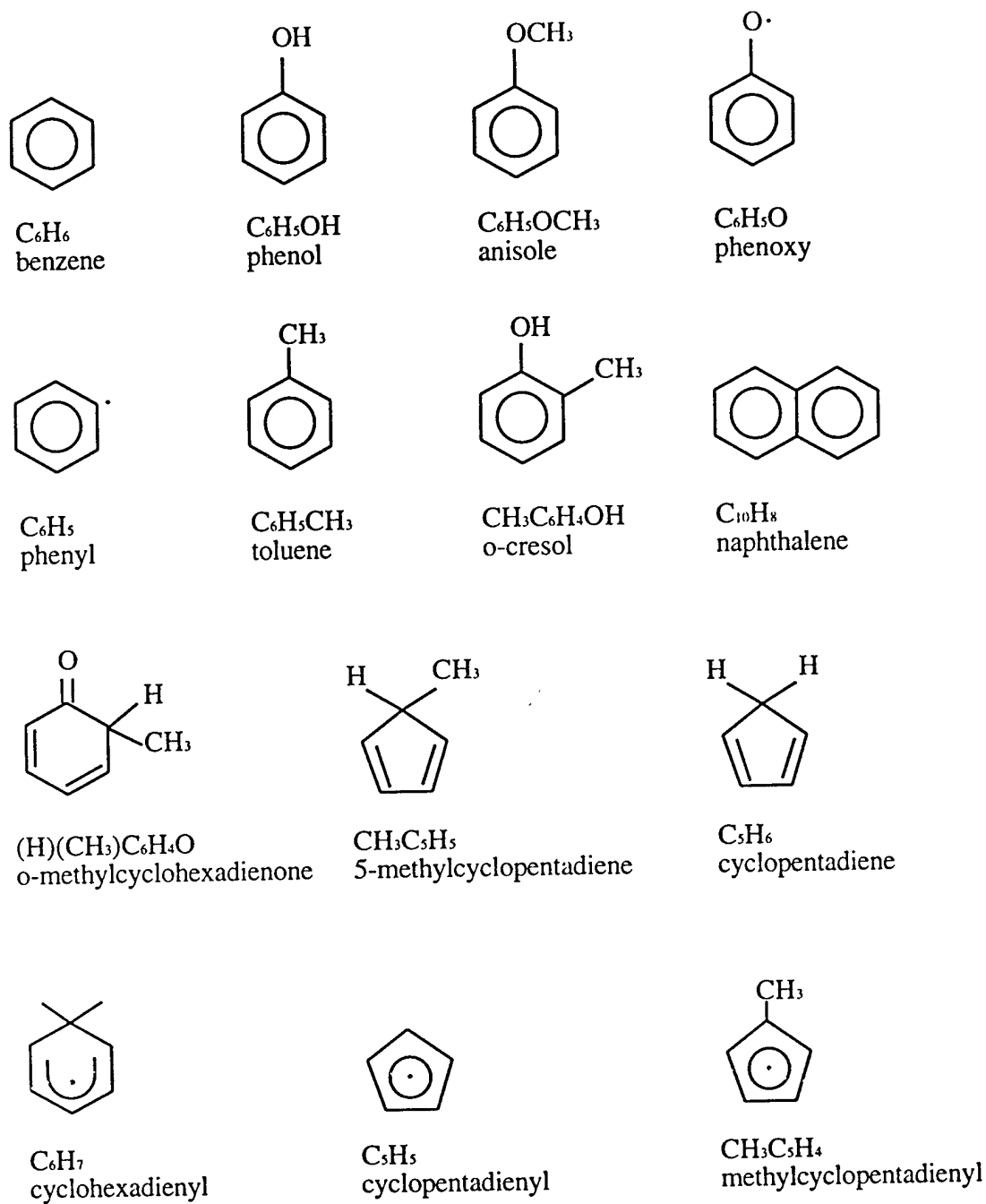
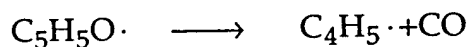
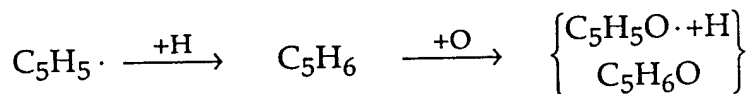
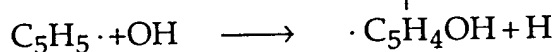
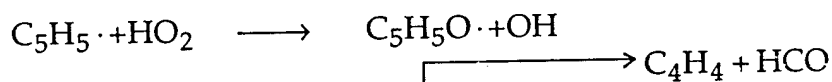
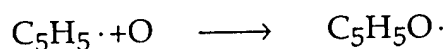
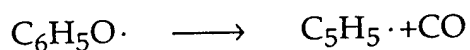
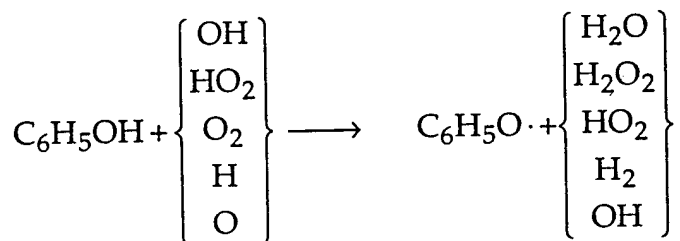
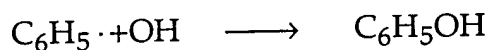
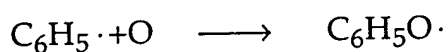
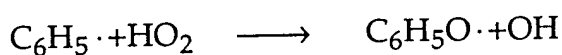
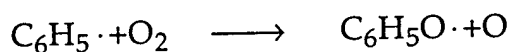
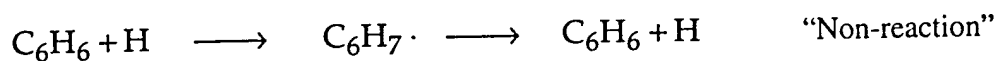
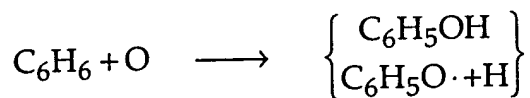
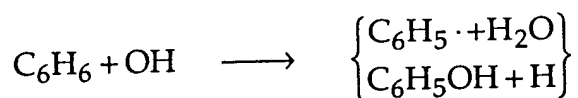


Figure 1.2: Select aromatic and aliphatic species relevant to the high-temperature oxidation of anisole and phenol.

Initiation Processes  $\longrightarrow$  Radical Pool (H, OH, O, HO<sub>2</sub>)



Ring is opened

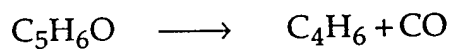


Figure 1.3: Benzene oxidation mechanism [Brezinsky, 1986].

## CHAPTER 2. EXPERIMENTAL TECHNIQUE

---

The Princeton Atmospheric Pressure Flow Reactor in its present configuration is the product of almost four decades of evolution. Since its conception in the late 1950s [Crocco et al., 1957, 1959], the APFR has been used to study the high-temperature oxidation chemistry of species ranging in chemical complexity from CO and H<sub>2</sub> to 1-methylnaphthalene (C<sub>11</sub>H<sub>10</sub>). Nevertheless, throughout the course of its adaptation to new applications, the flow reactor's essential concept has remained unchanged: to isolate the combustion chemistry from the fundamental transport and fluid mechanical processes intrinsic to the propagation of flames. The flow reactor's task is then to produce, as nearly as possible, a reacting flow which is radially uniform in temperature and composition, is subject to negligible axial diffusion of heat or species, and whose convection is sufficient to achieve adequate spatial resolution of the reaction chemistry.

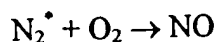
This chapter will provide a description of the flow reactor, its basic operation, and the associated analytical system and techniques. When it is appropriate, the added complexities and difficulties inherent in the present study and any changes to the flow reactor effected during the author's tenure will be noted.

## 2.1 THE PRINCETON ATMOSPHERIC PRESSURE FLOW REACTOR

### Reactor and Reactor Operation

A schematic of the flow reactor is shown in Figure 2.1 along with a list of typical operating conditions. The reactor is an adiabatic, continuous flow device consisting of an Inconel inlet section ( $\approx 10$  cm I.D.  $\times$  100 cm length) joined to a quartz test section ( $\approx 10$  cm I.D.  $\times$  130 cm length). Temperature-controlled electric resistance "clamshell" heaters surround each section. Fire brick and Kaowool (ceramic fiber blanket) insulate the test and inlet sections, respectively. The heaters and insulation maintain the walls of the two sections at a chosen reaction temperature. The nitrogen carrier gas is heated to reaction temperature by passing a small fraction (arc  $N_2$ ) through a plasma torch and mixing this flow with the remaining nitrogen (plenum  $N_2$ ). The total carrier mass flow rate is determined, for a given temperature, by the residence time requirement. The plenum to arc  $N_2$  ratio and the torch power are adjusted to achieve a desired reaction temperature. During an experiment, these settings are held fixed and the temperature of the gas entering the test section is maintained by regulating a small flow ( $< 0.5$  g/s) of nitrogen diluent. In all, the carrier constitutes approximately 98–99% of the total molar flow. The reacting mixture is then sufficiently dilute as to absorb any heat released in the reaction process while maintaining isothermicity.

The temperature of the plasma arc is of the order  $10^4$  K, and thus some arc  $N_2$  is expected to be ionized. It has been suggested [Yetter, 1985; Emdee, 1991] that recombination results in metastable nitrogen ( $N_2^*$ ) which has the potential to react with  $O_2$  to form NO:



Therefore, a large surface area ceramic honeycomb section is located just downstream of the torch to promote collisional de-excitation of  $\text{N}_2^*$ .

Downstream of the honeycomb, oxygen may be introduced and, prior to fuel injection, is well-mixed with the  $\text{N}_2$  carrier [Litzinger, 1985]. An Inconel injector tube (0.18" I.D.) extends into the reactor along the horizontal centerline of the inlet cross-section. To promote mixing, the pressurized flow of oxygen is injected against the oncoming  $\text{N}_2$  stream through six small (0.80" I.D.) holes along the length of the injector. Prior to February, 1995, oxygen was injected radially through a flange in the inlet section. At that time, the inlet was actually comprised of three distinct sections separated by hollow stainless steel flanges for the injection of oxygen and other gases (e.g.  $\text{NO}_2$ ). Anomalous results obtained in a separate study of cyclopentadiene oxidation [Butler, 1992] (thought to be associated with the erosion of iron oxide from stainless steel surfaces in contact with the hot flow) demanded removal of the flanges. The entire inlet section was then replaced with one of single-piece construction. This redesign allowed for greater ease in removal of the inlet, required occasionally for repairs. Furthermore leakage of room air into the reactor, kept at slightly subatmospheric pressure during operation (about -0.1 in.  $\text{H}_2\text{O}$ ), was diminished.

Vaporized fuel diluted with  $\text{N}_2$  is injected radially at the throat of a converging-diverging nozzle which joins the inlet and test sections. Four small diameter ( $\approx 2$  mm I.D.) quartz tubes are arranged in an opposed flow configuration, i.e. spaced at  $90^\circ$  intervals

around the circumference of the throat. Again, mixing is fast by comparison with convection and is completed prior to arrival at the first sampling point.

The reacting flow is sampled at fifteen locations along the centerline of the test section, each corresponding to a distinct axial distance from fuel injection which can be equated through the flow velocity to a reaction time. Samples are quenched upon extraction by a water-cooled stainless steel probe and preserved in a heated multi-position valve (MPV) storage system for subsequent analysis by gas chromatography. The local reaction temperature is measured at the probe tip by a type B thermocouple (Pt-Pt/13% Rh), silica-coated to block catalysis by bare platinum.

Oxygen, CO, and CO<sub>2</sub> are monitored on-line by a Siemens Ultramat 22/O<sub>2</sub> Gas Analyzer with three independent measurement devices, an electrochemical cell for oxygen and NDIR absorption cells for CO and CO<sub>2</sub>. The on-line measurements of CO and CO<sub>2</sub> serve to guide the placement of the reaction in the test section. For a given temperature and equivalence ratio ( $\phi \equiv ([\text{fuel}]/[\text{O}_2])/([\text{fuel}]/[\text{O}_2])_{\text{stoichiometric}}$ ), selection of the flow rate is governed in part by the requirement to capture within the reactor the fuel decay and production of reaction intermediates without conversion of CO to CO<sub>2</sub> and the accompanying heat release.

#### Fuel Preparation and Delivery

Since rapid mixing of the fuel and oxidizer is imperative, liquid fuels like anisole are vaporized prior to injection. A schematic of the flow reactor's liquid fuel vaporization and injection system is given in Figure 2.2. Liquid fuel is supplied from a pressurized fuel tank and metered by a motorized valve. Flow rate is measured through a rotameter

calibrated for the particular fuel. The liquid fuel is atomized upon injection into the evaporator by a coaxial flow of preheated nitrogen diluent. In the evaporator, liquid fuel is sprayed into a hot quartz vessel. The vessel is filled with quartz wool providing a large surface area for rapid (ideally, "flash") vaporization of the fuel. The evaporator is typically maintained at a temperature 50–100 K above the boiling point of the fuel. The quartz manifold and injector tubes are maintained at the same temperature to prevent condensation of the fuel in these passages.

Prior to January, 1995, the evaporator consisted of a sintered stainless steel tube, through which the nitrogen diluent flowed, encased in a non-porous stainless steel sleeve. The results of Butler, mentioned above, motivated the replacement of the steel evaporator with one constructed of quartz. This change was found to have no effect on the composition of the evaporator effluent.

The flow reactor's fuel injection system, originally designed for liquid and gaseous fuels, required modification for the handling of a solid fuel like phenol. Preparation of a room-temperature solid reactant for introduction into the evaporator demands a melting device as well as accurate metering of the hot liquid flow rate. Prior phenol [Lovell, 1989], trioxane [Hochgreb, 1991] and naphthalene [Shaddix, 1993] studies employed a fluid driven piston system. Two stainless steel cylinders filled with solid fuel were heated to and maintained at a temperature well above the fuel's melting point. A free-floating piston, displaced by a metered flow of driver fluid (e.g. water, isopropanol), was designed to deliver the same accurately controlled flow of liquid fuel to the evaporator. But fuel flow rate variations of  $\pm 5\%$  and more recently  $\pm 20\%$  were observed by Hochgreb and

Shaddix, respectively. Some sort of "seal chatter" associated with at least one of the pistons was suspected. For the present study of phenol a new, greatly improved fuel delivery system was installed. A motor driven syringe pump, able to maintain precisely a given flow rate of liquid, was fitted with heaters allowing the phenol to be melted in its reservoir and held at an appropriate temperature throughout the course of an experiment.

As mentioned earlier, a delay in procurement of the syringe pump (donated by Mobil) postponed commencement of the phenol study. Once the syringe pump was in place it was used even in the anisole experiments (without heating) because it was deemed superior to the standard liquid fuel delivery system.

#### Gas Sample Collection

A schematic of the gas sample collection system is given in Figure 2.3. Gas samples are extracted from the reacting flow along the centerline of the test section through a water-cooled, stainless steel probe. Water-cooling provides rapid quenching of the reacting sample, an issue which will be addressed further in a discussion of reaction time uncertainty. Samples are drawn through the probe and heated transfer line and pressurized to about 10 psig by a bellows pump. Two sets of pressurized samples are stored in MPVs for subsequent analysis. Downstream of the MPVs, the sample flow is passed through an iso-propanol cold trap (a slush made by mixing  $i\text{-C}_3\text{H}_7\text{OH}$  with liquid  $\text{N}_2$ ) to condense any heavy hydrocarbons before proceeding to the on-line gas analyzers. Two sets of identical samples are collected in a single experiment in case one set is lost due to some failure (e.g. GC power outage) during post-run analysis.



The MPV consists of 16 stainless steel coils ( $\approx 10$  cc volume) accessed by a 16-position, pressure-actuated Valco valve. During operation, one loop is always open to the MPV lead lines and therefore only 15 samples can be collected and stored. The valve and coil system is temperature-controlled and encased in a cylindrical, stainless steel housing. Temperature control of the sample during collection, storage, and analysis is critical to prevent condensation of low vapor pressure aromatic species in transfer lines or in the MPVs themselves. It is required then that the samples be maintained at a temperature at which the saturation vapor pressure of each constituent species exceeds its partial pressure. This requirement was met by maintaining the sample at 100–150 C in the MPVs and heated transfer lines associated with the reactor and the analysis system.

Some condensation of high molecular weight species in the sampling probe did occur. After both anisole and phenol experiments, a thin layer of brown condensate remained on both the inside and outside surfaces of the probe. Acetone washes of this material were analyzed by GC-FTIR revealing, for the anisole experiments, the presence of phenol dimers (2,2'-biphenol and 4-phenoxyphenol). However, the concentrations of these species present in the gas phase could not be quantified precisely.

For each of the fifteen samples collected in a given experiment, a carbon total was computed from GC measurements, i.e.

$$C_{\text{total}} = \sum_{i=1}^I X_i n_i$$

where  $X_i$ =mole fraction of species  $i$ ,  $n_i$ =number of carbon atoms in species  $i$ , and

$I$ =number of observed species.  $C_{\text{total}}$  was compared with the known initial carbon loading,

$X_{\text{fuel}} n_{\text{fuel}}$  at  $t=0$ , to determine whether losses of gas-phase species due to condensation

were significant. Typical species and total carbon profiles are shown in Figure 2.4. Here it is shown that the total carbon measured in each sample was found to balance, within experimental uncertainty ( $\pm 10\%$ ), the initial carbon loading. However, this uncertainty (addressed below) may mask condensation losses of trace high molecular weight species. For example, a loss of 65 ppm of a  $C_{12}$  species (e.g. phenol/phenoxy dimers) is required to effect a 10% deficiency in the carbon total.

#### Gas Sample Analysis

Captured gas samples are analyzed on a Hewlett-Packard model 5890 Gas Chromatograph fitted with two capillary columns, each with its own flame-ionization detector (FID), and an SGE column switching unit. The gas sample is injected onto a DB-5 column (J&W Scientific, 30 m, 0.32 mm I.D., 0.25 mm film).  $C_4$  and smaller species are eluted quickly from the DB-5 onto a PoraPLOT Q column (Chrompack, 25 m, 0.32 mm I.D., 10 mm film) where they are separated. A nickel catalyst methanizer upstream of the PoraPLOT Q detector permits FID detection of CO and CO<sub>2</sub>. Prior to elution of any larger species from the DB-5, the column switcher is activated. Species subsequently eluted from the DB-5 are routed to the DB-5 detector, bypassing the PLOT column. This configuration makes possible the separation and quantification, from a single sample, of carbon containing reaction intermediates over a wide range ( $C_1$ - $C_{10}$ ) of molecular weights. GC peaks were assigned to species by several techniques including GC-MS, GC-FTIR, and retention time matching. All reported species were identified previously by MS [Emdee, 1991; Venkat et al., 1982], and the aromatics were confirmed in the course of the present study by FTIR. In addition, all peak assignments were

confirmed by retention time matching to known standards. FID signals were converted to species mole fractions via calibration of the detectors to pure standards for each of the identified species or, in the case of trace species, by carbon number correlations [O'Brien, 1985].

The largest uncertainty in the reported yields of reaction intermediates is expected to be that associated with GC calibration. Calibration factors for C<sub>4</sub> and smaller hydrocarbons, CO, CO<sub>2</sub>, and benzene were determined by analysis of a custom calibration gas containing these species in known concentrations. Prior to the analysis of each set of fifteen samples taken from the flow reactor, this gas mixture was re-analyzed to confirm the calibrations of its constituents. The uncertainty in measurements of these species is estimated to be  $\pm 5\%$ . Calibration factors for the cyclopentadienes and aromatics other than benzene were determined via comparison of their FID responses to that of an internal standard (i.e. benzene, whose FID response was well-characterized). For a given species, a solution was prepared of solvent ethanol and small, measured masses of the species in question and benzene. The unknown calibration factor could be correlated to benzene's by the known component masses in solution, molecular weights, and relative FID responses measured from a liquid injection. Measurements of species whose calibrations were determined in this way are estimated to be accurate to within  $\pm 10\%$ .

GC analysis of anisole reaction intermediates was complicated by the presence of copious amounts of phenolic species. At the longer reactor residence times, 60–70% of the initial fuel had been converted to phenol and cresols. Strongly polar phenolic compounds readily bond to active sites on quartz surfaces. The GC's quartz injector port

liner was found to retain these species, shedding them during subsequent sample injections. Measurements of phenol and cresols in the samples analyzed early in the sequence (the *longer* residence time samples) were unusually low; measurements of these species in the samples analyzed later (the *shorter* residence time samples) were unusually high. For a set of fifteen samples analyzed consecutively, the result was a gradual growth in the total carbon count with a 50% carbon deficiency in the first sample and a 50% excess of carbon in the fifteenth. This situation was remedied by deactivating the port liner prior to each experiment by rinsing it in Sylon CT (Supelco, 5% dimethyldisiloxane in toluene). With the implementation of this procedure, GC measurements of phenolic species were found to evolve with increasing residence time in the expected way. Consequently, a carbon balance of unity was readily achieved for the anisole experiments (within the uncertainties discussed, the total carbon contained in measured species was equal to the carbon supplied in the initial fuel).

Inexplicably, similar success was not achieved in analyzing the phenol contained in gas samples taken from experiments in which phenol itself was the fuel. For the first phenol experiments, the initial fuel fraction was set at 1000 ppm. For the anisole experiments and in general, this fuel loading has been found to be desirable, i.e. yields of fuel and reaction intermediates fall within the detection limits of the GC and species measurements are repeatable. But for these phenol experiments, the problem described above was encountered despite deactivation of the injector port liner prior to the start of an analysis sequence. The fuel loading was reduced to 500 ppm for subsequent experiments. Still, reliable phenol decay profiles were not consistently obtained. This

result was unexpected since the maximum phenol fraction possibly present in any of these samples (500 ppm) was less than the fraction of total phenolics present in some successfully analyzed samples in the anisole study (as much as 700 ppm). Therefore, the phenol decay profiles were reconstructed from the remaining species data. That is, the carbon contained in all other observed species was summed, subtracted from the initial carbon loading, and divided by the number of carbons per molecule of phenol. The greatest source of error in this procedure is due to the uncertainty in the GC measurements of reaction intermediates; the uncertainty in the initial fuel loading is negligible by comparison. Fortunately, only 15–20 reaction intermediates were detected in the phenol experiments, and all were positively identified and possessed reliable calibration factors. Nevertheless, caution is exercised in interpretation of the phenol profiles.

Despite the analytical difficulties described above, species measurements were repeatable. That is, for duplicate experiments the mole fraction vs. time profiles for a given reaction intermediate were virtually identical (Figures 2.5 and 2.6).

## 2.2 CALCULATION OF REACTION TIME

The reaction time was defined as the flow time along the reactor centerline from the throat to the probe tip. A number of individual sources of uncertainty contribute to the overall uncertainty in both the absolute reaction time at each sampling point as well as the uncertainty in the relative time between points. Some obvious contributions are those resulting from uncertainties in the probe position and the mass flow rates of  $N_2$  and  $O_2$ . The probe position is given by a position encoder on the probe drive motor. Norton

[1990] found the uncertainty in the relative distance between sampling locations to be  $\approx 0.6$  cm, roughly 10% of the total 6–7 cm. The absolute uncertainty in the probe position was estimated to be 3 cm or 2–3% of the total sampling distance, nominally 120 cm. The carrier mass flow rate is determined almost entirely by the calibrations of the plenum and arc N<sub>2</sub> rotameters (auxiliary nitrogen flows, i.e. manifold and inlet diluents, amount to about 3% of the total N<sub>2</sub> mass flow). Emdee [1991] recently calibrated the arc and plenum N<sub>2</sub> rotameters. Prior to this latest calibration, these rotameters had not been calibrated since 1972 due to the prohibitively large flow rates. The calibration of the plenum rotameter (which supplies the bulk of the flow) was within 10% of the previous calibration over the range of typical operating conditions (30–100 % full scale). The arc N<sub>2</sub> rotameter calibration was within 5% of the 1972 calibration. The pressure gauges associated with each rotameter were also checked and found to be accurate to within 2 psig. Since the experiments reported in this thesis were performed within 5 years of the most recent plenum and arc calibrations, the uncertainty in the flow rates is expected to be small ( $\sim \pm 2-3\%$ ). The O<sub>2</sub> rotameter was recalibrated for the present study.

Other contributions to the uncertainty in the reaction time exist and are associated with inexact knowledge of the flow field within the reactor, uncertainty in the gas density (derived from the temperature measurement), and uncertainty in the chemical quench time. These will be discussed in the following sections and summed to evaluate the overall uncertainty in the reaction time.

## Flow Field

An extensive review of the effects of non-plug flow and flow separation and recirculation in the APFR has been given by Shaddix [1993]. The following will be limited to a brief synopsis of the experimental findings regarding the flow field within the reactor's test section.

At one time, the APFR velocity field was assumed to be characterized by fully-developed turbulent pipe flow. Some early pitot static probe measurements [Dryer, 1972] were re-analyzed by Litzinger [1985] who determined that the flow in the APFR is more appropriately considered a developing turbulent pipe flow. Later, hot-wire anemometry measurements [Chang, 1989; Hochgreb, 1991] showed that the actual velocities in the first third of the reactor deviate substantially from those predicted under the plug flow assumption. The average centerline velocity (normalized by the local plug flow velocity) was determined as a function of distance from fuel injection over a range of Reynolds numbers. These measurements showed that the assumption of plug flow is reasonable for distances  $\geq 40$  cm from the throat. The results were very weakly dependent on Reynolds number and a Reynolds-independent expression was accepted for the velocity as a function of axial distance from injection. Reaction times in the region of non-plug flow are thus calculated by an "effective" area formulation as suggested by Norton [1990]:

$$t = \int_0^x \frac{dx}{U} = \int_0^x \frac{U_{\text{plug}}}{U} \frac{dx}{U_{\text{plug}}} = \int_0^x \frac{A_{\text{eff}}}{A} \frac{dx}{U_{\text{plug}}} = \int_0^x A_{\text{eff}} \frac{dx}{\dot{m} / \rho}$$

where

$x$  axial distance from reactor throat

$U$  centerline velocity

$U_{\text{plug}}$	local plug flow velocity
$A$	local duct cross-sectional area
$A_{\text{eff}}$	effective area, $\frac{A_{\text{eff}}}{A} \equiv \frac{U_{\text{plug}}}{U}$
$\dot{m}$	mass flow rate
$\rho$	local fluid density

$A_{\text{eff}}(x)$  was determined by a polynomial fit to the  $\frac{U}{U_{\text{plug}}}(x)$  data. The uncertainty in the velocity measurements was estimated by Hochgreb to be 10–13% although it has been suggested [Shaddix, 1993], due to improvements in calibration of the hot-wire technique, that this value is actually substantially lower.

Reaction times for sampling points within the plug flow region were calculated from the time corresponding to the previous point, the distance between the two, and the average of the two velocities:

$$t_{n+1} = t_n + 2(x_{n+1} - x_n) / (v_{n+1} + v_n).$$

Flow visualization [Chang, 1989] has revealed that boundary layer separation occurs in the diffuser resulting in the creation of a recirculation zone. The presence of a recirculation zone has implications regarding the near one-dimensionality of the flow. As discussed by Shaddix, experimental and computational evidence suggest that the near one-dimensionality of the system is not significantly affected. The primary consequence of recirculation in the flow reactor is to shorten the chemical induction time (i.e. by the transport of radicals upstream, against the direction of the bulk flow). As a result,



measured species profiles must often be shifted in time in order to match model predictions based on zero-dimensional chemistry.

### Temperature Measurement

The local density of the reacting mixture is determined from pressure (always 1 atm) and temperature by the ideal gas law. Therefore the uncertainty in the reaction time (which has an explicit dependence upon density as shown above) will include a contribution associated with the uncertainty in the measurement of local reaction temperature. The overall uncertainty in the determination of temperature is the sum of 1) the uncertainty in the knowledge of the thermocouple *bead* temperature, and 2) the uncertainty associated with deviation of the bead temperature from the actual *gas* temperature. Held [1993] gives an exhaustive review of these which include uncertainties associated with the manufacturer's calibration, electronics, the effect of the thermocouple coating process on the wire calibration, and the effect of radiative heat loss from the thermocouple to the nearby water-cooled sampling probe. The uncertainty from these sources is estimated to be roughly  $\pm 2-3$  K.

Some concern regarding the effect of mismatched thermocouple and lead wires was raised by Roesler [1992]. The probe tip thermocouple is constructed of 0.002" platinum-platinum/13% rhodium wire held perpendicular to the flow by 0.010" support wires. Roesler pointed out that, because the two sets of wire stock do not come from the same material bar, the welds between the 0.002" and 0.010" wires may generate small voltages. The resultant uncertainty was estimated to be within  $\pm 0.5\%$  ( $\pm 5$  K at 1000 K).

Therefore the sum uncertainty in the temperature measurement is estimated to be no more than  $\pm 7-8$  K.

While the effect of temperature uncertainty on reaction time uncertainty is small, the accuracy of the temperature measurement has important implications for the interpretation of experimental data. Meaningful comparison of kinetic model predictions with experiment relies upon accurate knowledge of the experimental conditions, i.e. initial temperature and pressure, mass flow rates of carrier gas and reactants. The effect of input temperature on model predictions can be particularly profound as reaction rate constants have an exponential dependence on temperature. However, predictions of the anisole pyrolysis model to be presented in Chapter 4 were found not to be particularly sensitive to a small ( $\pm 5$  K) variation in initial temperature (Figures 2.7 and 2.8).

#### Sample Quench

The reaction time calculation is based upon a reaction length defined as the centerline distance from the reactor throat to the probe tip. The gas sample continues to evolve chemically, however, for some short distance down the length of the probe before it is thermally quenched. Thus, there is an uncertainty in the reaction time due to the time required for a sample to be cooled to a temperature sufficiently low such that no further reaction takes place, i.e. the reaction rates are effectively zero. Litzinger [1985] has suggested a time of  $\sim 0.5$  ms to quench the sample to 400 K. More recently, Emdee [1991], on the basis of a detailed heat transfer model, calculated a quench time of 0.5 ms to 600 K and a time of 2 ms to reach 400 K. The calculations indicated that the quench

time is not particularly sensitive to the initial gas temperature over the range of typical flow reactor operating conditions.

Another important aspect of the quenching process is the loss of radicals in the sampling probe. The loss of radicals by gas-phase recombination may perturb the observed species yields from those actually present in the gas phase. For example, the modeling results of Emdee et al. [1992] suggested that almost all of the bibenzyl observed in their toluene oxidation experiments was formed by recombination of benzyl radicals in the probe. Little bibenzyl was predicted by the model. However the sum of the predicted bibenzyl and one half the predicted benzyl was comparable to the measured bibenzyl yield, i.e.

$$[\phi\text{CH}_2\text{CH}_2\phi]_{\text{model}} + 0.5 \times [\phi\text{CH}_2\cdot]_{\text{model}} \approx [\phi\text{CH}_2\text{CH}_2\phi]_{\text{experiment}}.$$

Radical loss may also occur heterogeneously. In this case, the parent species is produced from the gas-phase radical via some heterogeneous reaction at the probe wall (e.g. the abstraction of H from condensed material). Emdee's benzene modeling results indicated that a significant fraction (~50%) of the experimentally observed cyclopentadiene was derived from  $\text{C}_5\text{H}_5$  in the sampling probe.

#### Reaction Time Uncertainty

Summing the contributions to the reaction time uncertainty due to probe positioning ( $\pm 2-3\%$ ), mass flow rate calibration ( $\pm 2-3\%$ ), velocity measurement ( $\pm 10-13\%$ ), temperature measurement ( $\pm 1\%$ ), and sample quenching ( $\pm 2\%$ ) yields a total fractional uncertainty in the absolute reaction time of  $\pm 16-22\%$ .

### 2.3 EFFECTS OF DIFFUSION ON KINETICS

As stated earlier one of the essential requirements imposed upon this experiment in order to isolate and examine reaction kinetics is to minimize the diffusion of heat and species. The ability to meet this demand is in fact the fundamental advantage of this type of reactor, a *flow* reactor, over flames and static reactors where diffusional transport complicates interpretation of the chemistry. The length scales (length and diameter of test section) and operating conditions (carrier gas velocity and dilution of reacting mixture) of the APFR were chosen to minimize gradients of temperature and species and thus diffusion of heat and mass. The need to neglect diffusion in the interpretation of species data arises from the desire to model the experiment as a zero-dimensional, chemically evolving mixture. However, the reactor is at least one-dimensional since the flow is evolving chemically in the axial direction. Furthermore, the potential for heterogeneous reaction at the reactor wall warrants consideration of the significance of radial diffusion. So long as some, albeit small, gradients of temperature and species do exist, a practical estimation of the effects of diffusion is necessary. At least two attempts to estimate the actual influence of diffusion on kinetics in the flow reactor have been made and the interested reader is directed to the theses of Hochgreb [1991] and Emdee [1991] for the details of these analyses. The following will be limited to a review of the key points.

#### Longitudinal Diffusion

The conditions under which longitudinal diffusion can be neglected in the flow reactor can be determined by a comparison of the characteristic times of diffusion and convection. That is, the time required for a chemically reacting "particle" of fluid to be

convected over some length scale of interest must be small compared to the time required for reacting species to diffuse over that length, or  $\tau_c/\tau_D \ll 1$ . The characteristic time for longitudinal diffusion is given by

$$\tau_D \sim \frac{L^2}{D_t}$$

where  $L$  is a characteristic length and  $D_t$  is the turbulent diffusivity.  $D_t$  is estimated by

$$D_t \sim u' L_t$$

where  $u'$  is the root mean square of the turbulent velocity fluctuations and  $L_t$  is the integral length scale of turbulence. From hot-wire measurements, Hochgreb [1991] quoted an average value of  $u'/U=0.3$ . The integral length scale is a fraction of the diameter  $d$  of the test section. Thus,  $L_t = fd$  where  $f < 1$ . Now,

$$\tau_D \sim \frac{L^2}{0.3Ufd}$$

The characteristic time of convection is

$$\tau_c \sim \frac{L}{U}$$

The requirement  $\tau_c/\tau_D \ll 1$  now becomes

$$\frac{0.3fd}{L} \ll 1.$$

The length scale of interest  $L$  is the length over which species concentration changes significantly. For such a change which takes place over the entire length of the reactor test section ( $L \approx 100$  cm,  $d \approx 10$  cm),

$$\tau_c/\tau_D \sim 0.03f.$$

Therefore, provided the selection of  $L$  equal to the total length of the test section is valid, longitudinal diffusion may be neglected. It follows then that diffusion in the longitudinal direction cannot be neglected when  $L$  is short, i.e. when significant changes in species concentration occur over distances which are short with respect to the length of the reactor. The rapid conversion of  $\text{CO}$  to  $\text{CO}_2$  is one such example.

An argument for negligible diffusion of heat may also be made from the comparison of characteristic times given above. In this case, the length scale of interest is the length over which a significant change in temperature occurs. For the experiments reported here, the axial temperature profile was essentially isothermal. A typical temperature profile is shown in Figure 2.4. The temperature change from fuel injection to the latest sampling point was always less than 5 K and was more or less linear. So, for temperatures typical of this study (1000 K and higher), the length scale over which temperature changes significantly is  $\gg$  the length of the reactor.

### Radial Diffusion

Heterogeneous chemistry at the reactor wall (so-called "wall effects") has the potential to influence the gas-phase kinetics in the flow reactor. The test section is constructed of quartz, a fairly inert material, in order to minimize the prospect of surface chemistry. However even quartz surfaces have been found to be catalytic, facilitating the recombination of radicals [Pallix and Copeland, 1996]. The distribution of reaction intermediates will be perturbed only if species in the boundary layer have sufficient time to diffuse to the reactor centerline where samples are collected. Again, the requirement for negligible diffusion is  $\tau_c/\tau_D \ll 1$ . Here the diffusion time is given by

$$\tau_D \sim \frac{(d/2)^2}{D_t},$$

and the condition for negligible diffusion in the radial direction is

$$\frac{1.2fL}{d} \ll 1.$$

As given previously, the product  $fd$  defines the integral (i.e. largest) length scale of turbulence. The characteristic dimension of the largest eddies is, in general, of the same order as the characteristic dimension of the whole volume of fluid (i.e. the reactor diameter). Thus,  $f$  is taken to be between 0.1 and 1. For the longest sampling times,  $L/d \approx 10$  and

$$1.2 < \tau_C/\tau_D < 12.$$

From this analysis it is found that the condition for negligible radial diffusion is not met, in particular for the longer sampling times (large  $L/d$ ). Late in the reaction  $\tau_C$  and  $\tau_D$  are, at best, of the same order.

The above arguments suggest that wall effects may interfere with the investigation of homogeneous gas-phase kinetics in the flow reactor. However, experimental evidence does not support this conclusion [Dryer, 1972]. As will be discussed in Chapter 4, the possibility of surface-mediated chemistry was investigated in the present study. A series of experiments was performed with the reactor test section replaced by another of one half the original diameter, increasing the surface to volume ratio by a factor of 2 and thus reducing the characteristic time of diffusion to the reactor wall by a factor of 4. It was postulated that condensed high molecular weight material on the test section surface might provide labile hydrogen for abstraction by gas-phase radicals. No change in the product

distribution was observed in the initial trials. In an attempt to coat the quartz surface with a large amount of condensed material, anisole was then pyrolyzed in the reactor at an initial concentration several times that normally used. The experiments were repeated and still no change in the chemistry was revealed. Diffusion of species to and from the reactor wall is therefore concluded to have a negligible impact on the gas-phase kinetics and measured species data are presumed to be representative of strictly homogeneous chemistry.

## 2.4 EFFECTS OF MIXING AND TURBULENCE ON KINETICS

### Mixing

In order to properly characterize the fuel/oxidizer ratio of the reacting flow, turbulent mixing of fuel with the  $O_2/N_2$  stream in the diffuser must be fast by comparison with the total reaction time. The finite time associated with mixing can also be thought of as a mixing length, i.e. an axial distance from fuel injection after which a radially uniform mixture of fuel,  $O_2$ , and  $N_2$  exists. Litzinger [1985] determined experimentally a mixing length of roughly 6 cm at a Reynolds number of 8000. Oxygen was introduced into the nitrogen carrier gas at the reactor throat (where the fuel is normally introduced) and its concentration was measured along the centerline of the diffuser. For the fixed  $Re=8000$ , the mixing length was found to be independent of the oxygen flow rate. Similarly, Dryer [1972] measured a mixing length of approximately 20 cm for  $Re=6000$ . Reynolds numbers typical of the present study were 8000 and 5000 for the anisole and phenol experiments, respectively, and the measurements quoted above are considered to be



reasonable estimates of the corresponding mixing lengths. Nevertheless, the earliest sampling point was always more than 25 cm from the throat of the diffuser.

Although sampling is postponed until mixing is complete, an effect of finite mixing times is still seen experimentally. Emdee [1991] observed that substantially more fuel was consumed in the diffuser than could be explained by reasonable reaction rates. And as will be discussed in Chapter 5, the phenol oxidation data presented here also indicate that the chemistry in the diffuser is more rapid than would be expected for a uniform, zero-dimensional, chemically evolving mixture. It has been suggested [Litzinger, 1985] that prior to the completion of mixing, the existence of fuel-lean "pockets" may be responsible for the acceleration of the diffuser chemistry. However, computational results [ibid.] do not support this explanation. It has also been suggested [Emdee, 1991; Held, 1993] that the enhanced turbulent diffusion of radicals in the diffuser may accelerate the consumption of the incoming charge. And as mentioned earlier, the existence of a recirculation zone in the diffuser region is also likely to speed the induction chemistry. The post-induction chemistry, however, is found to be unaffected. Modeling results [ibid.] have shown that perturbations of the radical pool due to finite-rate mixing are quickly damped due to the speed of radical reactions. The prevailing effect of the mixing zone is then merely a shortening of the chemical induction time.

In general, zero-dimensional calculations do not predict well the induction phase of the reaction. Comparison of post-induction model predictions to experimental data thus often requires a shift in time of the calculated species profiles. Often the time at which 50% of the initial fuel has been consumed is selected as the alignment point [Hochgreb,

1991; Emdee et al., 1992; Held, 1993]. However, other criteria have and may be used [Held, 1993].

### Turbulence

The effect of turbulence on reaction kinetics in the flow reactor was addressed by Glassman and Eberstein [1963] and the key points of their analysis are reviewed here. Although flow in the reactor is turbulent, flow within the smallest eddies is no longer turbulent and molecular effects are dominant. It was argued that, during its lifetime in the flow reactor, such an eddy encounters only a 2% change in concentration and a 2 K difference in temperature. It was then concluded that these gradients are sufficiently shallow that diffusion will not result in rapid fluctuations of temperature or concentration within an eddy. Furthermore, the time required for the radical pool to adjust to a temperature change of a few degrees is much less than the characteristic time of turbulent oscillation and therefore steady-state kinetics do prevail in the flow reactor. Aside from steady-state considerations, the variation of reaction rate due to turbulent fluctuations in concentration and temperature was considered. The effect of temperature was determined to dominate in the flow reactor, and a time averaged reaction rate was found to deviate by less than 3% from a reaction rate based upon the time averaged temperature.

### **2.5 HYDROCARBON, OXIDIZER, AND CARRIER PURITIES**

The anisole and phenol used in this study were obtained from Aldrich. Anisole and phenol purities, both quoted as 99%, were confirmed by GC analysis. Both fuels were used without further purification. Oxygen was obtained from Airco, quoted >99.993%

pure. The nitrogen carrier gas, derived from a reserve of liquid  $N_2$  supplied by Liquid Carbonic, was found to contain 25–30 ppm  $O_2$ .

Calibration standards used in GC liquid injections were, with the exception of the cyclopentadienes, quoted 99% pure. Methylcyclopentadiene and cyclopentadiene were derived from their dimers which were specified as 93 and 95% pure, respectively.

## 2.6 SUMMARY

The pyrolysis and oxidation of both anisole and phenol have been performed in the Princeton Atmospheric Pressure Flow Reactor. A description of the physical device and its operation have been given in this chapter. In particular, recent changes to the reactor and the analytical procedure have been duly recorded. The most noteworthy of these was the addition and modification of a syringe pump for solid fuel melting and delivery.

An estimate of the uncertainties associated with the species measurements has been given. Also, contributions to the uncertainty in calculated reaction times have been identified and quantified. Finally, the impacts of molecular and fluid mechanical processes (i.e. diffusion, finite-rate mixing, and turbulence) on the chemistry in the flow reactor have been examined. In summary, these effects have been determined to be small, allowing comparison of flow reactor data with zero-dimensional model calculations.

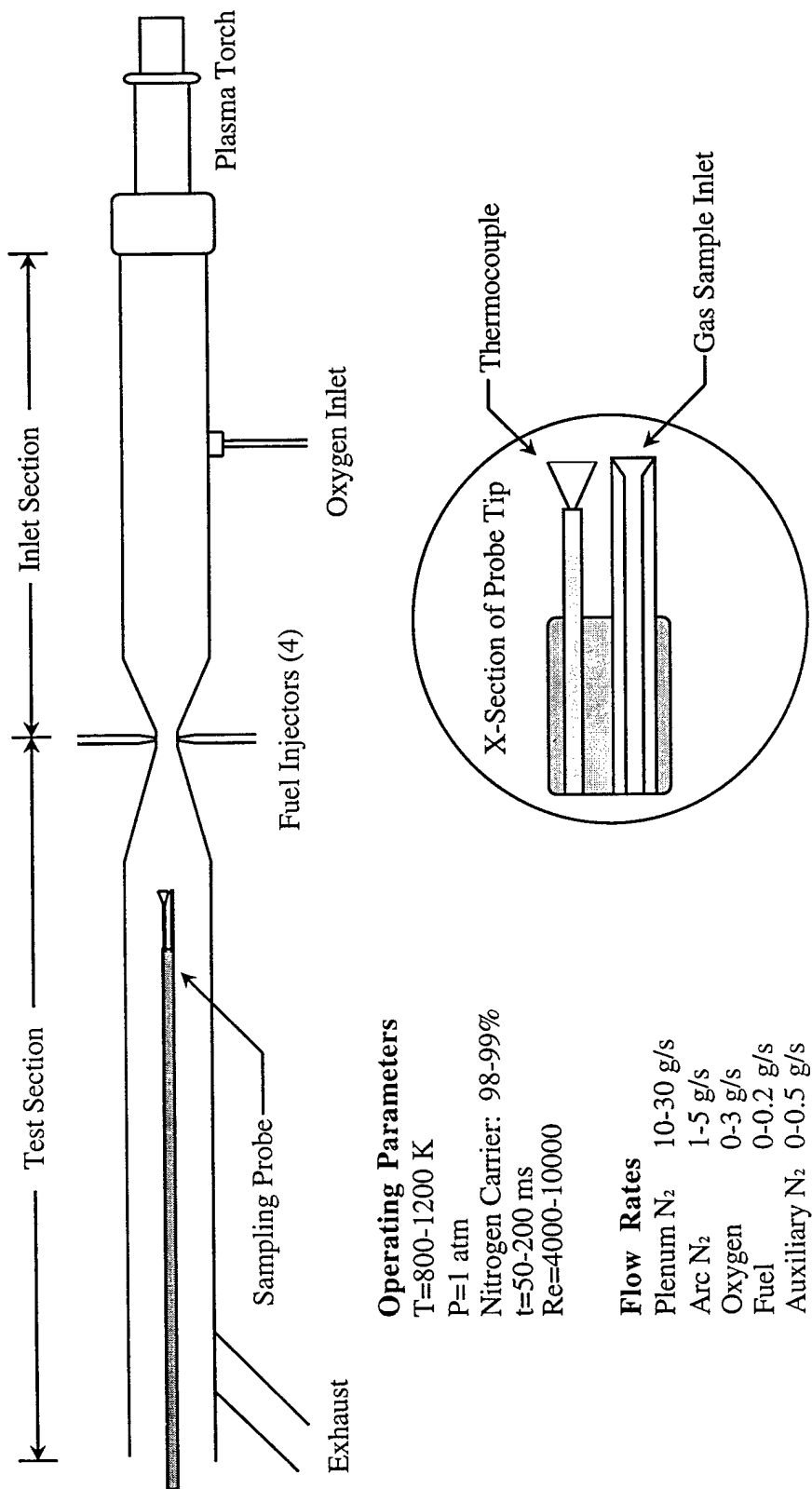


Figure 2.1: Schematic of the Princeton Atmospheric Pressure Flow Reactor. Adapted from Shaddix [1993].

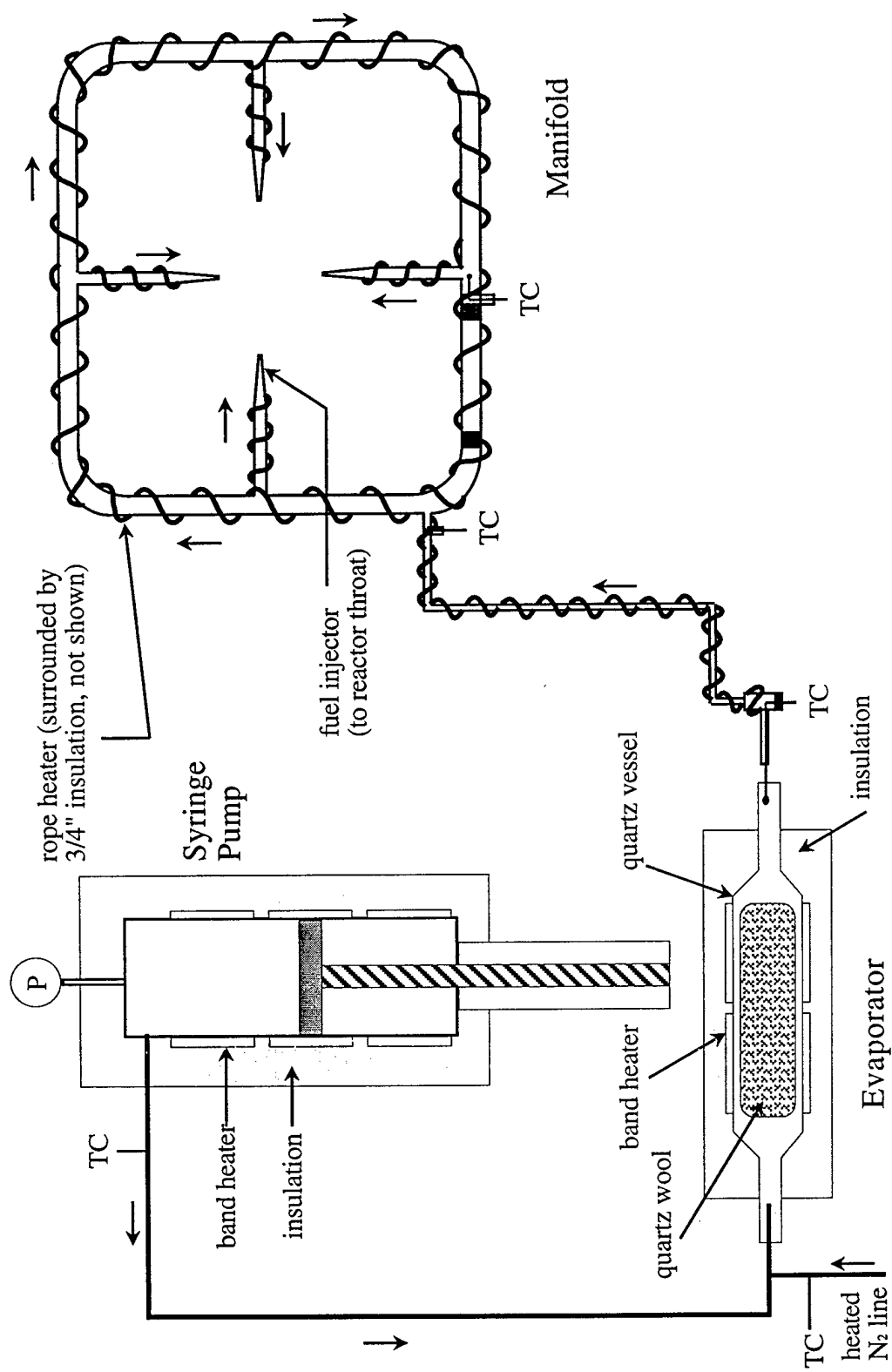


Figure 2.2: Schematic of fuel preparation and delivery system. Adapted from Shaddix [1993].

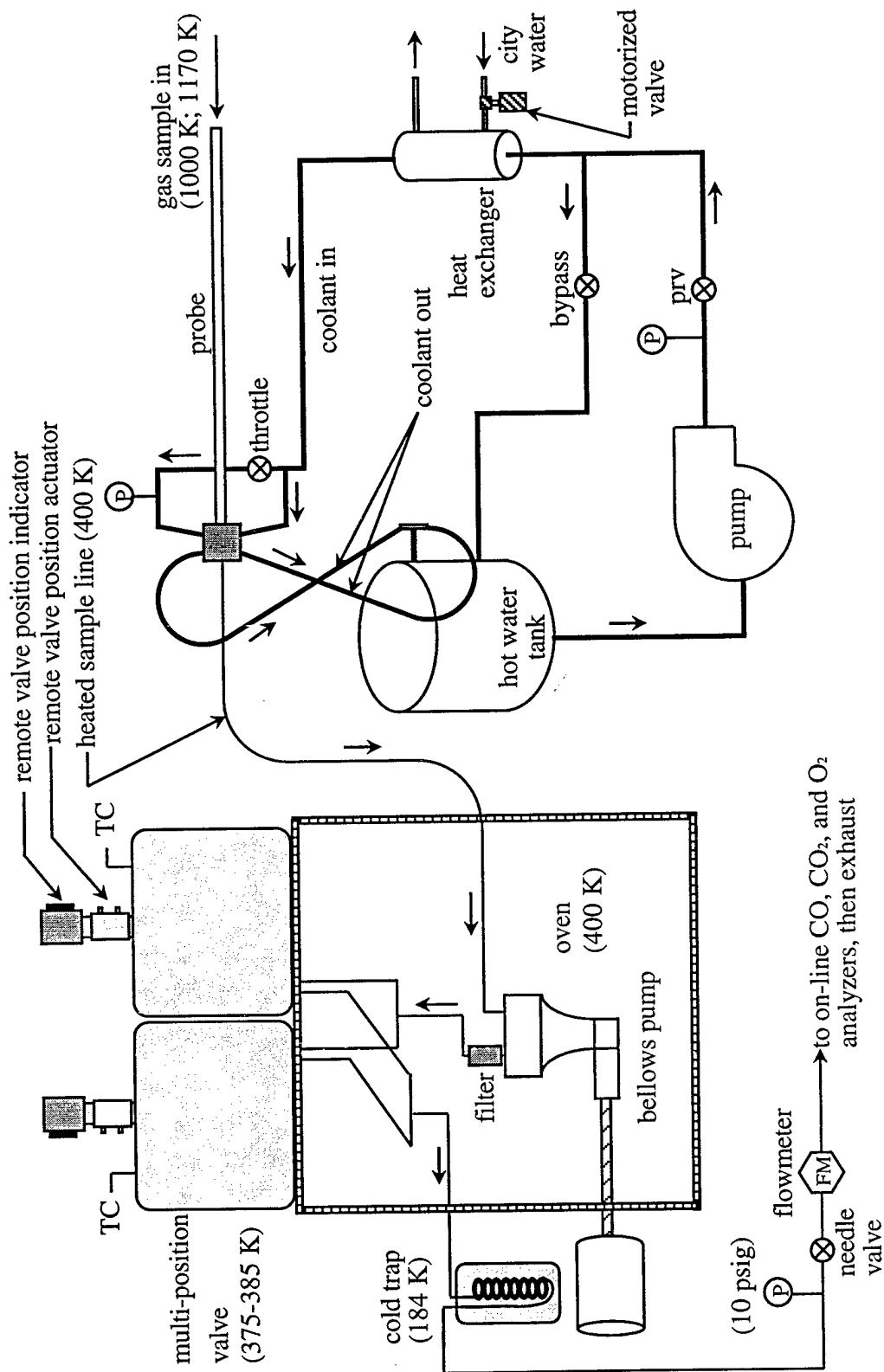


Figure 2.3: Schematic of gas sample collection system. Adapted from Shaddix [1993].

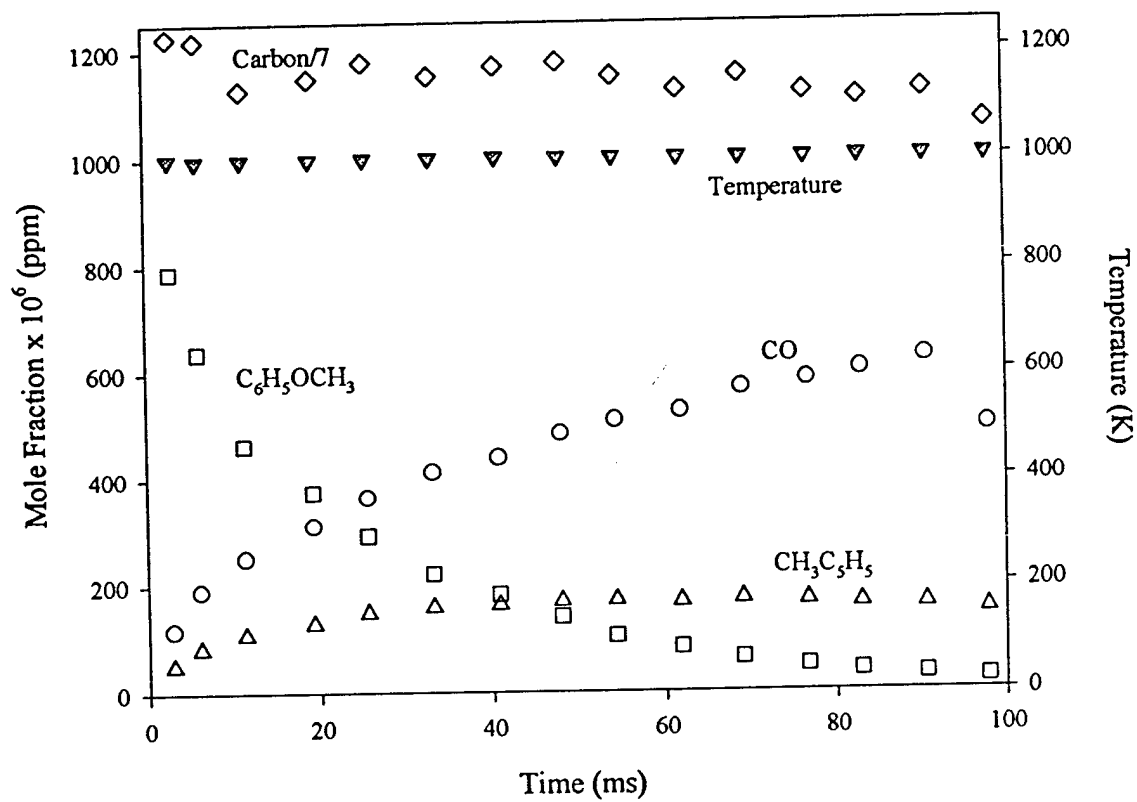


Figure 2.4: Representative species, total carbon, and temperature profiles from the oxidation of anisole near 1000 K.  $Carbon_i = 1079$  ppm.

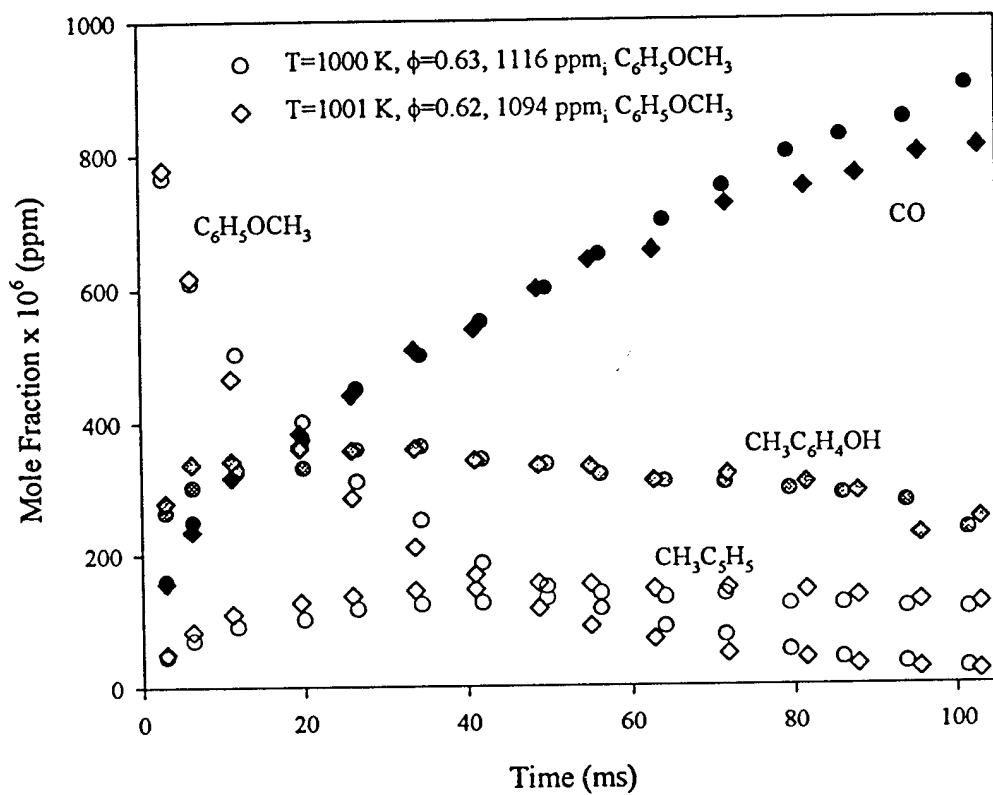


Figure 2.5: Major reaction intermediate profiles from duplicate anisole experiments.



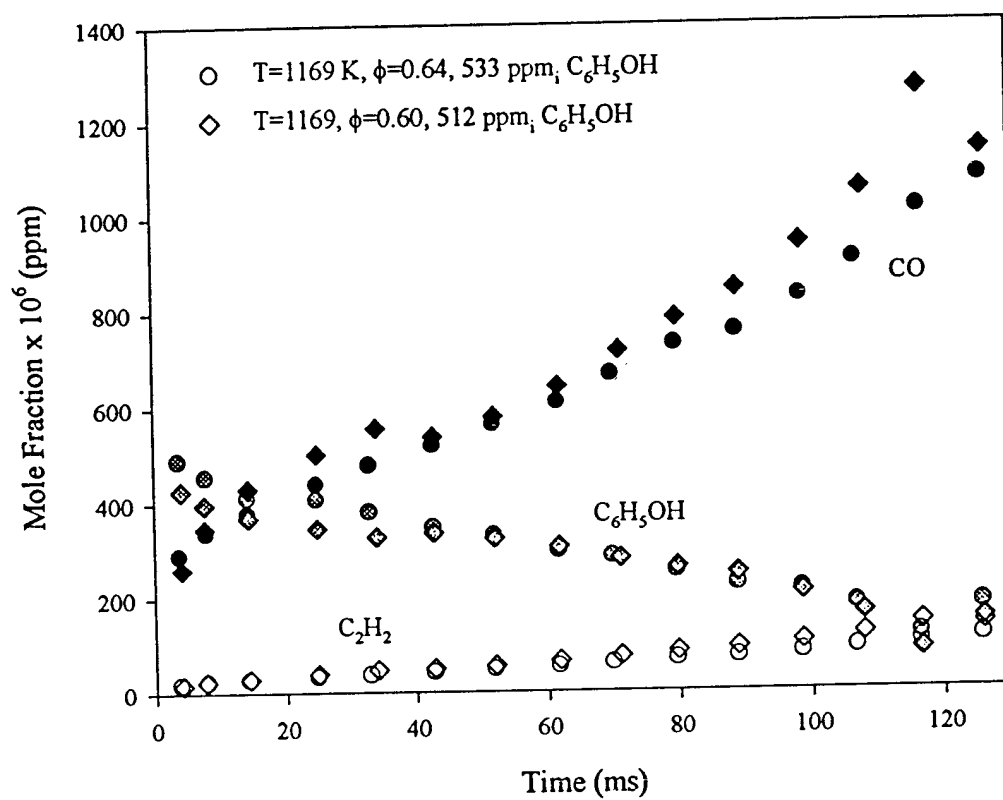


Figure 2.6: Major reaction intermediate profiles from duplicate phenol experiments.

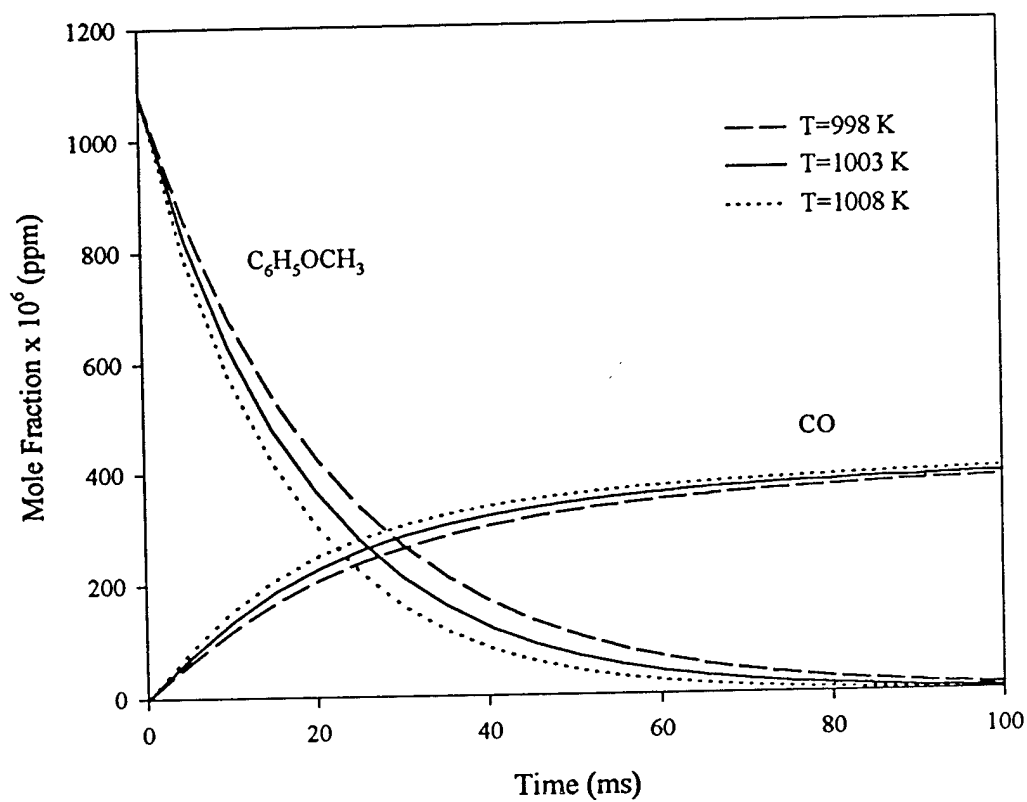


Figure 2.7: Anisole pyrolysis model (Table 4.1) predictions of fuel decay and carbon monoxide for T=998, 1003, and 1008 K. T=1003 K is actual experimental condition.

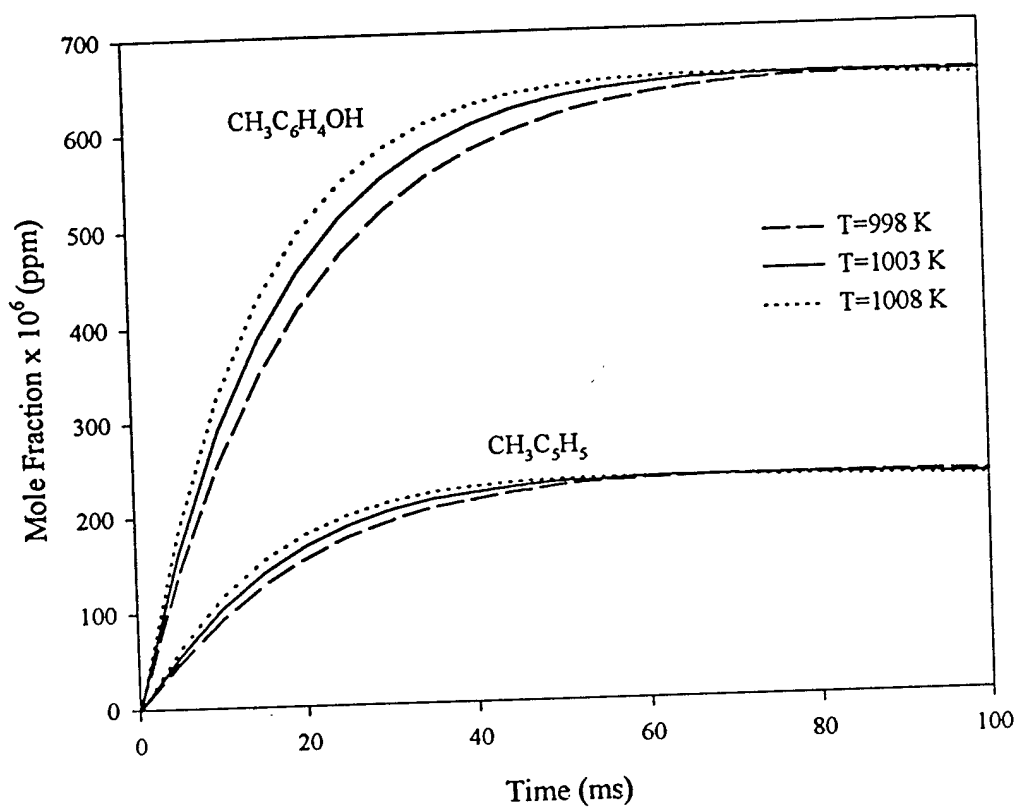


Figure 2.8: Anisole pyrolysis model (Table 4.1) predictions of cresol and methylcyclopentadiene for  $T=998$ ,  $1003$ , and  $1008\text{ K}$ .  $T=1003\text{ K}$  is actual experimental condition.

## CHAPTER 3. ANISOLE PYROLYSIS AND OXIDATION: EXPERIMENTAL RESULTS

---

Anisole is phenyl methyl ether and, as that name implies, contains the R–O–R' linkage where R=C<sub>6</sub>H<sub>5</sub> and R'=CH<sub>3</sub>. In this study anisole was exploited as a chemical source of the phenoxy radical. The weak C<sub>6</sub>H<sub>5</sub>O–CH<sub>3</sub> bond (≈64 kcal/mol) is readily ruptured at temperatures near 1000 K to yield the phenoxy and methyl radicals. As discussed, the phenoxy radical is an important reaction intermediate in the high-temperature oxidation of aromatic hydrocarbons; C<sub>6</sub>H<sub>5</sub>O· → C<sub>5</sub>H<sub>5</sub>· + CO is the dominant route by which the loss of aromaticity occurs in these systems. In this study it was observed that other phenoxy reaction paths are competitive with its unimolecular decomposition. In particular, reactions of phenoxy with methyl were found to dominate.

As explained in Section 1.2, the boundary (at 1 atm) between the low/intermediate- and high-temperature chemical regimes is approximately 1000 K. Thus the anisole experiments reported here may be classified as high-temperature. However, the relevance of these experiments to practical combustion processes where the flame temperature typically exceeds 2000 K is not immediately obvious and must be addressed. Consideration of the flame structure [Bittner and Howard, 1981; Glassman, 1996] reveals that at the flame front, the narrow region of peak temperature, virtually all of the initial

fuel has already been consumed; it is the lower temperature early part of the reaction zone in which the fuel is mainly oxidized to reaction intermediates. The combustion window accessible in the flow reactor ( $T < 1200$  K) falls within the range of temperature typical of this pre-flame zone. The kinetics in this region are critical to the development of a model which ultimately is to predict flame chemistry. Indeed, the composition of flame product gases is determined not only by the temperature at the flame front, i.e. the "flame temperature," but by the time/temperature history of the reactants.

The set of experimental conditions is given in Table 3.1. In each case the initial fuel fraction was nominally the same, 1000 ppm, and the oxygen mole fraction was varied to obtain the desired equivalence ratio. The pyrolysis of anisole was investigated first to provide bench mark data for the oxidation study. As will be discussed in detail in this chapter, even in the presence of oxygen pyrolytic chemistry was found to dominate.

Table 3.1: Experimental conditions for anisole experiments.

Equivalence Ratio, $\phi$	Temperature (K)	Residence Time (ms)	Fuel Loading (ppm)
pyrolysis	1003	98	1077
1.05	1001	98	1079
0.62	1001	103	1094
1.71	999	100	1090

### 3.1 EXPERIMENTAL RESULTS

#### C<sub>6</sub>H<sub>5</sub>OCH<sub>3</sub>

In the absence of oxygen, the destruction of the anisole fuel was found to proceed almost entirely through cleavage of the phenoxy-methyl bond. This result is consistent

with the known anisole bond strengths:  $\text{C}_6\text{H}_5\text{O}-\text{CH}_3$ , 64 kcal/mol;  $\text{C}_6\text{H}_5-\text{OCH}_3$ , 91 kcal/mol;  $\text{C}_6\text{H}_5\text{OCH}_2-\text{H}$ , 93 kcal/mol. In an inert [Lin and Lin, 1986; Mackie et al., 1989] or hydrogen [Arends, 1993] atmosphere, the  $\text{C}_6\text{H}_5\text{O}-\text{CH}_3$  cleavage has already been established as the dominant anisole decomposition pathway. In Figure 3.1 the natural log of fraction remaining anisole is plotted versus time for pyrolysis at 1003 K. A plot of this type will be linear if the decay is first order in anisole. More explicitly, the rate of change of anisole concentration is given by

$$\frac{d[\text{C}_6\text{H}_5\text{OCH}_3]}{dt} = -k_f[\text{C}_6\text{H}_5\text{OCH}_3] + k_r[\text{C}_6\text{H}_5\text{O}][\text{CH}_3]$$

where  $k_f$  and  $k_r$  represent the forward and backward rates of the anisole decomposition reaction and it is assumed that no other reactions either produce or consume anisole. As will be discussed later, the reverse reaction can be disregarded. The integration

$$\int_{[\text{C}_6\text{H}_5\text{OCH}_3]_0}^{[\text{C}_6\text{H}_5\text{OCH}_3]} \frac{d[\text{C}_6\text{H}_5\text{OCH}_3]}{[\text{C}_6\text{H}_5\text{OCH}_3]} = -\int_0^t k_f dt$$

can now be performed to give the linear relationship between the natural log of  $[\text{C}_6\text{H}_5\text{OCH}_3]$  and time

$$\ln\left(\frac{[\text{C}_6\text{H}_5\text{OCH}_3]}{[\text{C}_6\text{H}_5\text{OCH}_3]_0}\right) = -k_f t.$$

First-order profiles derived from reported rate parameters are also shown in Figure 3.1 for comparison with the experimental data. Literature values of  $k_f$ (1003 K) range roughly from 12 to 56  $\text{s}^{-1}$ . The pressure and temperature conditions under which each of these values was measured are listed in Table 3.2.  $k_f$  does not exhibit the appropriate dependence upon pressure required to attribute the discrepancy in its value to an effect of

falloff. Furthermore, no general relationship can be discerned between the measured values of  $k_f$  and their corresponding experimental conditions. Nevertheless the present pyrolysis data fall within the range predicted and, as expected, the observed decay is first order in anisole.

Table 3.2: Pressure and temperature conditions for measurement of rate constant for  $C_6H_5O-CH_3$  bond homolysis.

Pressure (atm)	Temperature (K)	$k_{1003\text{ K}} (s^{-1})$	Reference
0.1–0.5	800	12	Paul and Back, 1975
0.4–0.9	1000–1580	56	Lin and Lin, 1986a
$10^{-6}$	1092	46	Suryan et al., 1989
0.016–0.120	850–1000	33	Mackie et al., 1989
1	793–1020	28	Arends, 1993
1	1003	41	Present work

The present study revealed that, even in the presence of oxygen, the decay of anisole obeys first-order kinetics. In Figure 3.2 the natural log of  $\frac{[C_6H_5OCH_3]}{[C_6H_5OCH_3]_0}$  is demonstrated to be linear with respect to time for oxidation experiments over a range of equivalence ratios. Even for the leanest condition employed ( $\phi=0.6$ ), the fuel decay is still unaffected by oxygen. It is apparent though from the figure that the rate of anisole consumption is not identical among the four experiments, i.e. the slopes of the linear curvefits to each data set differ slightly. This difference is attributable to the variation in experimental temperature (999–1003 K). Figure 3.2 confirms that a higher temperature does indeed correspond to a steeper slope (or a faster rate of decay). The slope variation may, at first glance, seem too pronounced to be attributed to a temperature variation of

only a few degrees. But for a high activation energy process, the dependence of the rate constant on temperature is strong. In the case of anisole decomposition ( $E_a \approx 63$  kcal/mol) near 1000 K, a temperature difference of a few degrees effects roughly a 10% variation in the resulting rate constant.

Figures 3.3 and 3.5–9 illustrate the influence of oxygen on the production and consumption of some important reaction intermediates.

#### $C_6H_5OH$ and $CH_3C_6H_4OH$

Phenol and the related species cresol (or methylphenol) are major products and, as shown in Figure 3.3, their yields are independent of  $\phi$ . Over the 100 ms residence time, these species together constitute roughly 30–60% of the carbon initially contained in the fuel. Both phenol and cresol are direct products of the radical(s) produced in the initial anisole decomposition, a pyrolytic reaction step. The  $\phi$ -independence of the phenol and cresol yields suggests the absence of any subsequent oxidation of these species.

Two isomers of cresol, ortho and para, were observed experimentally. Their formation is best explained by consideration of the phenoxy radical as a hybrid of three resonance structures as shown in Figure 3.4. The unpaired electron is associated primarily with the ring [Mackie et al., 1989] as depicted in structures (ii) and (iii). Addition of methyl to a ring site produces *o*- or *p*-methylcyclohexadienone, the keto tautomers of *o*- and *p*-cresol. Tautomeric equilibrium favors enolization [Hart, 1979], and migration of the allylic hydrogen yields the observed *ortho*- and *para*-cresols. The recombination of methyl with phenoxy at the O atom (the reverse of the initial fuel decomposition) is not



expected to be a significant reaction path; the unpaired electron density in the phenoxy radical is just 9% on oxygen [Arends, 1993].

Following an initial period of rapid growth, i.e.  $0 < t < 15$  ms, cresol yield is found to reach a pseudo-steady-state which persists until  $\approx 70$  ms when a slow decay commences. Phenol undergoes a more gradual growth with its yield ultimately exceeding that of the cresols. A similar observation was made by Mackie and coworkers [1989]. In their investigation, runs at fixed temperature and pressure demonstrated that phenol yield increased with increasing residence time while cresol yield decreased. It is reasonable to assume that phenol is formed via reaction of phenoxy with a hydrogen donor. But in Mackie's study, some percentage of the total observed phenol (from 54% at 860 K to 98% at 984 K) could not be accounted for by abstraction reactions. It was suggested that the cresols were, at least in part, precursors to phenol. The only mechanism which was found to account for the "excess" phenol was a first-order decomposition of cresol to form phenol. An Arrhenius fit to their data yielded the rate constant  $k_{\text{fit}} = 10^{8.8 \pm 0.5} \exp(-35 \pm 2 \text{ kcal} \cdot \text{mol}^{-1} / RT) \text{ s}^{-1}$ . As noted by the authors, these empirically determined Arrhenius parameters are not suggestive of a homogeneous gas-phase reaction; at 900 K their estimated rate constant for the  $\text{CH}_3\text{--C}_6\text{H}_4\text{OH}$  bond homolysis is between 2 and 3 orders of magnitude slower than  $k_{\text{fit}}$ . Furthermore, supporting cresol pyrolysis experiments indicated that decomposition was significant only at temperatures above 1100 K. At 1000 K, the temperature employed in the current study, decomposition of cresol cannot be expected to be a significant source of phenol. For now it is assumed that phenol is derived

from the phenoxy radical although, as will be discussed later, the origin of the necessary H atoms is unclear.

### CH<sub>3</sub>, C<sub>2</sub>H<sub>6</sub>, and C<sub>2</sub>H<sub>4</sub>

Methane and ethane yields are shown in Figure 3.5. These species are derived from methyl radical(s):



Like phenol and cresol, CH<sub>4</sub> and C<sub>2</sub>H<sub>6</sub> are direct products of a radical which is produced pyrolytically and their yields are independent of  $\phi$ . Again, the data suggest an absence of oxidative chemistry.

Ethene yield is also shown in Figure 3.5 and does exhibit a dependence upon  $\phi$ . In the case of pyrolysis, ethene may arise by abstraction of H from ethane by any radical (e.g. C<sub>6</sub>H<sub>5</sub>O<sup>•</sup>, H, CH<sub>3</sub>) and subsequent loss of H from ethyl. In the oxidation experiments the potential exists for attack on ethane by O<sub>2</sub> or associated radicals (i.e. OH, HO<sub>2</sub>, O). But while the ethene yield depends upon equivalence ratio, the ethane yield does not. Thus the data do not suggest that ethene is a product of ethane oxidation. Instead ethene may be derived from the vinyl radical which, as will be discussed, is a product of methylcyclopentadiene oxidation.

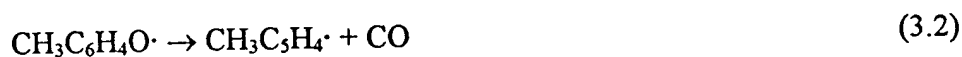
### C<sub>5</sub>H<sub>6</sub> and C<sub>6</sub>H<sub>6</sub>

Cyclopentadiene and benzene yields are independent of equivalence ratio as shown in Figure 3.6. Also shown are minor yields of naphthalene (C<sub>10</sub>H<sub>8</sub>) and dihydronaphthalene (C<sub>10</sub>H<sub>10</sub>). Cyclopentadiene is derived from the cyclopentadienyl

radical which, as explained previously, is a product of phenoxy decomposition. The naphthalenes are formed presumably from two cyclopentadienyl radicals [Klinkenberg and Louw, 1987; Manion and Louw, 1989; Melius et al., 1996] though the precise mechanism is not conclusively established. Benzene is evolved from the methylcyclopentadienyl radical. Methylcyclopentadiene is a significant reaction intermediate in both the pyrolysis and oxidation of anisole and its formation pathways will be addressed shortly. The methylcyclopentadienyl radical may be produced via loss of an allylic H either by homolysis or by abstraction. The radical rearranges to a cyclohexadienyl intermediate which rapidly loses an H atom to yield benzene [Ritter et al., 1990].

### CH<sub>3</sub>C<sub>5</sub>H<sub>5</sub>

Methylcyclopentadiene profiles are shown in Figure 3.7. Several mechanisms for CH<sub>3</sub>C<sub>5</sub>H<sub>5</sub> formation may be considered, the most obvious of which is the recombination of C<sub>5</sub>H<sub>5</sub>· and CH<sub>3</sub> radicals. Alternatively, the cresol radical methylphenoxy may eliminate CO, analogously to phenoxy, to yield methylcyclopentadienyl radical:



CH<sub>3</sub>C<sub>5</sub>H<sub>4</sub>· may then recombine with H. A third reaction pathway is proposed whereby methylcyclopentadiene is formed directly from methyl and phenoxy. This mechanism, to be detailed in Section 4.1, is the dominant mode of methylcyclopentadiene production.

For now, it is represented globally by



Like phenol and cresol, methylcyclopentadiene is formed predominantly from radicals which are produced pyrolytically. But, unlike these other species, the CH<sub>3</sub>C<sub>5</sub>H<sub>5</sub>

yield exhibits a distinct dependence upon  $\phi$ . Thus, the data suggest that methylcyclopentadiene is oxidized preferentially. A comparison of the relative R-H bond strengths (Table 3.3) among the observed reaction intermediates supports this conclusion. The most weakly bonded hydrogen in the system will be most susceptible to attack by  $O_2$  and related radicals.  $C_5H_6$  and  $CH_3C_5H_5$  possess the most readily abstractable hydrogens, i.e. allylic. Still,  $C_5H_6$  yield is independent of  $\phi$ . Presumably, the  $C_5H_6$  concentration is never sufficiently high to drive its reaction with oxygen. However, methylcyclopentadiene is a major product and is readily oxidized; in Figure 3.7,  $CH_3C_5H_5$  yield is shown to decrease with increasing equivalence ratio.

Table 3.3: R-H bond strengths for anisole reaction intermediates.

Bond	Energy (kcal/mol)	Reference
$CH_3C_6H_4O-H$	85	a
$H-CH_2C_6H_4OH$	85	b
$C_6H_5O-H$	85	Lowry and Richardson, 1987
$H-C_5H_5$	74	Emdee et al., 1992
$H-C_5H_4CH_3$	74	c
$H-CH_2C_5H_5$	98, 103	Moskaleva et al., 1996
$H-C_2H_5$	98	Lowry and Richardson, 1987
$H-CH_3$	104	Lowry and Richardson, 1987
$H-CH_2OC_6H_5$	93	d
$H-C_6H_5$	103	Lowry and Richardson, 1987

<sup>a</sup> Estimated from  $C_6H_5O-H$ .

<sup>b</sup> Estimated from  $H-CH_2C_6H_5$  [Lowry and Richardson, 1987].

<sup>c</sup> Estimated from  $H-C_5H_5$ .

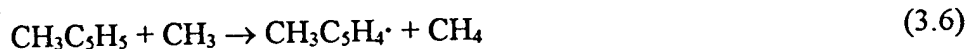
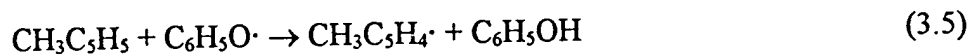
<sup>d</sup> Estimated from  $H-CH_2OH$  [ibid.].

Methylcyclopentadiene conversion is accompanied by the production of CO (Figure 3.8) and some C<sub>2</sub>–C<sub>4</sub> species including acetylene, propene, methylacetylene, allene, and 1,3-butadiene (Figure 3.9). Some CO<sub>2</sub> is observed in the oxidation experiments, but yield is not a function of  $\phi$ . In a typical hydrocarbon oxidation system, the conversion of CO to CO<sub>2</sub> is retarded until almost all of the fuel and intermediate hydrocarbon fragments have been consumed. Once these species have disappeared, the concentration of OH grows substantially and CO is rapidly oxidized via



[Glassman, 1996]. Consumption of anisole reaction intermediates is not completed on the time scale of the present experiments. Thus the exponential growth of CO<sub>2</sub>, indicative of rapid CO to CO<sub>2</sub> conversion, was not observed.

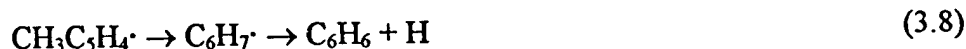
Regardless of oxygen concentration, methylcyclopentadiene is likely to be consumed to some extent via abstraction of H by phenoxy or methyl:



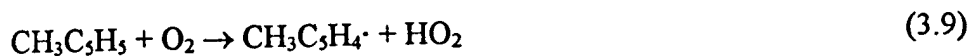
Also, it may decompose unimolecularly:



In the absence of oxygen the fate of the methylcyclopentadienyl radical is, almost exclusively, to form benzene via



As shown in Figure 3.6, benzene is indeed observed in the pyrolysis of anisole. In the presence of oxygen,  $\text{CH}_3\text{C}_5\text{H}_4\cdot$  is also produced by reactions of  $\text{CH}_3\text{C}_5\text{H}_5$  with  $\text{O}_2$  or other oxidizing radicals, e.g.



Therefore, it is reasonable to expect that the oxidation of methylcyclopentadiene should effect an increase in the production of benzene. Figures 3.6 and 3.7 illustrate that this supposition is not upheld by the experimental data;  $\text{CH}_3\text{C}_5\text{H}_5$  oxidation is not accompanied by a benzene yield in excess of that which is attributable to pyrolytic chemistry. This result suggests that  $\text{CH}_3\text{C}_5\text{H}_4\cdot$  is oxidized at a rate which is competitive with the rate of its conversion to  $\text{C}_6\text{H}_6$ . Alternatively, methylcyclopentadiene conversion may proceed by radical addition to the parent and subsequent decomposition (i.e.  $\text{CH}_3\text{C}_5\text{H}_4\cdot$  production is averted entirely). Thus, methylcyclopentadiene could be converted to CO and  $\text{C}_2\text{--C}_4$  hydrocarbons without a concomitant increase in benzene yield. The  $\text{CH}_3\text{C}_5\text{H}_5$  oxidation mechanism will be discussed further in Chapter 4.

#### CO and $\text{C}_5\text{H}_5$ Moieties

In the absence of oxidative chemistry, the mechanistic interpretation put forth implies a balance of CO and the sum of  $\text{C}_5\text{H}_5$  moieties. As discussed, CO is produced proportionately with the cyclopentadienes. The sum of  $\text{C}_5\text{H}_5$  moieties must comprise not only the cyclopentadienes themselves, but any species which are derived from secondary reactions of  $\text{C}_5\text{H}_6$  and  $\text{CH}_3\text{C}_5\text{H}_5$  or their respective radicals. These species include benzene, naphthalenes, and toluene. Benzene is derived from the methylcyclopentadienyl radical and trace toluene is presumed to be derived from benzene. Naphthalenes (i.e.

naphthalene and dihydronaphthalene) are evolved via reaction of either two cyclopentadienyl radicals or  $C_5H_5$  and  $C_5H_6$  and are therefore counted twice in the  $C_5H_5$  tally. The anisole pyrolysis data in Figure 3.10 confirm the suggested agreement between CO and the sum of  $C_5H_5$  derivatives. This result is very important in that it supports the chemistry proposed in this chapter.

### 3.2 SUMMARY

Experiments over a range of equivalence ratios ( $\phi=0.62-1.71$ ) revealed that the oxidation of anisole at atmospheric pressure near 1000 K does not differ significantly from its pyrolysis at the same nominal conditions; the distribution of reaction intermediates was virtually independent of  $\phi$ . Reactions of phenoxy with methyl, loosely termed "pyrolytic," were found to dominate the system chemistry even in the presence of oxygen. Oxidation was found to occur exclusively through intermediate methylcyclopentadiene. The preferential oxidation of  $CH_3C_5H_5$  (with respect to other major species like  $C_6H_5OH$  and  $CH_3C_6H_4OH$ ) is consistent with relative R-H bond strength arguments. Observed hydrocarbon oxidation products included acetylene, ethene, allene, propene, methylacetylene, and 1,3-butadiene. As expected, CO production increased with extent of methylcyclopentadiene conversion. Rapid oxidation of CO to  $CO_2$ , however, did not commence on the time scale of these experiments..

A mechanism has been presented which accounts qualitatively for reaction intermediates produced in the anisole experiments. In order to assess the relative importance of the various reaction pathways and to gain a more quantitative

understanding of the kinetics following the initial O-CH<sub>3</sub> bond homolysis, detailed reaction modeling was employed.



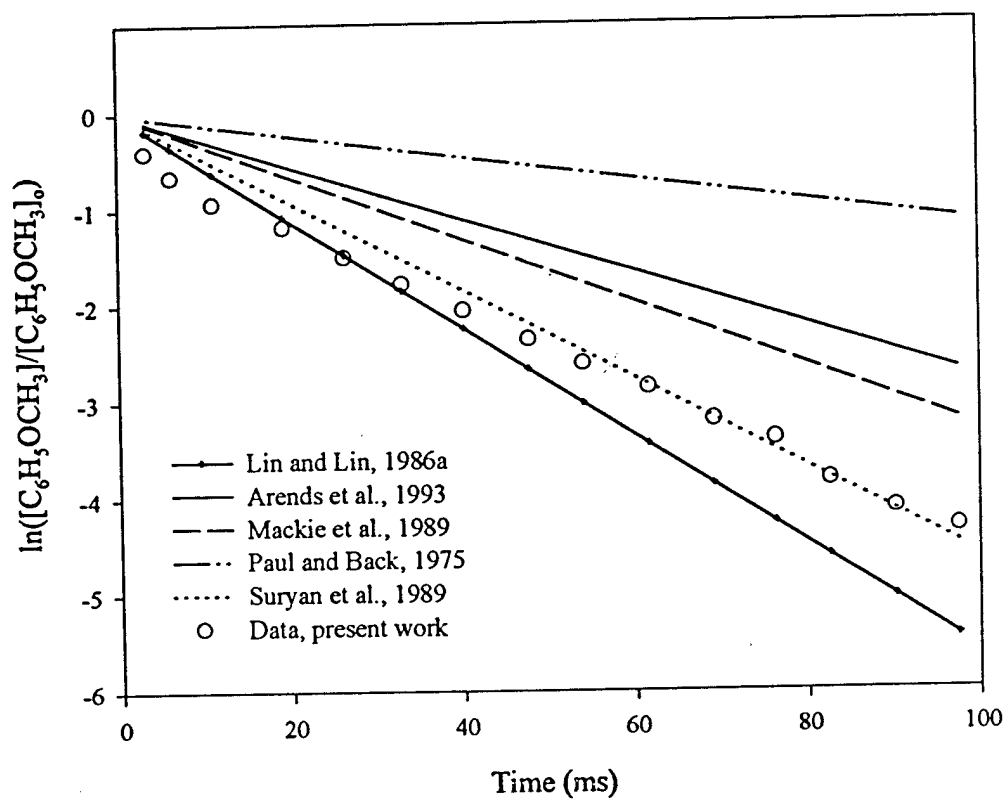


Figure 3.1: Comparison of experimental anisole data with first-order anisole decay profiles derived from reported rate constants ( $T=1003$  K).

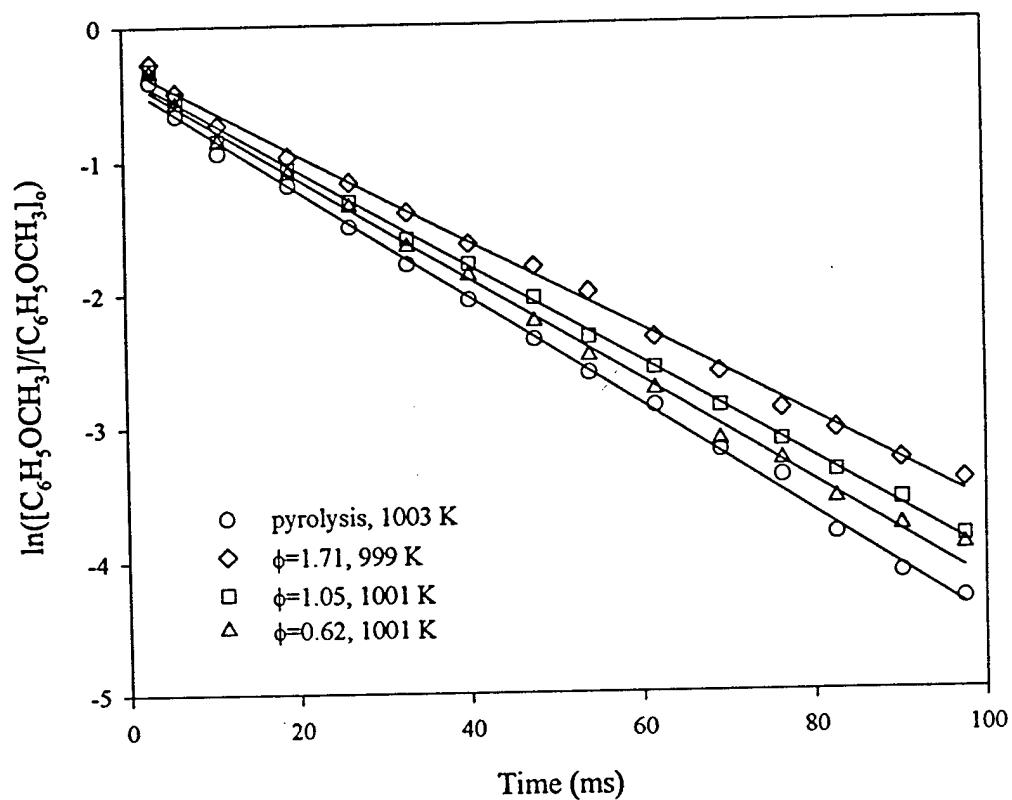


Figure 3.2: First-order anisole decay profiles from the pyrolysis and oxidation of anisole near 1000 K. Solid lines are linear curvefits to the data.

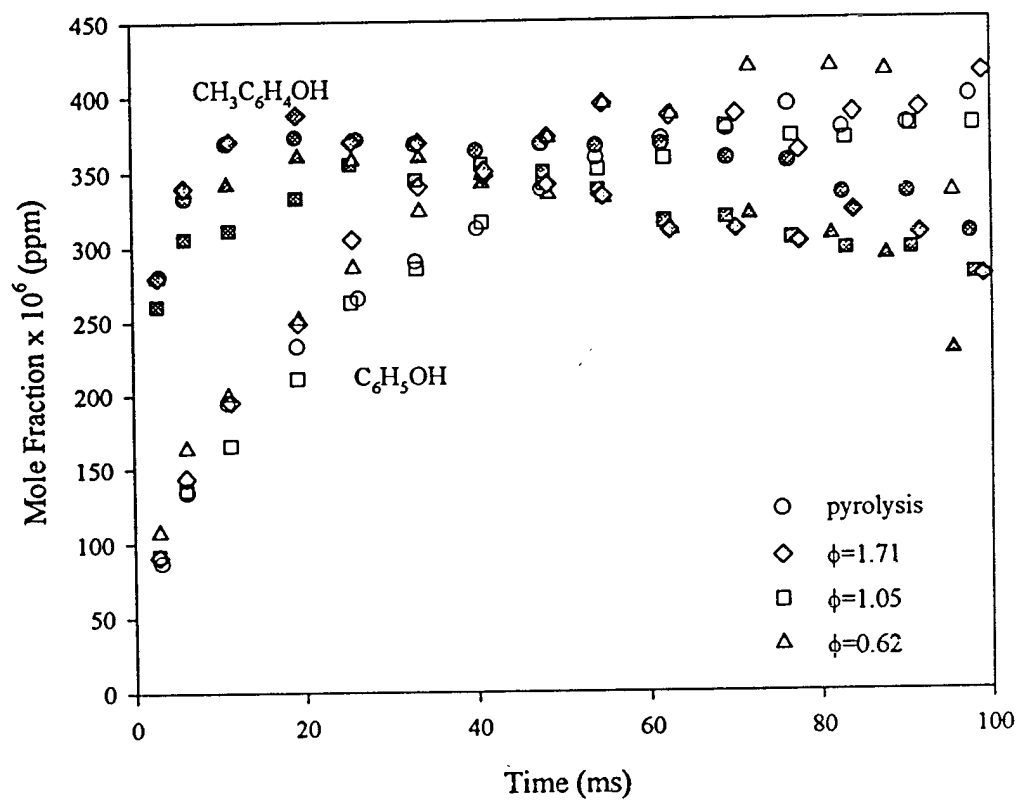


Figure 3.3: Phenol and cresol profiles from the pyrolysis and oxidation of anisole near 1000 K.

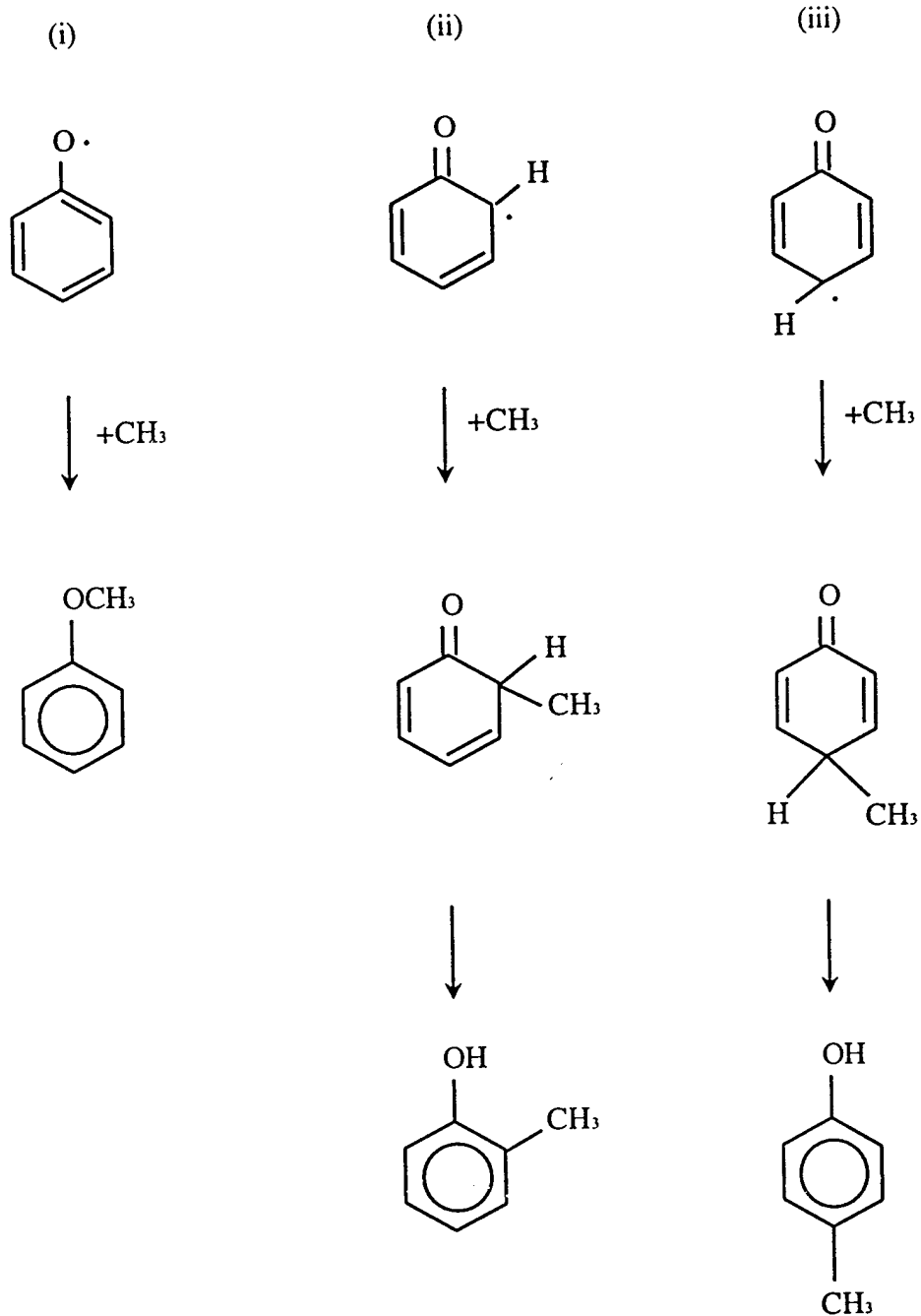


Figure 3.4: Formation of *o*- and *p*-cresols illustrated by consideration of the phenoxy radical as a hybrid of three resonance structures.

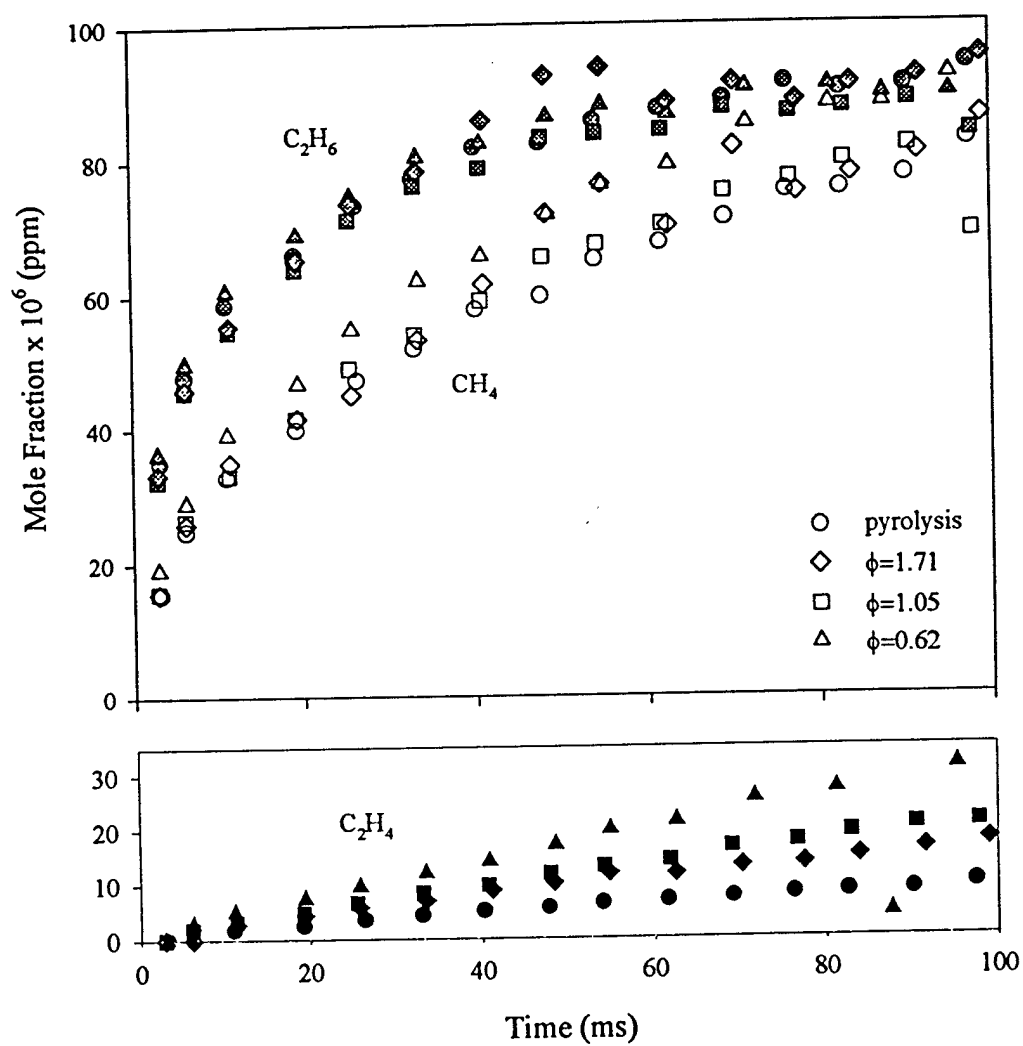


Figure 3.5: Methane, ethane, and ethene profiles from the pyrolysis and oxidation of anisole near 1000 K.

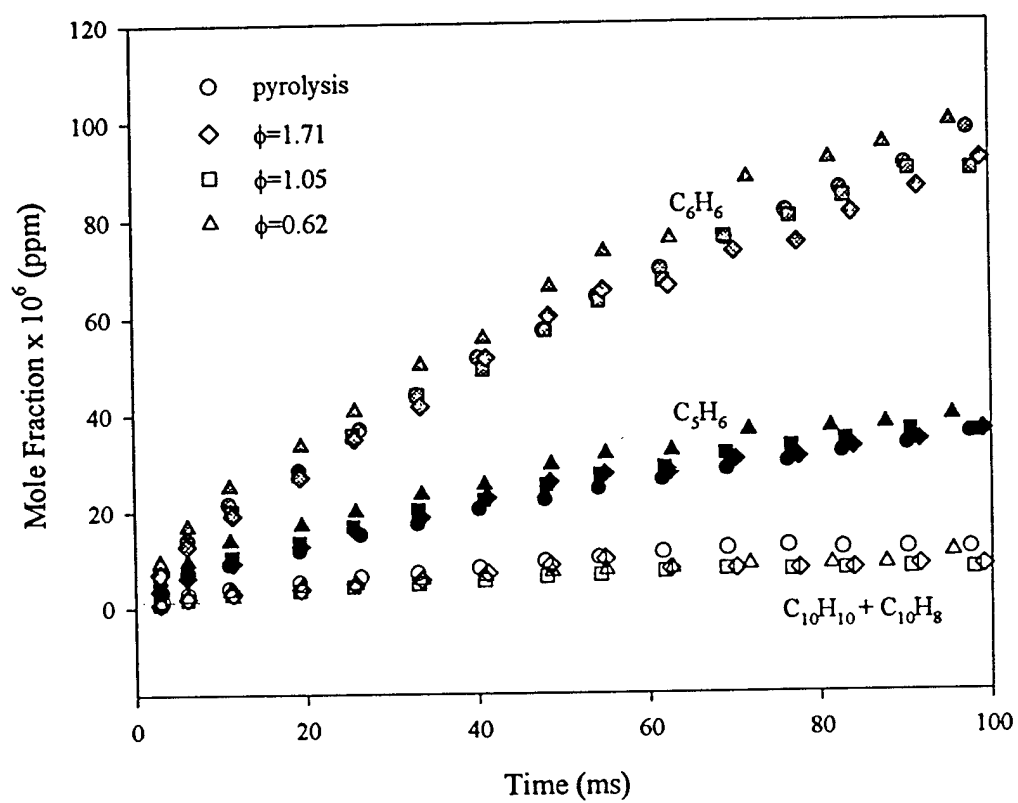


Figure 3.6: Cyclopentadiene, benzene, and naphthalene profiles from the pyrolysis and oxidation of anisole near 1000 K.

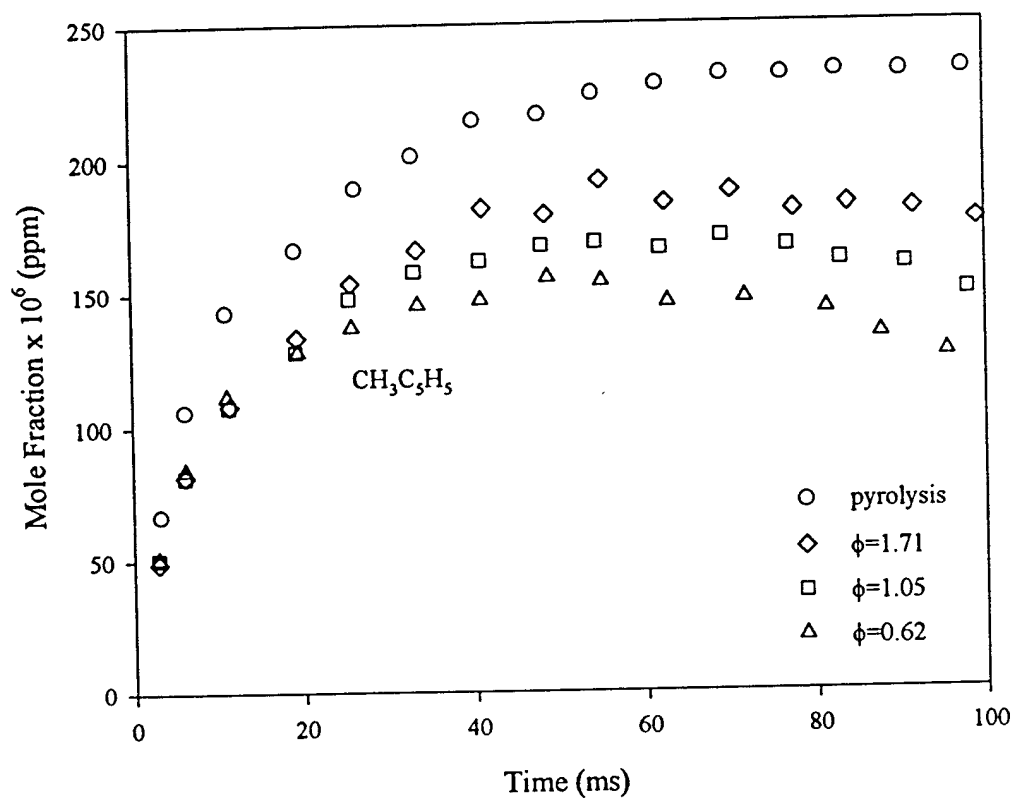


Figure 3.7: Methylcyclopentadiene profiles from the pyrolysis and oxidation of anisole near 1000 K.

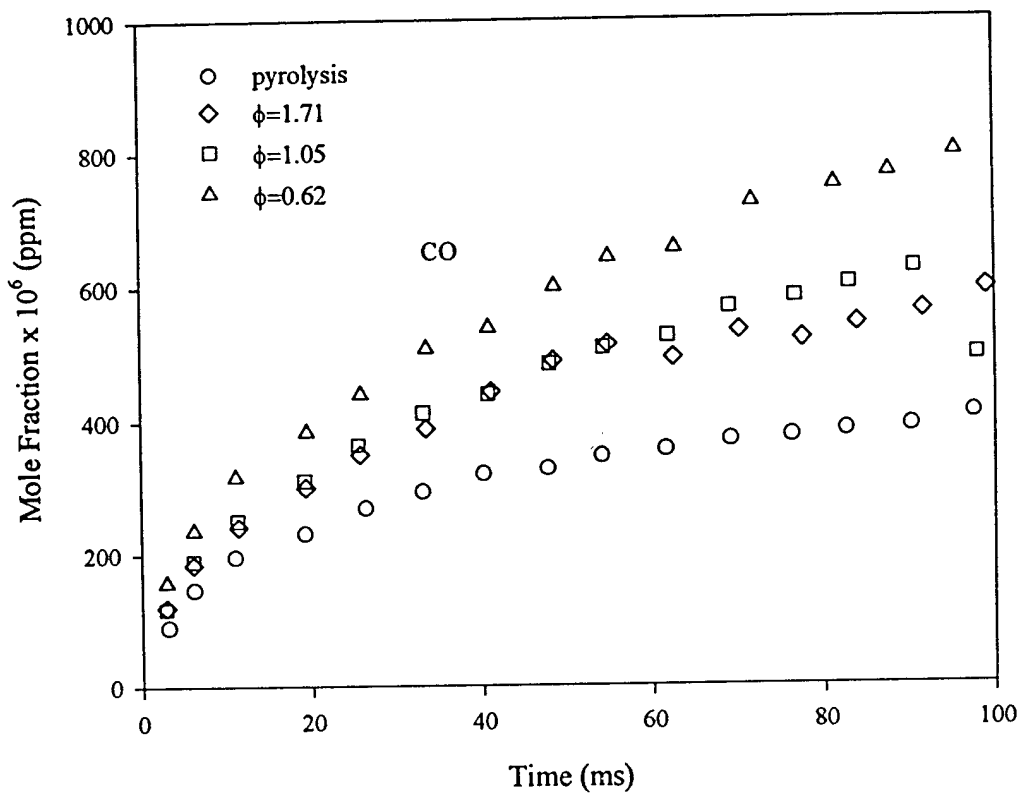


Figure 3.8: Carbon monoxide profiles from the pyrolysis and oxidation of anisole near 1000 K.



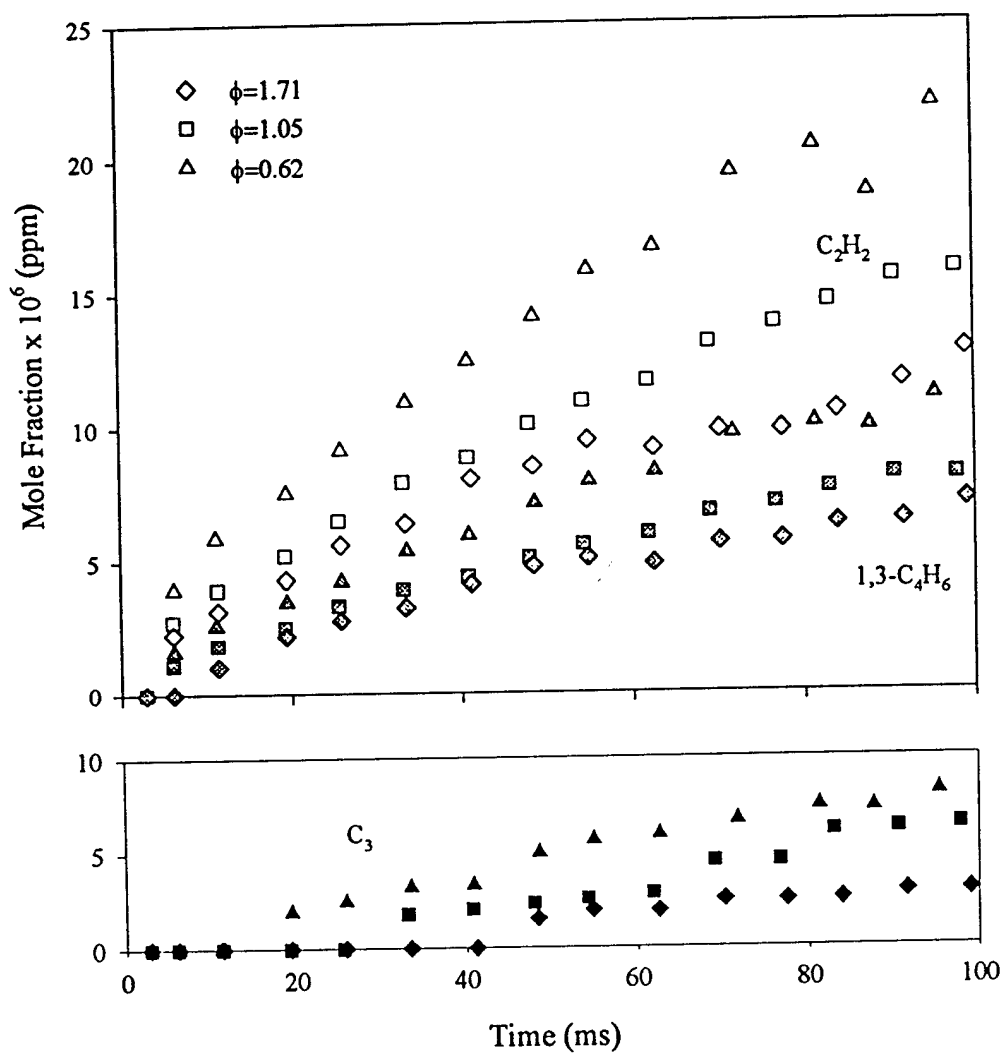


Figure 3.9: Acetylene,  $C_3$  (allene + propene + methylacetylene), and 1,3-butadiene profiles from oxidation of anisole near 1000 K.

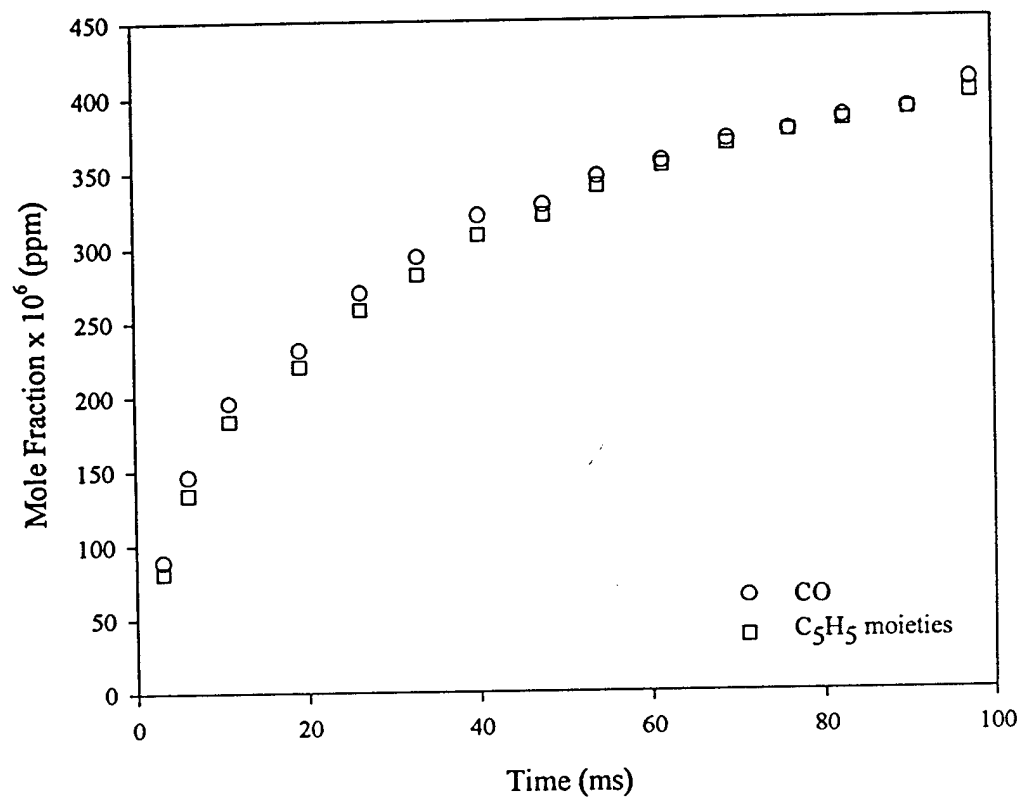


Figure 3.10: Comparison of carbon monoxide and sum of  $C_5H_5$  moieties =  $C_5H_6 + CH_3C_3H_5 + C_6H_6 + C_6H_5CH_3 + 2 \times (C_{10}H_8 + C_{10}H_{10})$  from anisole pyrolysis at 1003 K.

## CHAPTER 4. ANISOLE PYROLYSIS AND OXIDATION: KINETIC MODELING

---

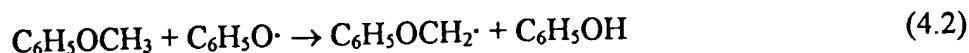
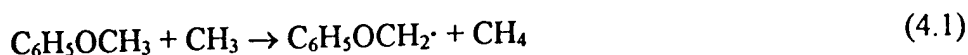
At the experimental conditions employed in this study the reaction intermediate yields are, with a few exceptions, insensitive to equivalence ratio. It can be inferred that, even in the presence of oxygen, the chemistry is primarily pyrolytic. Therefore, accurate characterization of the pyrolysis chemistry is essential to the development of a model for the oxidation of anisole.

### 4.1 PYROLYSIS MODEL DEVELOPMENT

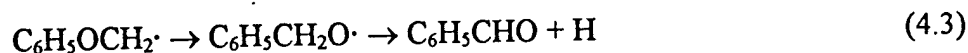
A set of 66 reversible reactions involving 31 species (Table 4.1, page 119) was developed to model the pyrolysis of anisole. Elementary reaction rate parameters for which measured values do not exist were obtained from thermodynamic estimations, QRRK analysis, semiempirical molecular orbital calculations, or by comparison with analogous reactions. Some salient features of this model are considered below.

#### Anisole Consumption

As stated previously, the destruction of anisole was found to occur almost exclusively via cleavage of the  $\text{C}_6\text{H}_5\text{O}-\text{CH}_3$  bond. However, the following H abstraction reactions were considered as well:



$\text{C}_6\text{H}_5\text{O}\cdot$  and  $\text{CH}_3$  radicals are the only abstractors present in sufficient concentration to potentially compete with the homolysis route.  $\text{C}_6\text{H}_5\text{OCH}_2\cdot$ , the anisyl radical, will undergo a 1,2 aryl shift to yield the benzoxy radical which eliminates H to form benzaldehyde [Arends et al., 1993]:



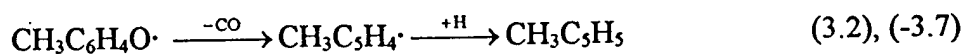
Trace (< 10 ppm) benzaldehyde was observed in the pyrolysis experiment. Thus, even though the anisole decay was found to be highly first-order, the three reactions above were included in the model for completeness.

As already shown in Table 3.2, a number of rate constants have been reported for the thermal decomposition of anisole. The rate constant of Suryan et al. [1989] was found to best fit the present experimental data.

#### Methylcyclopentadiene Formation

As explained earlier, the recombination of phenoxy and methyl radicals yields an *o*- or *p*-methylcyclohexadienone species which may isomerize to form the corresponding cresol. This reaction sequence is well-known and was first identified by Mulcahy and Williams [1963]. Here it is also considered that the ketone intermediate may decompose to methylcyclopentadiene and CO. The motivation for this proposal is detailed below.

In Section 3.1, two other sources of methylcyclopentadiene were considered:



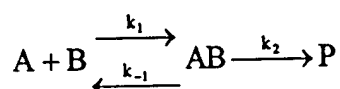
The first of these is not a significant producer of methylcyclopentadiene. The deficiency of H atom (a consequence of the scarcity of weak R-H bonds in the anisole system) is rate-limiting.  $\text{CH}_3\text{C}_5\text{H}_4\cdot$  is instead converted to benzene. The second reaction does contribute significantly to the production of methylcyclopentadiene.  $\text{C}_5\text{H}_5\cdot$  and  $\text{CH}_3$  are relatively unreactive radicals. Their lifetimes are sufficiently long as to facilitate recombination reactions. But while radical recombination is a significant source of methylcyclopentadiene, it is not a sufficient source. The observed fairly rapid growth of  $\text{CH}_3\text{C}_5\text{H}_5$  in the first 20 ms could not be reproduced by modeling the production of this species strictly via recombination of cyclopentadienyl and methyl. Arends [1993] suggested that H attack on methylcyclohexadienone, the keto precursor to cresol, may yield methylcyclopentenyl and CO. Subsequent loss of H might then give methylcyclopentadiene. Here it is considered instead that the methylcyclohexadienone complex may decompose unimolecularly to  $\text{CH}_3\text{C}_5\text{H}_5$  and CO. This molecular elimination reaction was first proposed by Cypres and Bettens [1974, 1975b] to explain the formation of methylcyclopentadiene in their cresol pyrolysis experiments. The authors postulated the expulsion of CO following an isomerization of cresol to a methylcyclohexadienone intermediate.

The potential energy diagram in Figure 4.1 illustrates the set of reactions considered to stem from the recombination of phenoxy and methyl radicals. The multichannel  $\text{C}_6\text{H}_5\text{O}+\text{CH}_3$  reaction scheme was treated by the bimolecular Quantum RRK (Rice-Ramsperger-Kassel) chemical activation approach as presented by Dean [1985].

Before the determination of actual rate constants is discussed, a review of chemical activation principles is appropriate.

### Review of Chemical Activation

Consider the addition of two species, A and B, to form products P. A conventional, thermal equilibrium approach would regard the reaction as



The rate of change of [AB] is given by

$$\frac{d[AB]}{dt} = k_1[A][B] - k_{-1}[AB] - k_2[AB]$$

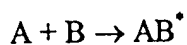
Assuming a steady-state concentration of AB,

$$[AB]_{ss} = \frac{k_1[A][B]}{k_{-1} + k_2}$$

The rate of change of [P] is then given by

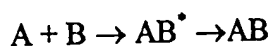
$$\frac{d[P]}{dt} = \frac{k_2 k_1 [A][B]}{k_{-1} + k_2} = \frac{k_2 k_1}{k_{-1} + k_2} [A][B]$$

In the chemical activation approach, A and B are considered to form initially an energized molecule  $AB^*$

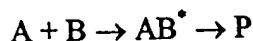


$AB^*$  is said to be chemically activated, i.e. it possesses a non-Boltzmann distribution of energies. Rather,  $AB^*$  has energy equal to the sum of the thermal energies of A and B plus the chemical energy released in the creation of the new bond [Westmoreland et al., 1986]. This chemical energy is the same as the energy barrier for dissociation of AB to

the original reactants, and  $AB^*$  may in fact simply decompose to A and B. Alternatively,  $AB^*$  may be stabilized (i.e. thermally equilibrated) by collisions

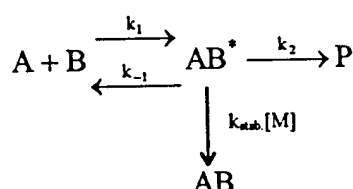


However, if the energy of  $AB^*$  exceeds the barrier for another decomposition (or an isomerization), then  $AB^*$  may react via that pathway to form products P



So, the fate of  $AB^*$  is determined by competition among the possible pathways:

redissociation to initial reactants, stabilization by collisions, or formation of products by decomposition or isomerization, i.e.



Invoking the steady-state assumption for  $[AB^*]$ , the rate of change of [P] is now given by

$$\frac{d[P]}{dt} = \frac{k_2 k_1 [A][B]}{k_{-1} + k_2 + k_{stab.}[M]} = \frac{k_2 k_1}{k_{-1} + k_2 + k_{stab.}[M]} [A][B]$$

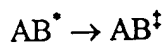
As in the well-known Lindemann model, a pressure dependence is introduced through [M]. But, the rate constant  $k_{A+B \rightarrow P}$  is pressure-independent at low pressure and pressure-dependent at high pressure, the inverse of the normal concept of falloff (i.e. as pertains to unimolecular reactions).

The QRRK formulation also differs from a Lindemann-type formulation in that the rate constants  $k_1$  and  $k_2$  are considered to be explicit functions of  $\epsilon^*$ , the energy of  $AB^*$ .

The reaction of  $AB^*$  to products P can be considered as



Here the distinction must be made between the energized molecule  $AB^*$  and the activated complex  $AB^\ddagger$ . An activated complex is a molecule that is at the top of the energy barrier which separates reactants from products and is actually passing over. An energized molecule, on the other hand, is one that possesses sufficient energy to become an activated complex but must undergo an internal redistribution of that energy in order to do so [Laidler, 1987]. That is, the QRRK theory asserts that reactions occur only when the critical energy  $\epsilon_0^*$  is concentrated in one normal mode of vibration. An essential feature of the theory is that  $\epsilon^*$  is distributed randomly among the various vibrational modes and the process



is treated statistically. The energy dependence of  $k_2$  ultimately takes the form

$$k_2 \propto \left( \frac{\epsilon^* - \epsilon_0^*}{\epsilon^*} \right)^{s-1}$$

where  $s$  is the number of oscillators. Further details of the QRRK formulation may be found elsewhere [Dean, 1985; Westmoreland et al., 1986; Laidler, 1987].

#### Estimation of Rate Constants by QRRK Analysis

The CHEMACT code [Dean et al., 1991] was used to estimate apparent rate constants for the various reactions proceeding through the formation of an energized  $C_6H_5O-CH_3$  complex (Figure 4.1).  $C_6H_5O$  and  $CH_3$  may form directly three distinct adducts depending upon the recombination site. Recombination at the O atom to form  $C_6H_5OCH_3^*$  is not expected to be a significant reaction path in accordance with the



electron density arguments given in Section 3.1. Therefore, discussion is limited to recombination at the ortho and para ring sites to form *o*- or *p*-(H)(CH<sub>3</sub>)C<sub>6</sub>H<sub>4</sub>O<sup>•</sup>.

Once formed the methylcyclohexadienone adduct may simply decompose to the initial radicals (effectively, no reaction). Alternatively, (H)(CH<sub>3</sub>)C<sub>6</sub>H<sub>4</sub>O<sup>•</sup> may be stabilized by collisions or may react further by isomerization and/or decomposition. As already proposed, the complex may eliminate CO to yield CH<sub>3</sub>C<sub>5</sub>H<sub>5</sub>. It is important to consider all reactions which may realistically be expected to occur since calculation of the rate constant for a given channel will be dependent upon the rate constants of other existing channels. Therefore loss of H to yield the methylphenoxy radical, in effect the displacement of H by methyl, is also considered. The initial adduct may also isomerize to form a second activated molecule, CH<sub>3</sub>C<sub>6</sub>H<sub>4</sub>OH<sup>•</sup>. CH<sub>3</sub>C<sub>6</sub>H<sub>4</sub>OH<sup>•</sup> may in turn decompose to CH<sub>3</sub> and <sup>•</sup>C<sub>6</sub>H<sub>4</sub>OH (hydroxyphenyl) or may be stabilized to yield cresol.

It should be noted here that no attempt has been made to distinguish between ortho and para isomers (i.e. of (H)(CH<sub>3</sub>)C<sub>6</sub>H<sub>4</sub>O<sup>•</sup>, CH<sub>3</sub>C<sub>6</sub>H<sub>4</sub>OH<sup>•</sup>, (H)(CH<sub>3</sub>)C<sub>6</sub>H<sub>4</sub>O, or CH<sub>3</sub>C<sub>6</sub>H<sub>4</sub>OH). Implicit in this treatment is the assumption that reactions of these species are not isomer selective. This is consistent with the RRKM treatment of C<sub>6</sub>H<sub>5</sub>O-CH<sub>3</sub> recombination by Lin and Lin [1986b]. Lin and Lin evaluated the branching ratio for isomerization versus stabilization of the methylcyclohexadienone complex and reported a single value for the energy barrier to isomerization. In the present analysis ortho and para forms have been treated equivalently, and the modeling results have given no indication that a distinction is necessary.

Inputs to the QRRK calculation include: 1) the high pressure rate constants  $k_1$ – $k_3$ ,  $k_{-1}$ , and  $k_{-4}$ , 2) the geometric mean vibrational frequency  $\langle \nu \rangle$  of the adduct  $(\text{H})(\text{CH}_3)\text{C}_6\text{H}_4\text{O}^\bullet$ , and 3) molecular parameters for both the adduct and the bath gas including molecular weight, collision diameter ( $\sigma$ ), well depth ( $\epsilon/k$ ), and the average energy transferred per collision. The determination of each of these inputs will be considered in turn followed by a discussion of the outputs.

#### *High pressure limit rate constants*

The high pressure rate constants  $k_1$ – $k_3$ ,  $k_{-1}$ , and  $k_{-4}$  (Table 4.2) were derived by comparison with similar or analogous reactions. Thermodynamic consistency was maintained for reaction pairs 1 and 4. Reaction 1, the recombination of phenoxy and methyl, was assumed to have zero energy barrier.  $k_1$  was estimated from the A factor for the reverse of  $\text{C}_6\text{H}_5\text{OCH}_3 \rightarrow \text{C}_6\text{H}_5\text{O}^\bullet + \text{CH}_3$ ,  $A_r$ .  $A_r$  was determined from the measured preexponential for the forward decomposition reaction [Arends, 1993] and thermodynamics.  $A_1$  was set equal to  $10A_r$  according to the unpaired electron density distribution in the phenoxy radical; the density associated with the o and p ring sites is roughly 10 times the density on the O atom.

Arrhenius parameters for reaction 2 were estimated from those measured for the similar CO expulsion from phenoxy [Frank, 1994].  $A_2$  was taken as the A factor for  $\text{C}_6\text{H}_5\text{O}^\bullet \rightarrow \text{C}_5\text{H}_5^\bullet + \text{CO}$ .  $E_{a,2}$  is equal to the sum of  $\Delta H_{R,2}$  (17 kcal/mol) plus the intrinsic activation energy of the phenoxy reaction (16 kcal/mol).  $E_{a,2}$  was ultimately reduced by 0.5 kcal/mol in order to improve agreement of the model with the experimental data. This

adjustment is reasonable in light of the uncertainty in the thermodynamic properties of  $(\text{H})(\text{CH}_3)\text{C}_6\text{H}_4\text{O}^\bullet$  which were estimated by group additivity methods.

Table 4.2: High pressure limit rate parameters for QRRK analysis of  $\text{C}_6\text{H}_5\text{O}^\bullet + \text{CH}_3$

k	$A^a$	$E_a$ (kcal/mol)
1	1.04E+14	0.0
-1	5.66E+17	57.4
2	7.40E+11	32.5
3	3.26E+15	67.9
4	5.67E+13	39.0
-4	1.75E+12	55.6
5	1.40E+16	99.8

<sup>a</sup> Units:  $\text{s}^{-1}$  (except  $A_1 \sim \text{cc} \cdot \text{mol}^{-1} \cdot \text{s}^{-1}$ ).

$A_3$  and  $E_{a,3}$  were calculated from thermodynamics with  $A_3 = 1.0 \times 10^{14}$  (a reasonable estimate for radical recombination with H).

$E_{a,4}$  was estimated by analogy with the tautomerization reaction 2-pyridone  $\rightarrow$  2-hydroxypyridine [Moreno and Miller, 1990].  $A_4$  was determined from transition state theory, i.e.  $A = (ekT/h)\exp(\Delta S^\ddagger/R)$ . The transition state was assumed to be tight [Lin and Lin, 1986b] and thus  $\Delta S^\ddagger \approx 0$ .

$E_{a,5}$  and  $A_5$  were obtained by comparison with the analogous reaction of toluene:



### Geometric mean vibrational frequency

One of the simplifying assumptions of the QRRK treatment is the use of a single characteristic frequency, the geometric mean, to represent the vibrational frequency distribution of the adduct. By this approach, the high pressure limit activation energy of a given reaction path can be related to a critical number of energy quanta required for reaction. The geometric mean vibrational frequency is given by

$$\langle \nu \rangle = \left( \prod_{i=1}^s \nu_i \right)^{1/s}$$

where  $s$  is the total number of vibrational modes. Often though, especially in the case of radicals or unfamiliar molecules, the  $\nu_i$  frequencies have not been measured and must be estimated from those of similar molecules. The vibrational frequencies of  $(\text{H})(\text{CH}_3)\text{C}_6\text{H}_4\text{O}^\bullet$  are assumed to be identical to those of the stabilized species. These frequencies, listed in Table 4.3, were estimated on the basis of the spectra of *p*-benzoquinone and toluene [Lin and Lin, 1986b].

Table 4.3: Vibrational frequencies of  $(\text{H})(\text{CH}_3)\text{C}_6\text{H}_4\text{O}$ .

$\nu \text{ (cm}^{-1}\text{)}$	
3018	(8)
1408	(10)
1139	(8)
871	(6)
610	(6)
402	(3)
289	(1)
$\langle \nu \rangle = 1141$	

### *Molecular parameters*

Lennard-Jones parameters for many species typically encountered in combustion applications are tabulated [Kee et al., 1983; Reid et al., 1987].  $\sigma$  and  $\epsilon/k$  of uncommon species like  $(H)(CH_3)C_6H_4O$  can be correlated to their boiling point or critical point properties by methods detailed by Reid et al. [1987]. In the case of  $(H)(CH_3)C_6H_4O$ , even the boiling point properties were required to be estimated thus introducing an additional uncertainty into the calculation of  $\sigma$  and  $\epsilon/k$ . The Lennard-Jones parameters are essential to the computation of the collision frequency  $Z$  which in turn determines  $k_{stab.}$ .  $Z$  is defined as the Lennard-Jones collision frequency  $Z_{L-J}$  given below:

$$Z \equiv Z_{L-J} = 2.708 \left( \frac{\sigma_1 + \sigma_2}{2} \right)^2 \left( \frac{8\pi kT}{\mu} \right)^{1/2} \left( \frac{\epsilon}{kT} \right)^{1/3}$$

$Z_{L-J}$  has only a weak dependence on  $\epsilon/k$  but depends strongly on  $\sigma$ . However, the determination of overall rate constants was found to be virtually insensitive to small variations in the values of  $\sigma$  and  $\epsilon/k$  assigned to the adduct. These have been estimated by the methods mentioned above and the calculations are summarized in Table 4.4.

Bath gas ( $N_2$ ) Lennard-Jones parameters and  $\langle \Delta E \rangle$ , the average energy transferred per collision, were taken from Gardiner et al. [1984] and are also listed in Table 4.4.  $\langle \Delta E \rangle$  is used to compute a collision efficiency,  $\beta$  [Troe, 1979]. Within the QRRK formulation is the assumption of a modified strong collision model. That is, the deactivation (and activation) of molecules is assumed to occur in single, large steps via strong collisions rather than by many weaker collisions.  $\beta$  (always  $< 1$ ) is a correction factor of sorts by

which the collision frequency  $Z$  is weighted in the calculation of  $k_{stab}$ . Physically,  $1/\beta$  can be thought of as the number of collisions required for deactivation.

Table 4.4: Molecular parameters for  $(H)(CH_3)C_6H_4O$  and  $N_2$  bath gas.

Species	$T_c^a$ (K)	$T_b^b$ (K)	$V_b^c$ (cc/mol)	$\mu^d$ (Debye)	$\sigma$ (Å)	$\epsilon/k$ (K)
<i>o</i> -(H)(CH <sub>3</sub> )C <sub>6</sub> H <sub>4</sub> O	611	406	105	3.1	5.11 <sup>e</sup>	598 <sup>e</sup>
<i>p</i> -(H)(CH <sub>3</sub> )C <sub>6</sub> H <sub>4</sub> O	594	395	105	3.1	5.09 <sup>e</sup>	588 <sup>e</sup>
(H)(CH <sub>3</sub> )C <sub>6</sub> H <sub>4</sub> O <sub>avg</sub>					5.10 <sup>f</sup>	595 <sup>f</sup>
N <sub>2</sub>					3.62	97.5
$\langle \Delta E \rangle = 830$ cal/mol						

<sup>a</sup>  $T_c$ =critical temperature, estimated by method of Forman and Thodos [Reid et al., 1987].

<sup>b</sup>  $T_b$ =boiling point (1 atm), determined by modified Guldberg rule with method of Lyderson [ibid.].

<sup>c</sup>  $V_b$ =molar volume at boiling, estimated by method of Schroeder [ibid.].

<sup>d</sup>  $\mu$ =dipole moment, estimated from  $\mu$  of cyclohexanone [ibid.].

<sup>e</sup> Estimated by method of Brokaw [ibid.].

<sup>f</sup> Properties computed from weighted average of ortho and para properties, e.g.

$$\sigma_{avg} = \frac{(2 \times \sigma_o + \sigma_p)}{3}.$$

#### Apparent rate constants

Computed apparent rate constants for reactions of  $C_6H_5O\cdot$  and  $CH_3$  to products are given in Table 4.5. A comparison of rate expressions evaluated at  $T=1000$  K reveals that reactions 4.7 and 4.8 are negligible at the experimental conditions. Stabilization of  $(H)(CH_3)C_6H_4O\cdot$  clearly dominates accounting for 60% of the collisions which form the adduct. In this context the term "stabilized" refers to *thermal* stabilization, i.e. a stabilized species possesses a Boltzmann distribution of energies. Further reaction of the thermalized species is possible and must be accounted for.

Table 4.5: Apparent reaction rate constants<sup>a,b</sup> calculated via QRRK analysis.

	Reaction	A	n	E <sub>a</sub>	k <sub>1000 K</sub>
(4.6)	$C_6H_5O\cdot + CH_3 \rightarrow (H)(CH_3)C_6H_4O$	2.277E+86	-21.56	36090	6.16E+13
(3.3)	$C_6H_5O\cdot + CH_3 \rightarrow 5-CH_3C_5H_5 + CO$	2.049E+75	-18.29	38880	8.78E+11
(4.7)	$C_6H_5O\cdot + CH_3 \rightarrow CH_3C_6H_4O\cdot + H$	3.331E+39	-7.78	31670	1.82E+09
(1.15)	$C_6H_5O\cdot + CH_3 \rightarrow CH_3C_6H_4OH$	2.313E+73	-17.37	38780	6.00E+12
(4.8)	$C_6H_5O\cdot + CH_3 \rightarrow \cdot C_6H_4OH + CH_3$	1.292E-31	13.20	15580	2.02E+05
(4.9)	$(H)(CH_3)C_6H_4O \rightarrow 5-CH_3C_5H_5 + CO$	1.180E+47	-10.32	51910	6.70E+04
(4.10)	$(H)(CH_3)C_6H_4O \rightarrow CH_3C_6H_4OH$	2.732E+60	-13.73	64300	1.92E+05

<sup>a</sup> Bath gas: N<sub>2</sub>. Pressure: 1 atm. Temperature range: 900–1300 K.

<sup>b</sup> Units: cc, mol, s, cal.

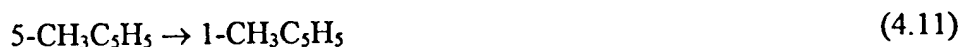
Decomposition of  $(H)(CH_3)C_6H_4O$  to the initial reactants is automatically included in the model since the reactions are written reversibly. However, decomposition/isomerization to other products, in particular  $CH_3C_5H_5 + CO$  and  $CH_3C_6H_4OH$ , must be considered as well. The multichannel unimolecular reaction of  $(H)(CH_3)C_6H_4O$  was treated using the CHEMACT companion code DISSOC and the resulting rate constants are also listed in Table 4.5. The relative importance of the direct (prior to stabilization of the adduct) product formation routes with respect to the indirect (following stabilization) routes will be discussed in Section 4.2.

#### Methylcyclopentadiene Isomerization

The formation of methylcyclopentadiene by recombination of  $CH_3$  and  $C_5H_5\cdot$  necessarily yields the 5- isomer as shown in Figure 4.2a. The decomposition  $(H)(CH_3)C_6H_4O^* \rightarrow CH_3C_5H_5 + CO$  is postulated to occur without any intermediate isomerization of the adduct and therefore must also yield the 5- isomer of methylcyclopentadiene (Figure 4.2b). The 1- and 2- forms are known to be derived via

sigmatropic rearrangement(s) [McClean and Haynes, 1965; Spangler, 1976]. A [1,5] sigmatropic hydrogen shift yields 1-CH<sub>3</sub>C<sub>5</sub>H<sub>5</sub> which may itself undergo a [1,5] shift to yield 2-CH<sub>3</sub>C<sub>5</sub>H<sub>5</sub> (Figure 4.2c). Two GC peaks have been identified by MS as isomers of methylcyclopentadiene [Emdee, 1991]. On the basis of thermodynamic stability considerations, these peaks were assigned to 1- and 2-CH<sub>3</sub>C<sub>5</sub>H<sub>5</sub>.

While thermodynamic properties do not differ vastly among the three isomers, the kinetic stability of the 5- isomer does contrast significantly with that of the 1- and 2- forms. Specifically, at 1000 K 5-CH<sub>3</sub>C<sub>5</sub>H<sub>5</sub> decomposes readily via cleavage of the C<sub>5</sub>H<sub>5</sub>-CH<sub>3</sub> bond ( $E_a=67.5$  kcal/mol) to yield the cyclopentadienyl and methyl radicals. In contrast, methyl loss from 1- or 2-CH<sub>3</sub>C<sub>5</sub>H<sub>5</sub> involves the formation of a C<sub>5</sub>H<sub>5</sub> cyclic carbene and is approximately 90 kcal/mol endothermic rendering these decompositions unfeasible at temperatures near 1000 K. The pyrolysis data in Figure 3.7 suggest that at the later residence times methylcyclopentadiene persists in a pseudo-steady-state. In order to reproduce the observed stability of this species in the anisole pyrolysis system, it is necessary to include CH<sub>3</sub>C<sub>5</sub>H<sub>5</sub> isomerization reactions in the model. Rate parameters for the two isomerization reactions



were estimated via a semiempirical approach using the MOPAC code [Stewart, 1989].

A semiempirical method is a quantum mechanical treatment of molecules which can be used for example to estimate thermodynamic properties and also to locate the transition state for a given reaction. It differs from the ab initio approach in that an



attempt is made to improve the accuracy of the results by introducing numerical parameters whose values are chosen to fit experiment [Dewar, 1992]. Because a semiempirical model contains adjustable parameters which are optimized for a finite set of molecules, caution must be observed in applying a given method to molecules which are unlike those in the optimization set. Specifically, it is useful to compare thermodynamic data determined by experiment with that predicted by the semiempirical model to gain a sense of the accuracy of the procedure.

In the case of methylcyclopentadiene, experimentally determined thermodynamic data could not be found in the literature. Observed enthalpies of formation for some related compounds are listed in Table 4.6 along with values determined by PM3 (the semiempirical model employed by MOPAC). The experimental and predicted values of  $\Delta H_f(298)$  are comparable. Rate parameters for the two isomerization reactions were derived from transition state theory according to the relations

$$E_a = \Delta H^\ddagger + RT$$

$$A = (ekT/h) \exp(\Delta S^\ddagger/R)$$

where  $\Delta H^\ddagger$  and  $\Delta S^\ddagger$  are the change in enthalpy and entropy involved in progressing from the reactant to the transition state. Note that the rate constant  $k = A \exp(-E_a/RT)$  depends exponentially upon  $\Delta H^\ddagger$  and  $\Delta S^\ddagger$ . Thus, errors in predicted thermodynamic properties on the order of several kilocalories may result in nontrivial errors in the computed rate constant. But small, systematic errors inherent in the estimation of thermodynamic quantities may to some extent be canceled in taking the differences  $\Delta H^\ddagger$  and  $\Delta S^\ddagger$ .

Table 4.6: Comparison of observed  $\Delta H_f$  with PM3 predictions for species similar to  $\text{CH}_3\text{C}_5\text{H}_5$ .

Species	$\Delta H_f$ Observed (kcal/mol)	$\Delta H_f$ PM3 (kcal/mol)
methylcyclopentane, $\text{CH}_3\text{C}_5\text{H}_9$	-25.4	-29.9
cyclopentadiene, $\text{C}_5\text{H}_6$	32.1	31.8

A summary of the PM3 calculations is given in Table 4.7. The results are consistent with the observations of McLean and Haynes [1965] who showed that 5- $\text{CH}_3\text{C}_5\text{H}_5$  rearranged "very rapidly" to 1- $\text{CH}_3\text{C}_5\text{H}_5$  which then rearranged "more slowly" to 2- $\text{CH}_3\text{C}_5\text{H}_5$ .

Table 4.7: Summary of PM3 calculations.

Reaction	$\Delta H^\ddagger$ (kcal/mol)	$\Delta S^\ddagger$ cal/(mol·K)	A ( $\text{s}^{-1}$ )	$E_a$ (kcal/mol)	$k_{1000\text{ K}}$ ( $\text{s}^{-1}$ )
5- $\text{CH}_3\text{C}_5\text{H}_5 \rightarrow$ 1- $\text{CH}_3\text{C}_5\text{H}_5$	33.1	-4.0	7.57E+12	35.1	1.62E+05
1- $\text{CH}_3\text{C}_5\text{H}_5 \rightarrow$ 2- $\text{CH}_3\text{C}_5\text{H}_5$	53.7	3.0	2.56E+14	55.7	1.72E+02

### Benzene Formation

As stated in Section 3.1, benzene is evolved from the methylcyclopentadienyl radical.  $\text{CH}_3\text{C}_5\text{H}_4\cdot$  rearranges to a cyclohexadienyl radical intermediate which rapidly loses H to yield benzene. Rate constants for the relevant reactions of  $\text{CH}_3\text{C}_5\text{H}_4\cdot$  and  $\text{C}_6\text{H}_7\cdot$  were taken from the QRRK analysis of Ritter et al. [1990] which considered the reverse reaction, addition of H to  $\text{C}_6\text{H}_6$ . As illustrated in Figure 4.3,  $\text{H} + \text{C}_6\text{H}_6$  yields a cyclohexadienyl complex. Prior to stabilization, it may undergo a ring opening reaction to

linear  $C_6H_7\cdot$  or may rearrange to a chemically activated methylcyclopentadienyl radical.

The radical may be stabilized or may decompose to fulvene + H.

The energy requirements of the two decomposition pathways are significantly greater than those of both the forward and reverse isomerization reactions. These decompositions were omitted from the anisole pyrolysis model since they were found to have virtually no effect on the predicted species yields. Ritter's rate constants for the reactions



and the corresponding reverse reactions (determined by thermodynamics) are listed in Table 4.8. The reverse reactions govern the production of benzene in the anisole system. A comparison of the reverse rate constants for the two H addition reactions suggests that both the direct and indirect (i.e. following stabilization of  $C_6H_7\cdot$ ) reactions of  $CH_3C_5H_4\cdot$  to benzene will be important.

Table 4.8: Rate constants<sup>a</sup> for formation of  $C_6H_6$  from  $CH_3C_5H_4\cdot$ .

Reaction	Forward			Reverse			
	A	n	E <sub>a</sub>	A	n	E <sub>a</sub>	k <sub>1000 K</sub>
$H + C_6H_6 \rightarrow CH_3C_5H_4\cdot$	5.22E+28	-4.3	28.8	5.21E+29	-5.1	52.8	1.12E+03
$H + C_6H_6 \rightarrow C_6H_7\cdot$	8.18E+57	-13.2	26.3	7.97E+57	-13.3	48.2	3.45E+07
$C_6H_7\cdot \rightarrow CH_3C_5H_4\cdot$	5.00E+12	0.0	38.1	5.12E+13	-0.6	40.2	1.27E+03

<sup>a</sup> Units: cc, mol, s, kcal.

### Phenoxy Decomposition

A number of rate constants for the unimolecular decomposition of phenoxy, determined both experimentally [Colussi et al., 1977; Lin and Lin, 1985, 1986a; Frank et al., 1994] and theoretically [Olivella et al., 1995; Liu et al., 1996] have been reported in the literature. The measurement of Lin and Lin was described in Chapter 1. In the more recent measurement by Frank et al., the preexponential was determined to be roughly a factor of 3 higher than Lin and Lin's value. It has been observed [Frank et al., 1994; Olivella, 1995] that there is a notable uncertainty in Lin and Lin's rate due to the effects of alternative reactions (i.e.  $\text{C}_6\text{H}_5\text{O} + \text{CH}_3 \rightarrow \text{CH}_3\text{C}_6\text{H}_4\text{OH}$ ) which compete with the phenoxy decomposition reaction. Frank et al.'s measurements, also accomplished via thermal decomposition of alkyl phenyl ethers in a shock tube, were less susceptible to such complications since they were made under far more dilute conditions (i.e. initial ether mole fraction=25–90 ppm). For this reason, the rate constant of Frank et al. was chosen for the anisole pyrolysis model. It should be noted however that the values of the A factor and  $E_a$  reported by both Lin and Lin and Frank et al. are significantly lower than those predicted by theory suggesting a need for further study of the phenoxy decomposition reaction.

### Naphthalene Formation

The mechanism of naphthalene formation during the oxidation of both aromatic and aliphatic hydrocarbons has been the subject of considerable study due to the importance of PAH (polycyclic aromatic hydrocarbon) formation in the overall process of

soot production. Thus, while naphthalene is only a trace reaction intermediate in the present anisole experiments, a brief discussion of its formation mechanism is included here.

The formation of naphthalene has been postulated to occur via recombination of two cyclopentadienyl radicals to yield initially an isomer of dihydrofulvalene [Klinkenberg and Louw, 1987; Melius et al., 1996]. Klinkenberg and Louw suggested that following a [1,5] H-shift, attack by H yields a  $C_5H_5C_5H_6$  species. This species was thought to undergo a series of ring openings and closures to form two fused  $C_6$  rings and, ultimately, naphthalene by loss of 3H. Melius et al. suggested that isomerization of dihydrofulvalene is followed by H elimination to form a  $C_{10}H_9$  radical. A species of two fused  $C_6$  rings is then formed through a series of closures and openings of a three-membered ring. Loss of another H yields naphthalene.

In short, the formation of fused  $C_6$  rings from a  $C_5H_5$  dimer is clearly a complex procedure. Rates of the many elementary reaction steps involved are still not well-defined. Dean determined a rate for the global reaction



by QRRK analysis [Dean, 1990]. The rate constant, reported for  $P=0.58\text{atm}$ , is roughly  $7 \times 10^7$  at 1000 K. Arends [1993] estimated the rate constant for the same reaction to be  $1 \times 10^8$  at 1 atm, and this is the rate constant used in the present modeling effort.

#### Analogous Reactions

While some measured or estimated rates exist in the literature for reactions of phenol and cyclopentadiene, rates for the methyl-substituted species cresol and methylcyclopentadiene are absent. Rates for abstractions of the phenolic H from cresol

were assumed to be equivalent to rates for the analogous abstractions from phenol. Also, expulsion of CO from the cresol radical methylphenoxy was assigned the rate for the analogous decomposition of phenoxy. Rates for abstractions of the allylic H from methylcyclopentadiene were taken to be equal to rates for the analogous abstractions from cyclopentadiene. In the case of the 5- isomer, however, the preexponential of the  $C_5H_6$  reaction was divided by two since 5- $CH_3C_5H_5$  possesses only one easily abstractable H.

Other reaction rates assigned by analogy are identified as such in Table 4.1.

## 4.2 PYROLYSIS MODELING RESULTS

The reacting flow was treated numerically as a homogeneous, zero-dimensional, adiabatic, constant pressure system using the SENKIN chemical kinetics code [Lutz et al., 1987]. Thermodynamic properties (Table 4.9, page 123) were taken from the CHEMKIN thermodynamic data base [Kee et al., 1987], Burcat and McBride [1993], and Ritter et al. [1990] or in many cases were estimated by group additivity methods [Benson, 1968] using THERM [Ritter and Bozzelli, 1987].

### Comparison of Model Predictions with Experimental Data

Experimental pyrolysis data are compared with model predictions of anisole decay and CO production in Figure 4.4. Predictions of these species which are global descriptors of overall reaction progress match experiment well.

Excellent agreement between model and experiment is obtained not only for *total* methylcyclopentadiene yield but for the individual isomer yields as illustrated in Figure 4.5. As stated earlier, two isomers of  $CH_3C_5H_5$  were observed experimentally and GC peaks

were assigned to the 1- and 2- forms initially on the basis of thermodynamic stability considerations. A steady-state analysis supports the designated assignments. As shown in Figure 4.5, both isomers reach a pseudo-steady-state which persists over the second half of the 100 ms residence time. Assuming that other reactions which consume or produce 2-CH<sub>3</sub>C<sub>5</sub>H<sub>5</sub> and 1-CH<sub>3</sub>C<sub>5</sub>H<sub>5</sub> are slow by comparison to the isomerizations, the following steady-state relations hold true:

$$\frac{d[1 - \text{CH}_3\text{C}_5\text{H}_5]}{dt} = k_{5 \rightarrow 1}[5 - \text{CH}_3\text{C}_5\text{H}_5] - (k_{1 \rightarrow 5} + k_{1 \rightarrow 2})[1 - \text{CH}_3\text{C}_5\text{H}_5] = 0$$

$$\frac{d[2 - \text{CH}_3\text{C}_5\text{H}_5]}{dt} = k_{1 \rightarrow 2}[1 - \text{CH}_3\text{C}_5\text{H}_5] - k_{2 \rightarrow 1}[2 - \text{CH}_3\text{C}_5\text{H}_5] = 0$$

$k_{5 \rightarrow 1}$ ,  $k_{1 \rightarrow 5}$ ,  $k_{1 \rightarrow 2}$ , and  $k_{2 \rightarrow 1}$  correspond to the forward and reverse rate constants of the reactions



It follows that

$$\frac{[5 - \text{CH}_3\text{C}_5\text{H}_5]}{[1 - \text{CH}_3\text{C}_5\text{H}_5]} = \frac{(k_{1 \rightarrow 5} + k_{1 \rightarrow 2})}{k_{5 \rightarrow 1}}$$

and

$$\frac{[2 - \text{CH}_3\text{C}_5\text{H}_5]}{[1 - \text{CH}_3\text{C}_5\text{H}_5]} = \frac{k_{1 \rightarrow 2}}{k_{2 \rightarrow 1}}$$

Therefore at 1000 K,  $\frac{[5 - \text{CH}_3\text{C}_5\text{H}_5]}{[1 - \text{CH}_3\text{C}_5\text{H}_5]} \approx 0.02$  and  $\frac{[2 - \text{CH}_3\text{C}_5\text{H}_5]}{[1 - \text{CH}_3\text{C}_5\text{H}_5]} \approx 0.88$ . Since the

observed isomers of CH<sub>3</sub>C<sub>5</sub>H<sub>5</sub> both reach steady-state mole fractions of the same order, they must be the 1- and 2- forms. The 5- isomer, predicted to be present on the order of

just a few ppm, could easily go undetected. Furthermore, the GC peak of greater magnitude must correspond to 1-CH<sub>3</sub>C<sub>5</sub>H<sub>5</sub>. Later, a reaction path analysis of modeling results will support the assumption that the isomerization reactions are by far the dominant producers and consumers of 1- and 2-CH<sub>3</sub>C<sub>5</sub>H<sub>5</sub>.

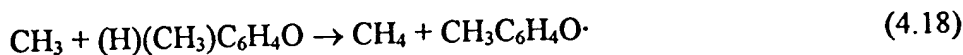
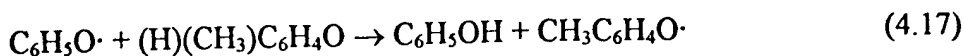
The cyclopentadiene profile is well-predicted as shown in Figure 4.6. However, the model predicts an early accumulation of the cyclopentadienyl radical. C<sub>5</sub>H<sub>5</sub>·, a resonantly stabilized radical, may realistically be expected to build to high concentration (relative to other, more reactive radicals) in the flow reactor. The radical may then encounter a source of H in the probe (e.g. condensate on the probe's inner surface) and be detected as the stable species C<sub>5</sub>H<sub>6</sub>. A deficit in the C<sub>5</sub>H<sub>6</sub> model prediction would support this notion. However, such a deficit is not observed in Figure 4.6. The C<sub>5</sub>H<sub>5</sub>· radical might also be expected to recombine with another in the quench region of the sampling probe yielding perhaps naphthalene, dihydronaphthalene, or some other C<sub>10</sub> species. In his flow reactor study of toluene, Emdee [1991] found that most of the observed bibenzyl was formed by recombination of two resonantly stabilized benzyl radicals in the probe; very little bibenzyl was predicted by the toluene model and the sum of the bibenzyl prediction and one half of the benzyl prediction was comparable to the measured yield of bibenzyl. A similar argument does not hold true for the present model with regard to the C<sub>5</sub>H<sub>5</sub>· and naphthalene. Without taking the C<sub>5</sub>H<sub>5</sub>· prediction into account, the naphthalenes are already overpredicted by the model as also shown in Figure 4.6. Some unknown trace species, tentatively identified as C<sub>5</sub>'s, were observed during anisole pyrolysis and may have been associated with C<sub>5</sub>H<sub>5</sub>· decomposition.



$C_3H_3\cdot$  production is attributed primarily to the unimolecular decomposition of phenoxy. Rate constants reported for this reaction differ by a factor of three. For reasons explained in Section 4.1, the faster rate constant of Frank et al. [1994] was chosen for the present model. Use of the slower rate constant of Lin and Lin [1986a] does improve the  $C_3H_3\cdot$  prediction, but Frank's value provides the best overall agreement between model and experiment.

Prediction of total phenolics (Figure 4.7) agrees well with experiment though the distribution among phenol and cresols exhibits poor agreement; at 98 ms total phenolics consist of approximately equal parts phenol and cresols while the model predicts essentially only cresols (Figure 4.8). A concomitant underprediction of methane and ethane (Figure 4.9) is consistent with this result; methyl groups are "trapped" in excess cresols, unavailable to reactions forming methane and ethane. All attempts to improve prediction of these species by optimization—within realistic limits—of rate parameters were unsuccessful.

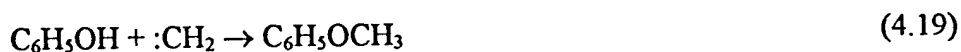
In particular, reactions of phenoxy and methyl radicals with the intermediate *o*- and *p*-methylcyclohexadienones were investigated. These molecules possess a weak, abstractable hydrogen atom and are also polar, so abstraction could be a fast (low  $E_a$ ) process. Mulcahy and Williams [1965], in their study of methyl radical reactions with phenol, observed larger yields of  $CH_4$  than could be accounted for by abstraction from phenol. They attributed their surplus  $CH_4$  to an unusually rapid reaction between  $CH_3$  and methylcyclohexadienone intermediates. Nevertheless, adoption of large rate constants (as high as  $10^{12} \text{ cc}\cdot\text{mol}^{-1}\cdot\text{s}^{-1}$ ) for the reactions:



did not reproduce the present experimental phenol and methane profiles. In the present system,  $[(\text{H})(\text{CH}_3)\text{C}_6\text{H}_4\text{O}]$  is at best two orders of magnitude less than  $[\text{CH}_3]$  or  $[\text{C}_6\text{H}_5\text{O}\cdot]$ , and thus the above reactions cannot compete with reactions of phenoxy and methyl with one another.

As will be illustrated shortly, recombination of phenoxy with H is virtually the sole source of phenol in the present model. The rate constant for the reaction ( $2 \times 10^{14} \text{ s}^{-1}$ , He et al. [1988]) is large. However, formation of phenol via this recombination is limited by the deficiency of atomic hydrogen in this system.

An attempt was made to model the production of phenol directly from anisole. Arends [1993] proposed the addition of H to anisole at the ortho or para position of the aromatic nucleus followed by methyl elimination to yield (keto)phenol. In the present study a phenol formation pathway not involving atomic hydrogen was sought. Unimolecular elimination of the methylene singlet from anisole was postulated. Insertion of  $:\text{CH}_2$  into O-H bonds to form methyl ethers is known to occur [Kerr et al., 1967]. In accordance with microreversibility the reverse reaction, expulsion from O-CH<sub>3</sub>, must therefore be possible. Reaction 4.19:



(assumed to have zero activation energy) was assigned  $A = 5 \times 10^{13} \text{ cc}\cdot\text{mol}^{-1}\cdot\text{s}^{-1}$ . This rate constant is reasonable according to the results of Kerr et al. [1967] who determined relative reactivities of roughly 10–20 for the insertion of methylene into hydroxyl groups

as compared with insertion into primary C-H bonds. But, the inclusion of reaction 4.19 in the anisole pyrolysis model had no effect on species yields. This result is not surprising since the reverse reaction of anisole is 97 kcal/mol endothermic and thus cannot be a significant source of phenol at 1000 K. Attempts to model phenol via pathways involving recombination of phenoxy radicals and subsequent consumption of the dimers [Gopalan and Savage, 1995] were also unsuccessful.

Arends and coworkers [1993] encountered a similar obstacle in predicting their observed phenol yields. In their anisole hydrogenolysis model, the rate of recombination of phenoxy and H to yield phenol had to be artificially increased (from He's value given above) by a factor of 50. Without this acceleration phenoxy concentration was grossly overpredicted, accompanied by unrealistic yields of cresols. It was acknowledged by the authors however that their rate was too high for gas-phase recombination. And, it was suggested that the conversion of phenoxy to phenol could have been accelerated by a heterogeneous process at the reactor wall; it is well known that quartz reactors adsorb H atoms and catalyze recombinations. Similarly, Mackie and coworkers [1989] found that significant fractions of both phenol and methane observed in their study could not be accounted for by homogeneous gas-phase recombination or abstraction reactions. The unaccounted for methane was shown to obey first-order kinetics and the authors suggested the possible occurrence of surface-catalyzed chemistry.

### Investigation of Surface Effects

The possibility of surface-mediated chemistry was investigated in the context of this effort. It was found that model profiles could be corrected by the inclusion of the heterogeneous reactions:



where  $\text{H}_{\text{wall}}$  was postulated to be labile hydrogen associated with condensed high molecular weight material on the test section surface. This chemistry was modeled by imposing a surface density  $\rho_{\text{surface}}$  ( $\sim$ moles  $\text{H}_{\text{wall}}/\text{cm}^2$ ) sufficiently high such that the above reactions became pseudo-first-order in  $\text{C}_6\text{H}_5\text{O}\cdot$  and  $\text{CH}_3$ , respectively. First-order rate constants are then given by

$$k_{\text{first-order}} = k \rho_{\text{surface}} \left( \frac{S}{V} \right)$$

where  $\left( \frac{S}{V} \right)$  is the reactor surface-to-volume ratio. It was found that the experimental data could be predicted well with  $k_{\text{first-order}} \sim 10^3 \text{ s}^{-1}$  for each of the two surface reactions. This value is reasonable in the context of kinetic theory. The kinetic theory of gases [Somorjai, 1994] gives the flux  $F$  of molecules reaching a surface as

$$F = \frac{N_A P}{(2\pi \overline{M} R_u T)^{1/2}}$$

where  $N_A$  is Avogadro's number and  $\overline{M}$  is the mean molecular weight. For the experimental conditions of this study,  $F \approx 0.265 \text{ mol}\cdot\text{cm}^{-2}\cdot\text{s}^{-1}$ .  $F$  can be converted to a

volumetric rate  $Z$  by multiplying by  $\left(\frac{S}{V}\right)$ , i.e.  $Z = F\left(\frac{S}{V}\right) \sim \text{mol}\cdot\text{cc}^{-1}\cdot\text{s}^{-1}$ . Now, the first-order rate for wall reaction of species  $A$  is

$$\frac{d[A]}{dt} = Z\eta X_A$$

where  $\eta$  is the fraction of successful collisions and  $X_A$  is the mole fraction of species  $A$ .

Based on the modeling results (exclusive of heterogeneous reaction steps),  $X_{\text{phenoxy}} \sim 1 \times 10^{-5}$  at the early residence times. The maximum rate of phenoxy conversion to phenol at the reactor wall is then roughly  $1 \times 10^{-6} \text{ mol}\cdot\text{cc}^{-1}\cdot\text{s}^{-1}$ . For  $k_{\text{first-order}} \sim 10^{-3}$  as given above,

$$\frac{d[\text{C}_6\text{H}_5\text{OH}]}{dt} \text{ at the wall is only of order } 10^{-7}.$$

An experimental justification for the assumption of heterogeneous chemistry was sought. A series of experiments was performed with the reactor test section replaced by another of one half the original diameter (i.e. 5 vs. 10 cm) increasing the surface to volume ratio by a factor of 2. The anisole and diluent flow rates were adjusted in order to match the fuel loading and Reynolds number ( $\approx 8000$ ) of the 10 cm duct experiments. As a result the residence time for the 5 cm duct experiments is one half the residence time of the 10 cm duct experiments. The set of experimental conditions is listed in Table 4.10.

No change in the product distribution was observed in the initial trials. In an attempt to coat the quartz surface with a large amount of condensed material, anisole was then pyrolyzed in the reactor at an initial concentration several times that normally used. The experiments were repeated and still revealed no change in the chemistry. A comparison of the phenol and cresol profiles for the set of experiments is shown in Figure

4.10. While this result represents a further validation of the Princeton APFR as a device capable of capturing homogeneous gas-phase chemistry, it leaves the mechanism of phenoxy conversion to phenol in the flow reactor as yet unresolved.

Table 4.10: Experimental conditions for anisole pyrolysis experiments in 5 and 10 cm reactor test sections.

Reactor Diameter (cm)	Temperature (K)	Residence Time (ms)	Fuel Loading (ppm)	Reynolds Number
5	999	50	1009	8214
5	999	50	1009	8217
5	996	50	4134	8092
5	1000	50	1005	8248
10	1003	98	1077	8110

#### Reaction Path Analysis

Reaction path analysis examines the contributions of individual reactions to the production and destruction of particular species. The analysis involves the determination of the instantaneous “flux” or rate ( $\text{mol}\cdot\text{cc}^{-1}\cdot\text{s}^{-1}$ ) of each reaction at each time step. The relative importance of competing reaction paths is then readily ascertained by comparison of their respective fluxes. Furthermore, flux information can be summarized pictorially as in Figure 4.11 to provide a convenient illustration of the flow of reaction intermediates. In Figure 4.11 each arrow represents the flux of a given reaction in the indicated direction; the forward and reverse of a reaction are depicted individually. The magnitude of a flux is indicated by the weight of its arrow. The analysis pictured in Figure 4.11 was performed for the residence time corresponding to  $\approx 50\%$  anisole conversion, i.e.  $t_{50}=15$  ms. The

relative ranking of reactions at this time is indicative of their relative importance overall.

Note that every reaction in Table 4.1 is not represented on the flux diagram; only the most significant reactions have been included.

The results of the reaction path analysis (Figures 4.11–13) reveal the following:

1. Both the forward and reverse of the recombination



are significant reaction paths;  $(\text{H})(\text{CH}_3)\text{C}_6\text{H}_4\text{O}$  is both a continuous sink and source of the phenoxy and methyl radicals. The isomerization to cresol



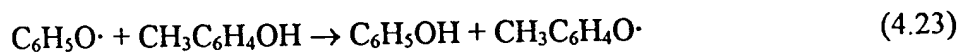
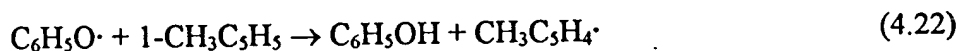
is only marginally more significant than the decomposition of  $(\text{H})(\text{CH}_3)\text{C}_6\text{H}_4\text{O}$  to initial reactants.

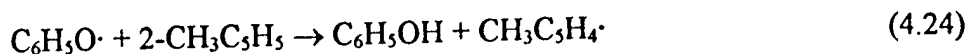
2. The indirect reaction paths (i.e. via stabilized  $(\text{H})(\text{CH}_3)\text{C}_6\text{H}_4\text{O}$ ) are more significant sources of 5- $\text{CH}_3\text{C}_5\text{H}_5$  and  $\text{CH}_3\text{C}_6\text{H}_4\text{OH}$  than the direct reactions of phenoxy and methyl. During the first half of the reaction ( $t < 50$  ms), the flux of cresol through  $(\text{H})(\text{CH}_3)\text{C}_6\text{H}_4\text{O}$  is roughly 5 times the flux via direct reaction. Similarly, the flux of  $\text{CH}_3\text{C}_5\text{H}_5$  via the indirect route exceeds the flux of the direct reaction by an order of magnitude.

3. The recombination



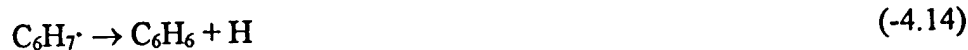
is the most significant producer of phenol. The next most significant phenol sources, in order of importance, are the H abstractions





However, these reactions account for only a trivial amount of phenol.

4. Atomic hydrogen is liberated almost exclusively via the reaction sequence



5. The assumptions essential to the steady-state analysis of 1- and 2- $\text{CH}_3\text{C}_5\text{H}_5$  are valid. Specifically, it was assumed that isomerization reactions are fast by comparison to other reactions which produce or consume 1- and 2- $\text{CH}_3\text{C}_5\text{H}_5$ . Figure 4.13 confirms that this is true.

### 4.3 PYROLYSIS SUMMARY

The pyrolysis of anisole near 1000 K has been modeled with excellent agreement between experimental data and predictions of fuel decay and major reaction intermediates including methylcyclopentadiene, carbon monoxide, and total phenolics. Much of the important chemistry—specifically, reactions of  $\text{C}_6\text{H}_5\text{O}\cdot$  with  $\text{CH}_3$  and methylcyclopentadiene isomerization reactions—had not been quantified previously. Unknown rate constants were rigorously estimated without subsequent adjustment to better fit the experimental data. The model's primary shortcoming is its inability to predict correctly the relative distribution of phenol and cresols.

Reaction path analysis has revealed that the recombination





is the primary phenol production reaction. The rate of this reaction is limited in the anisole pyrolysis system not by the rate constant but by the concentration of H. The series of reactions which produce benzene are virtually the sole means by which H is liberated. Presently benzene is underpredicted by roughly 25%. Optimization of the benzene production reactions was found to boost phenol production, but the increase was not nearly sufficient to predict the phenol data. Prediction of phenol was not improved significantly by acceleration (within the bounds of physically realistic rate parameters) of H abstraction reactions.

Difficulty in predicting successfully yields of phenoxy and phenol in intermediate- to high-temperature combustion experiments is pandemic. In reactor studies of anisole [Mackie et al., 1989; Arends et al., 1993], investigators have tentatively ascribed the production of phenol to some heterogeneous process. But attempts to model the benzene flame—where it is to be noted that no surface effect is possible—have also been plagued by gross inaccuracies in the prediction of phenoxy and phenol [Bittker, 1991; Zhang and McKinnon, 1995; Lindstedt and Skevis, 1994]. The hypothesis of surface chemistry was not supported in the present flow reactor study of anisole. The results of the present study suggest rather that there is some gas-phase chemistry of phenoxy and/or phenol which is as yet unknown. Nevertheless, a subset of phenoxy chemistry has been developed here from reactions which, until now, had not been linked and, in some cases, had not been treated quantitatively. This modeling effort represents an extension of our fundamental

knowledge of phenoxy and thus a contribution to the comprehensive understanding of the complex chemistry of aromatics.

#### 4.4 OXIDATION MODEL DEVELOPMENT

Reaction intermediate data from the oxidation of anisole over a range of equivalence ratios ( $\phi=0.62-1.71$ ) were shown not to differ substantially from the anisole pyrolysis data acquired at the same nominal temperature. More specifically, yields of anisole, cresols, phenol, benzene, cyclopentadiene, methane, and ethane were independent of  $\phi$ . Oxidation was found to occur preferentially through methylcyclopentadiene, accompanied by the production of CO and some  $C_2-C_4$  hydrocarbons. These results suggest that: 1) a model for the oxidation of anisole will rely heavily on the pyrolytic chemistry developed in Section 4.1 and 2) extension of the pyrolysis model will involve primarily the addition of reaction steps describing the oxidation of methylcyclopentadiene.

To some extent, the oxidation of methylcyclopentadiene can be described by analogy to the oxidation of the unsubstituted species, cyclopentadiene. The oxidation of cyclopentadiene proceeds in part via addition of radicals to its unsaturated bonds. Oxidation may also proceed through the radical  $C_5H_5\cdot$  by recombination with O or  $HO_2$ . Addition of a radical to either  $C_5H_5\cdot$  or the parent species yields an energized adduct which can decompose to lower energy, non-cyclic products by  $\beta$ -scission reactions [Bozzelli et al., 1990]. While the oxidation of methylcyclopentadiene may be considered to occur analogously, development of the comprehensive set of elementary reactions is significantly more complex. For the substituted cyclopentadiene, radical addition products

may exist in different isomeric forms which react subsequently via distinct  $\beta$ -scission pathways. Presently, development of a detailed kinetic model for quantitative prediction of  $\text{CH}_3\text{C}_5\text{H}_5$  oxidation must rely strongly on estimates of rate parameters; even the less complex cyclopentadiene chemistry has not yet been conclusively established. Furthermore, thermodynamic data for partially oxidized intermediate species must be estimated as well. In this section, a methylcyclopentadiene mechanism will be presented which accounts, qualitatively, for the  $\text{C}_2$ – $\text{C}_4$  reaction intermediates observed in the anisole oxidation experiments.

#### Radical Recombination

As stated earlier, two isomers of methylcyclopentadiene are observed experimentally but all three are present in the reacting system. 5- $\text{CH}_3\text{C}_5\text{H}_5$  is formed initially and is rapidly converted to 1- $\text{CH}_3\text{C}_5\text{H}_5$  which in turn is converted to 2- $\text{CH}_3\text{C}_5\text{H}_5$ . Abstraction of an allylic H from any one of the three forms yields the same resonantly stabilized methylcyclopentadienyl radical as shown in Figure 4.14.<sup>†</sup> It is more likely that the radical is derived from either 1- or 2- $\text{CH}_3\text{C}_5\text{H}_5$  since the 5- isomer is short-lived and, in contrast to the others, possesses only one loosely-bound H. In terms of modeling ease, it is fortunate that the three isomers yield only one radical. However, recombination with oxidizing radicals like O and  $\text{HO}_2$  may yield again three distinct isomers corresponding to addition at  $\text{C}_1$ , either of two equivalent 2 sites, or either of two equivalent 3 sites.

---

<sup>†</sup> According to the rules for nomenclature of organic chemistry, double (and/or triple) bonds in unsaturated monocyclic hydrocarbons are assigned numbers as low as possible. In the specific case of methylcyclopentadiene, the double bonds are labeled 1 and 3. The position of the methyl group then becomes 5, 1, or 2 depending on the isomeric form. For radicals derived from monocyclic hydrocarbons, the carbon atom with the free valence is numbered as 1 [Weast and Astle, 1980]. The unpaired electron in the methylcyclopentadienyl radical, however, is delocalized. Therefore, the carbon atom possessing the methyl group is labeled as 1.

Addition of radicals at the sole 1 site is statistically unfavorable and subject to steric hindrance. Thus the ensuing discussion will be limited to additions at C<sub>2</sub> and C<sub>3</sub>.

The potential energy diagrams in Figures 4.15a and 4.15b illustrate the reaction of CH<sub>3</sub>C<sub>5</sub>H<sub>4</sub>· and HO<sub>2</sub>. The radical recombination yields a methylcyclopentadienyl hydroperoxide which will rapidly dissociate either back to reactants or to a methylcyclopentadienyl-oxy radical and OH. In the oxidation of benzene at flow reactor temperatures, the analogous reaction of C<sub>5</sub>H<sub>5</sub>· and HO<sub>2</sub>:



is one of the most important chain branching reactions; the OH product is more reactive than HO<sub>2</sub> and thus accelerates the overall reaction via abstractions [Bozzelli et al., 1990].

The methylcyclopentadienyl-oxy radical may also be formed directly by recombination of O atom with CH<sub>3</sub>C<sub>5</sub>H<sub>4</sub>· as shown in Figures 4.16a and 4.16b. The radical will undergo rapid unimolecular dissociation near 1000 K via two low energy channels. One of these yields a methylcyclopentadienyl ketone and H atom. The second is a ring opening reaction to form a methylpentadienyl aldehyde radical. This radical may decompose to acetylene and a C<sub>4</sub> aldehyde radical but is more likely to undergo rapid internal abstraction of the aldehydic hydrogen to form a more thermodynamically stable carbonyl radical. The carbonyl radical will decompose to CO and a C<sub>5</sub> hydrocarbon radical. The structure of this hydrocarbon radical is determined by the site at which the initial recombination (i.e. of O or HO<sub>2</sub> with CH<sub>3</sub>C<sub>5</sub>H<sub>4</sub>·) took place; either the straight-chain 1,3-pentadien-4-yl radical or the branched 2-methyl-1,3-butadien-1-yl radical is formed. Subsequent reactions of these radicals are detailed in Figure 4.17. The straight-

be formed at the 4 position. In this case, ring opening would proceed via  $\beta$ -scission of the vinylic C–C bond resulting in the formation of a vinylic methyl-1,4-pentadienyl radical. The more reactive vinylic radical would rapidly decompose to methylacetylene and allyl radical [Bozzelli et al., 1990].

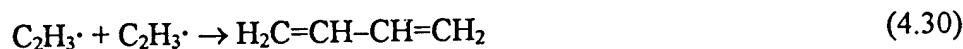
In their benzene model, Emdee et al. [1992] did not consider the addition of radicals to the  $C_5H_6$  ring due to the presence of easily abstractable hydrogens. But for the conditions of the present anisole experiments, radical addition to  $CH_3C_5H_5$  is expected to be a competitive reaction path. At 1000 K, the rate constant for abstraction of an allylic hydrogen by H is approximately  $1 \times 10^{13}$  (Table 4.1). The rate constant for addition of H to the ring, estimated from the rate expression for H addition to ethene [Dean, 1985], is roughly the same.

Several of the reaction paths mentioned above (e.g.  $HO_2$  or O recombination with  $CH_3C_5H_4\cdot$ ) may lead to the formation of a methylcyclopentadien-one. Preliminary modeling results have shown that this ketone intermediate is long-lived and may build to relatively high concentration. Therefore, further reaction of this species via radical addition to an unsaturated bond must be considered. An example of H addition is shown in Figures 4.19a and 4.19b.

#### Additional Reactions

As discussed in Section 3.1, the production of acetylene, ethene, allene, propene, methylacetylene, and 1,3-butadiene were observed to result from the oxidation of methylcyclopentadiene. Oxidation channels have been outlined above which describe the formation of methylacetylene as well as methyl and vinyl radicals. Allene may be formed

via isomerization of methylacetylene [Wu and Kern, 1987]. Recombination of vinyl with H, methyl, or vinyl yields ethene, propene, and 1,3-butadiene, respectively. Alternatively, vinyl may unimolecularly decompose to acetylene + H. A list of these reactions, not intended as a comprehensive set, is given below:



#### 4.5 OXIDATION SUMMARY

From the anisole data reported in Chapter 3, it was inferred that oxidation occurs preferentially through intermediate methylcyclopentadiene. Observed hydrocarbon oxidation products included acetylene, ethene, allene, propene, methylacetylene, and 1,3-butadiene. A general mechanism for the oxidation of methylcyclopentadiene has been developed which accounts for the production of these species. It is proposed that oxidation of methylcyclopentadiene proceeds in part via H abstraction followed by  $\text{CH}_3\text{C}_5\text{H}_4\cdot$  recombination with  $\text{HO}_2$  or O. Recombination is followed by ring opening and subsequent decomposition reactions which yield CO and non-cyclic hydrocarbon molecules and radicals. Methylcyclopentadiene conversion was considered to occur also by addition of radicals (i.e. H, O, and OH) to unsaturated bonds of the parent molecule. An energized adduct is thereby formed which may undergo ring opening and subsequent dissociation. In both cases, the relative positions of the methyl substituent and the radical

addition site determine a distinct  $\beta$ -scission channel. Development of a detailed model for quantitative prediction of methylcyclopentadiene oxidation is best postponed until the oxidation chemistry of the unsubstituted cyclopentadiene has been more conclusively established. As yet, measured rates and thermodynamic data are scarce and models must rely heavily on estimations.

In conclusion, the anisole experiments have demonstrated that at temperatures typical of the flame's preheat zone, phenoxy may undergo recombination reactions which are competitive with its decomposition. The resultant phenolic species, phenol and cresol, were found to be resistant to oxidation at temperatures near 1000 K. Phenol and related species have been observed in benzene flames [Bittner and Howard, 1981; Hausmann et al., 1992] and are expected to play a role in the flame chemistry of aromatics in general. Thus, the oxidation of phenol near 1170 K has also been investigated and is reported in the following chapter.

Table 4.1: Anisole pyrolysis mechanism.<sup>a</sup>

	Reaction	A	n	E <sub>a</sub>	Reference
1.14	$C_6H_5OCH_3 \rightarrow C_6H_5O + CH_3$	3.00E+15	0.00	63000	b
4.1	$C_6H_5OCH_3 + CH_3 \rightarrow C_6H_5OCH_2 + CH_4$	5.01E+11	0.00	10500	Arends, 1993
4.2	$C_6H_5OCH_3 + C_6H_5O \rightarrow C_6H_5OCH_2 + C_6H_5OH$	4.17E+11	0.00	16060	Arends, 1993
4.3	$C_6H_5OCH_2 \rightarrow C_6H_5CHO + H$	3.16E+12	0.00	21500	Arends, 1993
4.6	$C_6H_5O + CH_3 \rightarrow (H)(CH_3)C_6H_4O$	2.28E+86	-21.60	36090	c
3.3	$C_6H_5O + CH_3 \rightarrow 5-CH_3C_3H_5 + CO$	2.05E+75	-18.30	38880	c
4.7	$C_6H_5O + CH_3 \rightarrow CH_3C_6H_4O + H$	3.33E+39	-7.80	31670	c
1.15	$C_6H_5O + CH_3 \rightarrow CH_3C_6H_4OH$	2.31E+73	-17.40	38780	c
4.8	$C_6H_5O + CH_3 \rightarrow C_6H_4OH + CH_3$	1.29E-31	13.20	15580	c
4.10	$(H)(CH_3)C_6H_4O \rightarrow CH_3C_6H_4OH$	2.73E+60	-13.70	64300	c
4.9	$(H)(CH_3)C_6H_4O \rightarrow 5-CH_3C_3H_5 + CO$	1.18E+47	-10.30	51910	c
1.12	$C_6H_5O \rightarrow CO + C_3H_5$	7.40E+11	0.00	43853	Frank, 1994
1.13	$C_6H_5O + H \rightarrow C_6H_5OH$	2.50E+14	0.00	0	He, 1988
1.18	$C_6H_5OH + H \rightarrow C_6H_6 + OH$	2.21E+13	0.00	7930	He, 1988
	$C_6H_5OH + CH_3 \rightarrow C_6H_5O + CH_4$	2.51E+11	0.00	8000	Mulcahy, 1965
	$C_6H_5O + C_2H_6 \rightarrow C_6H_5OH + C_2H_5$	3.02E+11	0.00	11500	d
1.17	$C_6H_5OH + H \rightarrow C_6H_5O + H_2$	1.15E+14	0.00	12400	He, 1988
4.11	$5-CH_3C_3H_5 \rightarrow 1-CH_3C_3H_5$	7.57E+12	0.00	35100	c
4.12	$1-CH_3C_3H_5 \rightarrow 2-CH_3C_3H_5$	2.56E+14	0.00	55700	c
	$1-CH_3C_3H_5 + H \rightarrow CH_3C_3H_4 + H_2$	2.19E+08	1.77	3000	e
	$2-CH_3C_3H_5 + H \rightarrow CH_3C_3H_4 + H_2$	2.19E+08	1.77	3000	e
	$5-CH_3C_3H_5 + H \rightarrow CH_3C_3H_4 + H_2$	1.08E+08	1.77	3000	f
-3.7	$CH_3C_3H_4 + H \rightarrow 1-CH_3C_3H_5$	1.00E+14	0.00	0	g



	Reaction	A	n	E <sub>a</sub>	Reference
-3.7	$\text{CH}_3\text{C}_3\text{H}_4 + \text{H} \rightarrow 2\text{-CH}_3\text{C}_3\text{H}_5$	1.00E+14	0.00	0	g
-3.7	$\text{CH}_3\text{C}_3\text{H}_4 + \text{H} \rightarrow 5\text{-CH}_3\text{C}_3\text{H}_5$	1.00E+14	0.00	0	g
-4.4	$5\text{-CH}_3\text{C}_3\text{H}_5 \rightarrow \text{CH}_3 + \text{C}_3\text{H}_5$	1.00E+16	0.00	67500	Ritter, 1990
-4.25	$\text{CH}_3\text{C}_3\text{H}_4 + \text{H} \rightarrow \text{C}_3\text{H}_5 + \text{CH}_3$	8.00E+13	0.00	0	Ritter, 1990
3.6	$1\text{-CH}_3\text{C}_3\text{H}_5 + \text{CH}_3 \rightarrow \text{CH}_3\text{C}_3\text{H}_4 + \text{CH}_4$	3.11E+11	0.00	5500	e
3.6	$2\text{-CH}_3\text{C}_3\text{H}_5 + \text{CH}_3 \rightarrow \text{CH}_3\text{C}_3\text{H}_4 + \text{CH}_4$	3.11E+11	0.00	5500	e
3.6	$5\text{-CH}_3\text{C}_3\text{H}_5 + \text{CH}_3 \rightarrow \text{CH}_4 + \text{CH}_3\text{C}_3\text{H}_4$	1.56E+11	0.00	5500	f
3.5, 4.22	$1\text{-CH}_3\text{C}_3\text{H}_5 + \text{C}_6\text{H}_5\text{O} \rightarrow \text{CH}_3\text{C}_3\text{H}_4 + \text{C}_6\text{H}_5\text{OH}$	3.16E+11	0.00	8000	e
3.5, 4.24	$2\text{-CH}_3\text{C}_3\text{H}_5 + \text{C}_6\text{H}_5\text{O} \rightarrow \text{CH}_3\text{C}_3\text{H}_4 + \text{C}_6\text{H}_5\text{OH}$	3.16E+11	0.00	8000	e
3.5	$5\text{-CH}_3\text{C}_3\text{H}_5 + \text{C}_6\text{H}_5\text{O} \rightarrow \text{CH}_3\text{C}_3\text{H}_4 + \text{C}_6\text{H}_5\text{OH}$	1.58E+11	0.00	8000	f
	$1\text{-CH}_3\text{C}_3\text{H}_5 + \text{C}_3\text{H}_5 \rightarrow \text{CH}_3\text{C}_3\text{H}_4 + \text{C}_3\text{H}_6$	3.16E+11	0.00	8000	h
	$2\text{-CH}_3\text{C}_3\text{H}_5 + \text{C}_3\text{H}_5 \rightarrow \text{CH}_3\text{C}_3\text{H}_4 + \text{C}_3\text{H}_6$	3.16E+11	0.00	8000	h
	$5\text{-CH}_3\text{C}_3\text{H}_5 + \text{C}_3\text{H}_5 \rightarrow \text{CH}_3\text{C}_3\text{H}_4 + \text{C}_3\text{H}_6$	1.58E+11	0.00	8000	h
4.13	$\text{H} + \text{C}_6\text{H}_6 \rightarrow \text{CH}_3\text{C}_3\text{H}_4$	5.22E+28	-4.30	28800	Ritter, 1990
4.14	$\text{H} + \text{C}_6\text{H}_6 \rightarrow \text{c-C}_6\text{H}_7$	8.18E+57	-13.20	26300	Ritter, 1990
4.15	$\text{c-C}_6\text{H}_7 \rightarrow \text{CH}_3\text{C}_3\text{H}_4$	5.00E+12	0.00	38100	Ritter, 1990
	$\text{CH}_2\text{C}_6\text{H}_4\text{OH} + \text{H} \rightarrow \text{CH}_3\text{C}_6\text{H}_4\text{OH}$	1.80E+14	0.00	0	Arends, 1993
	$\text{CH}_3\text{C}_6\text{H}_4\text{OH} + \text{CH}_3 \rightarrow \text{CH}_3\text{C}_6\text{H}_4\text{O} + \text{CH}_4$	2.51E+11	0.00	8000	i
	$\text{CH}_3\text{C}_6\text{H}_4\text{OH} + \text{C}_6\text{H}_5\text{O} \rightarrow \text{CH}_3\text{C}_6\text{H}_4\text{O} + \text{C}_6\text{H}_5\text{OH}$	1.05E+11	0.00	9500	j
4.23	$\text{C}_6\text{H}_5\text{OH} + \text{CH}_2\text{C}_6\text{H}_4\text{OH} \rightarrow \text{C}_6\text{H}_5\text{O} + \text{CH}_3\text{C}_6\text{H}_4\text{OH}$	1.05E+11	0.00	9500	j
	$\text{CH}_3\text{C}_6\text{H}_4\text{OH} + \text{CH}_3 \rightarrow \text{CH}_2\text{C}_6\text{H}_4\text{OH} + \text{CH}_4$	3.16E+11	0.00	9500	k
	$\text{CH}_3\text{C}_6\text{H}_4\text{OH} + \text{H} \rightarrow \text{CH}_3\text{C}_6\text{H}_4\text{O} + \text{H}_2$	1.15E+14	0.00	12400	i
	$\text{CH}_3\text{C}_6\text{H}_4\text{O} + \text{H} \rightarrow \text{CH}_3\text{C}_6\text{H}_4\text{OH}$	2.50E+14	0.00	0	l
3.2	$\text{CH}_3\text{C}_6\text{H}_4\text{O} \rightarrow \text{CO} + \text{CH}_3\text{C}_3\text{H}_4$	7.40E+11	0.00	43853	l
4.16	$\text{C}_3\text{H}_5 + \text{C}_3\text{H}_5 \rightarrow \text{C}_{10}\text{H}_8 + \text{H}_2$	1.00E+11	0.00	0	Arends, 1993

Reaction	A	n	E <sub>a</sub>	Reference
$C_3H_6 + CH_3 \rightarrow CH_4 + C_3H_5$	3.11E+11	0.00	5500	Dean, 1990
$C_3H_6 + C_2H_5 \rightarrow C_3H_5 + C_2H_6$	4.67E+11	0.00	5500	m
$C_3H_5 + H \rightarrow C_3H_6$	1.00E+14	0.00	0	Emdee, 1992
$C_3H_6 + H \rightarrow C_3H_5 + H_2$	2.19E+08	1.77	3000	Emdee, 1992
$C_3H_6 + C_6H_5O \rightarrow C_3H_5 + C_6H_5OH$	3.16E+11	0.00	8000	Emdee, 1992
$C_3H_6 + CH_3C_6H_4O \rightarrow C_3H_5 + CH_3C_6H_4OH$	3.16E+11	0.00	8000	1
$C_6H_6 + CH_3 \rightarrow C_6H_5 + CH_4$	2.00E+11	0.00	11233	Kopinke, 1994
$C_6H_5 + H \rightarrow C_6H_6$	2.20E+14	0.00	0	Ackermann, 1990
$C_6H_6 + H \rightarrow C_6H_5 + H_2$	2.50E+14	0.00	16000	Kiefer, 1985
$C_6H_5 + C_6H_5OH \rightarrow C_6H_6 + C_6H_5O$	4.91E+12	0.00	4400	Fahr, 1988
$C_6H_5CH_3 \rightarrow C_6H_5 + CH_3$	1.40E+16	0.00	99800	Rao, 1989
$CH_3 + CH_3 (+M) \rightarrow C_2H_6 (+M)$	2.12E+16	-0.97	620	Bowman
4.5	Low pressure limit:	1.77E+50	6220	
	Troe parameters:	0.532	151	4970
3.1	$H + CH_4 \rightarrow CH_3 + H_2$	1.62	10840	Bowman
	$H + CH_3 (+M) \rightarrow CH_4 (+M)$	-0.63	383	Bowman
	Low pressure limit:	2.48E+33	2440	
	Troe parameters:	0.783	74	6964
	$H + C_2H_4 (+M) \rightarrow C_2H_5 (+M)$	0.45	1820	Bowman
	Low pressure limit:	1.20E+42	6970	
	Troe parameters:	0.975	210	4374

Reaction	A	n	E <sub>a</sub>	Reference
H + C <sub>2</sub> H <sub>6</sub> → C <sub>2</sub> H <sub>5</sub> + H <sub>2</sub>	1.15E+08	1.90	7530	Bowman
CH <sub>3</sub> + CH <sub>3</sub> → H + C <sub>2</sub> H <sub>5</sub>	4.99E+12	0.10	10600	Bowman
CH <sub>3</sub> + C <sub>2</sub> H <sub>6</sub> → C <sub>2</sub> H <sub>5</sub> + CH <sub>4</sub>	6.14E+06	1.74	10450	Bowman

<sup>a</sup> Units: cc, mol, s, cal. In this and all tables  $E \pm n \equiv \times 10^{+n}$ .

<sup>b</sup> Suryan et al. [1989], adjusted from  $10^{15.5} \exp(-63.5 \text{ kcal} \cdot \text{mol}^{-1}/RT)$ .

<sup>c</sup> This work.

<sup>d</sup> Estimated from  $\text{HO}_2 + \text{C}_2\text{H}_6 \rightarrow \text{H}_2\text{O}_2 + \text{C}_2\text{H}_5$  [Pitz et al., 1984].

<sup>e</sup> Estimated from analogous abstraction of H from C<sub>3</sub>H<sub>6</sub>.

<sup>f</sup> Estimated from analogous abstraction of H from C<sub>3</sub>H<sub>6</sub>; A factor divided by 2 since 5-CH<sub>3</sub>C<sub>3</sub>H<sub>5</sub> possesses only one easily abstractable H.

<sup>g</sup> A factor for C<sub>3</sub>H<sub>5</sub>+H.

<sup>h</sup> Rate parameters from CH<sub>3</sub>C<sub>3</sub>H<sub>5</sub>+C<sub>6</sub>H<sub>5</sub>O.

<sup>i</sup> Estimated from analogous abstraction of H from phenol.

<sup>j</sup> Estimated from CH<sub>3</sub>C<sub>6</sub>H<sub>4</sub>OH+C<sub>6</sub>H<sub>5</sub>CH<sub>2</sub>→CH<sub>3</sub>C<sub>6</sub>H<sub>4</sub>O+C<sub>6</sub>H<sub>5</sub>CH<sub>3</sub> [Emdee et al., 1992].

<sup>k</sup> Estimated from analogous reaction of toluene and methyl [Kerr and Parsonage, 1976].

<sup>l</sup> Rate parameters from analogous reaction of phenoxy.

<sup>m</sup> Estimated from C<sub>3</sub>H<sub>6</sub>+CH<sub>3</sub>→C<sub>3</sub>H<sub>5</sub>+CH<sub>4</sub>.

\* Indicates rate parameters are pressure dependent, calculated for P=1 atm.

Table 4.9: Thermodynamic properties for select species.<sup>a</sup>

Species	H <sub>f</sub> (298)	S(298)	C <sub>P</sub> (300)	C <sub>P</sub> (400)	C <sub>P</sub> (500)	C <sub>P</sub> (600)	C <sub>P</sub> (800)	C <sub>P</sub> (1000)	C <sub>P</sub> (1500)	Reference
C <sub>3</sub> H <sub>5</sub> <sup>•</sup>	63.60	66.80	18.43	24.47	29.57	33.63	38.95	42.76	48.06	Burcat, 1993
C <sub>3</sub> H <sub>6</sub>	32.10	65.52	18.13	24.46	30.12	34.82	41.22	45.87	52.36	Burcat, 1993
C <sub>6</sub> H <sub>5</sub> <sup>•</sup>	78.50	68.91	19.00	25.45	30.96	35.52	42.10	46.58	52.76	Burcat, 1993
C <sub>6</sub> H <sub>6</sub>	19.81	64.37	19.92	27.09	33.25	38.38	45.87	51.05	58.31	Burcat, 1993
C <sub>6</sub> H <sub>5</sub> O <sup>•</sup>	9.30	73.63	22.65	29.88	35.80	40.59	47.53	52.22	58.96	Burcat, 1993
C <sub>6</sub> H <sub>5</sub> OH	-23.03	75.33	24.93	32.38	38.63	43.68	50.73	55.56	62.37	Burcat, 1993
C <sub>6</sub> H <sub>5</sub> OCH <sub>3</sub>	-17.10	84.01	29.67	38.91	46.53	52.77	62.06	68.33	77.22	b
C <sub>6</sub> H <sub>5</sub> OCH <sub>2</sub> <sup>•</sup>	79.99	88.28	28.35	37.07	43.97	49.42	57.08	62.04	69.80	b
•CH <sub>2</sub> C <sub>6</sub> H <sub>4</sub> OH	7.15	86.21	30.71	40.82	49.33	56.47	67.43	75.11	72.77	b
CH <sub>3</sub> C <sub>6</sub> H <sub>4</sub> OH	-31.62	85.06	29.97	38.82	46.53	52.93	62.08	68.61	77.64	Burcat, 1993
CH <sub>3</sub> C <sub>6</sub> H <sub>4</sub> O <sup>•</sup>	2.80	78.89	50.37	52.48	54.65	56.85	61.20	65.29	73.43	Burcat, 1993
(H)(CH <sub>3</sub> )C <sub>6</sub> H <sub>4</sub> O	-15.02	78.12	28.78	38.42	46.39	52.96	62.76	69.39	78.70	b
•C <sub>6</sub> H <sub>4</sub> OH	39.25	77.68	23.52	30.35	35.95	40.51	47.24	51.75	58.15	b
5-CH <sub>3</sub> C <sub>3</sub> H <sub>5</sub>	28.30	73.01	22.23	29.25	35.56	41.18	50.48	57.46	67.19	Ritter, 1990
2-CH <sub>3</sub> C <sub>3</sub> H <sub>5</sub>	24.38	74.16	28.07	35.72	41.88	46.85	54.29	59.98	67.74	Burcat, 1993
1-CH <sub>3</sub> C <sub>3</sub> H <sub>5</sub>	22.81	74.44	24.35	32.19	38.73	44.17	52.44	58.22	66.80	b
CH <sub>3</sub> C <sub>3</sub> H <sub>4</sub> <sup>•</sup>	48.06	75.37	23.15	29.92	35.94	41.23	49.78	55.93	63.86	Ritter, 1990
c-C <sub>6</sub> H <sub>7</sub> <sup>•</sup>	49.86	72.02	20.88	28.59	35.04	40.43	48.66	54.39	62.67	Ritter, 1990

<sup>a</sup> Units: H<sub>f</sub>, kcal/mol; S and C<sub>P</sub>, cal/(mol·K).

<sup>b</sup> Estimated using group additivity methods [Benson, 1968; Ritter et al., 1987].

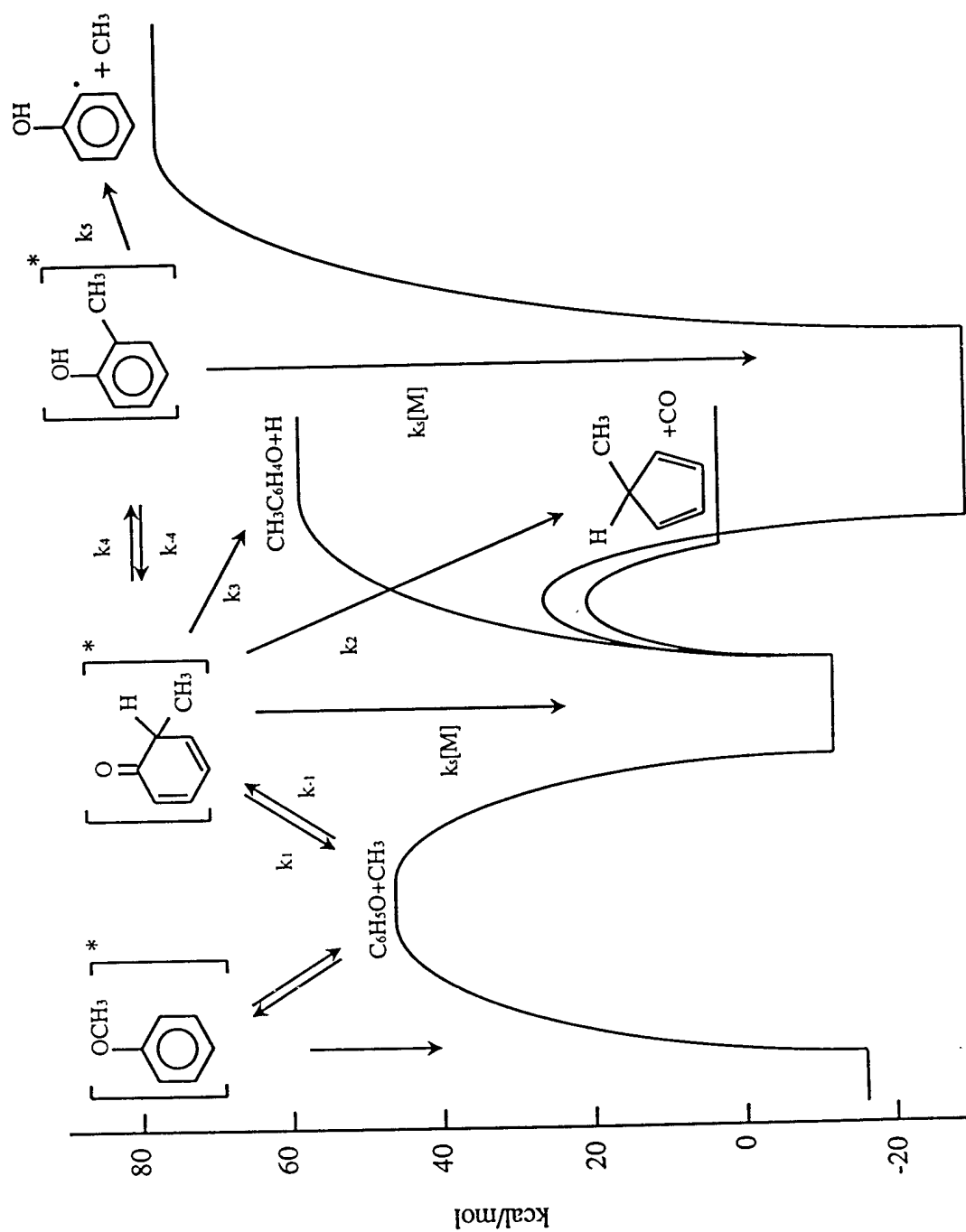


Figure 4.1: Potential energy diagram for  $\text{C}_6\text{H}_5\text{O} + \text{CH}_3$  as evaluated by QRRK.

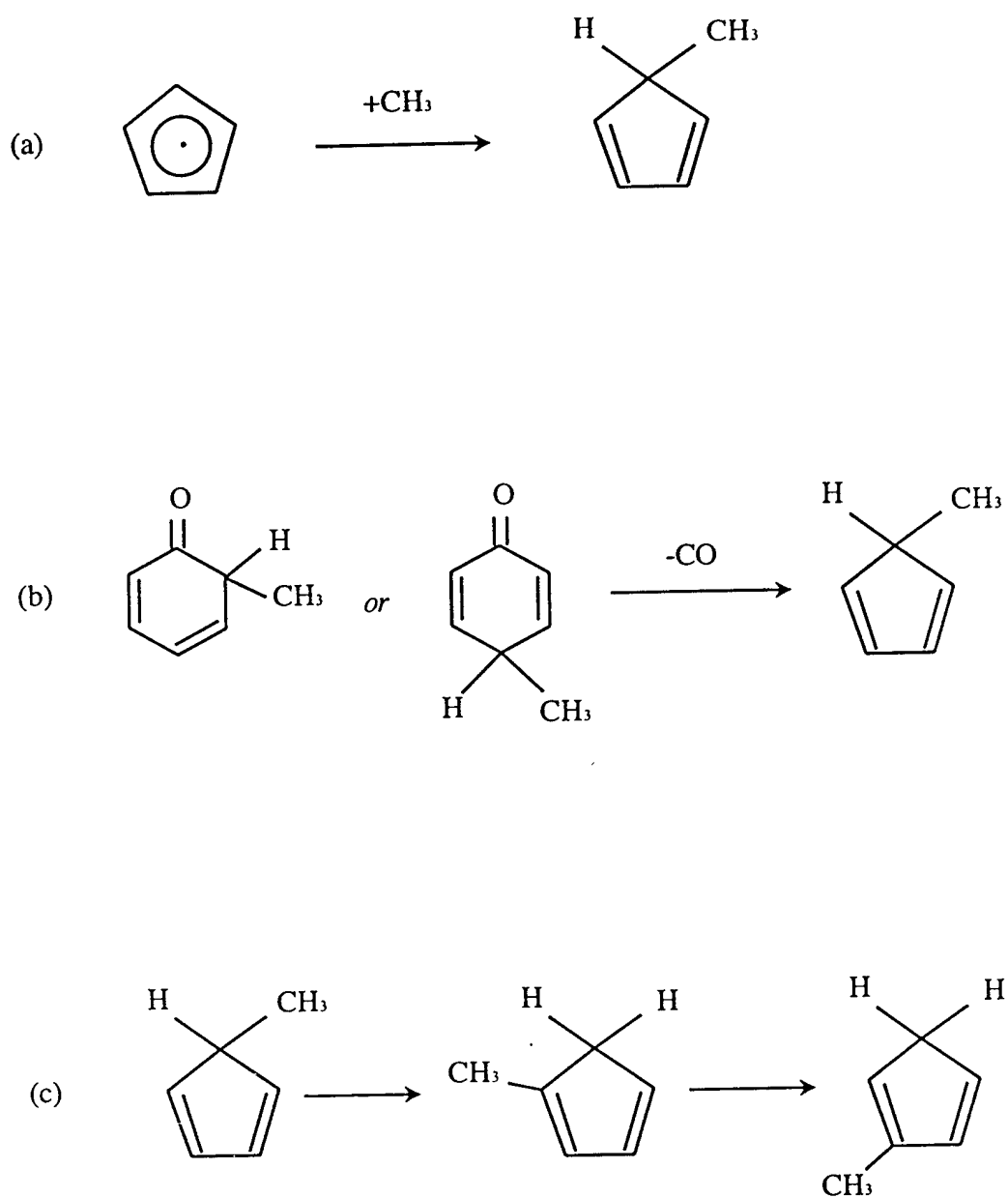


Figure 4.2: Direct formation of 5-CH<sub>3</sub>C<sub>5</sub>H<sub>5</sub> via (a) C<sub>5</sub>H<sub>5</sub>-CH<sub>3</sub> recombination or (b) decomposition of (H)(CH<sub>3</sub>)C<sub>6</sub>H<sub>4</sub>O and (c) subsequent formation of the 1- and 2- isomers by sigmatropic rearrangement(s).

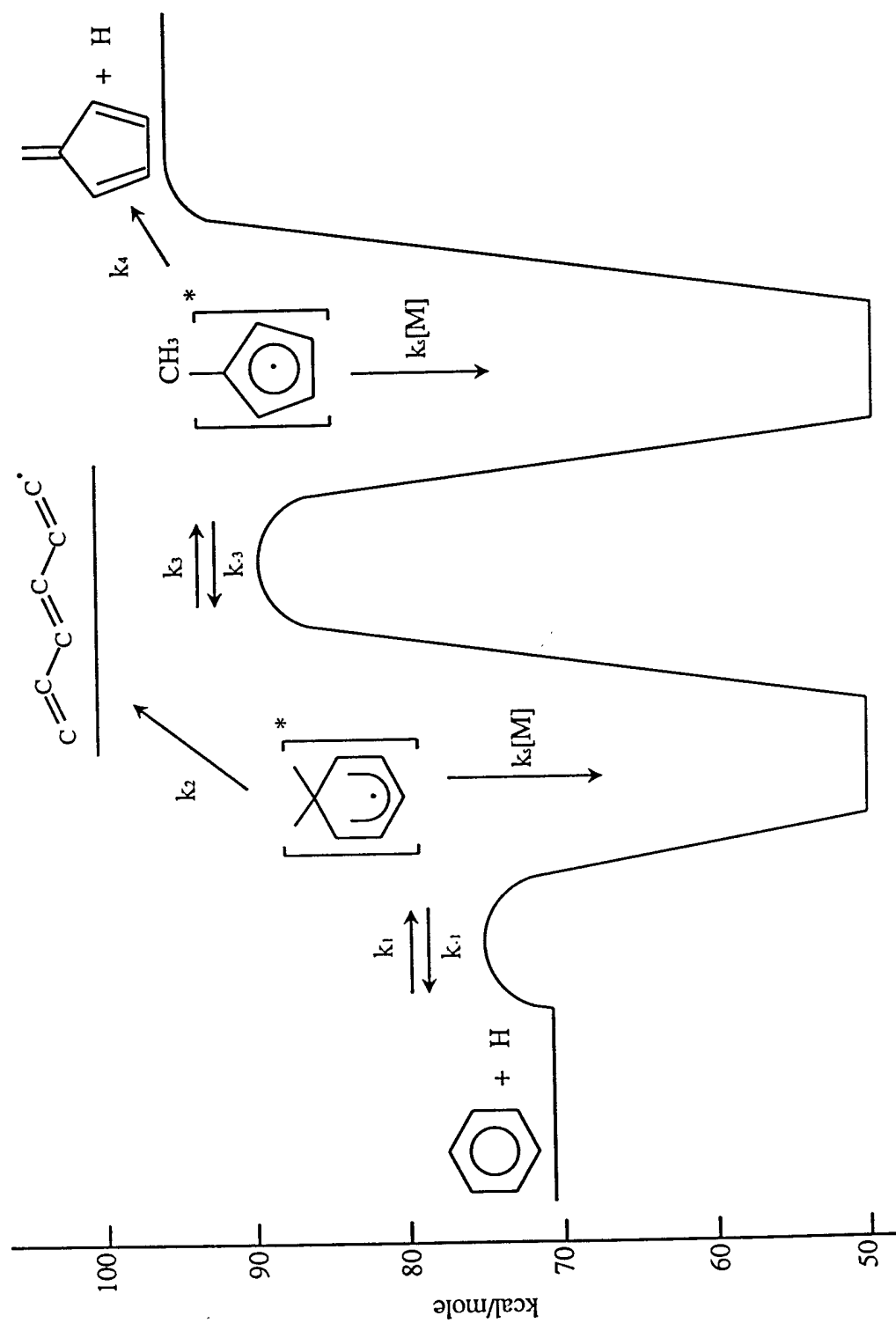


Figure 4.3: Potential energy diagram for  $H + C_4H_6$  addition as evaluated by QRRK [Ritter et al., 1990].

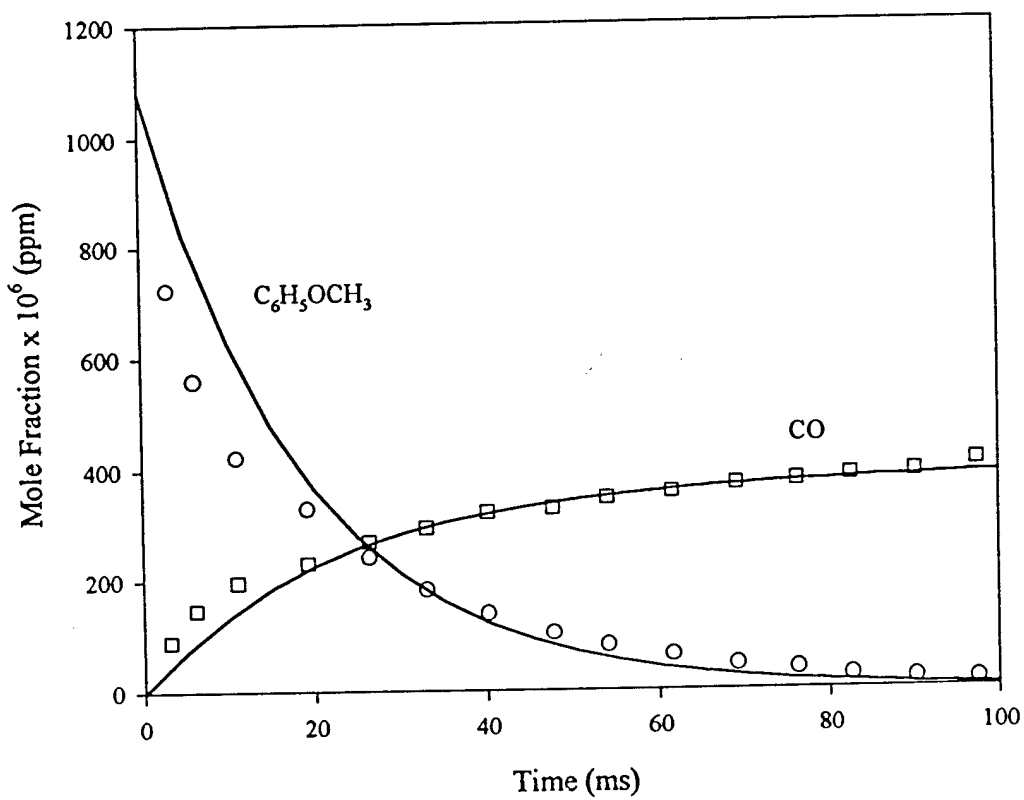


Figure 4.4: Comparison of anisole pyrolysis data ( $T=1003$  K) with model predictions of carbon monoxide and anisole. Symbols represent experimental data; solid lines are model predictions.



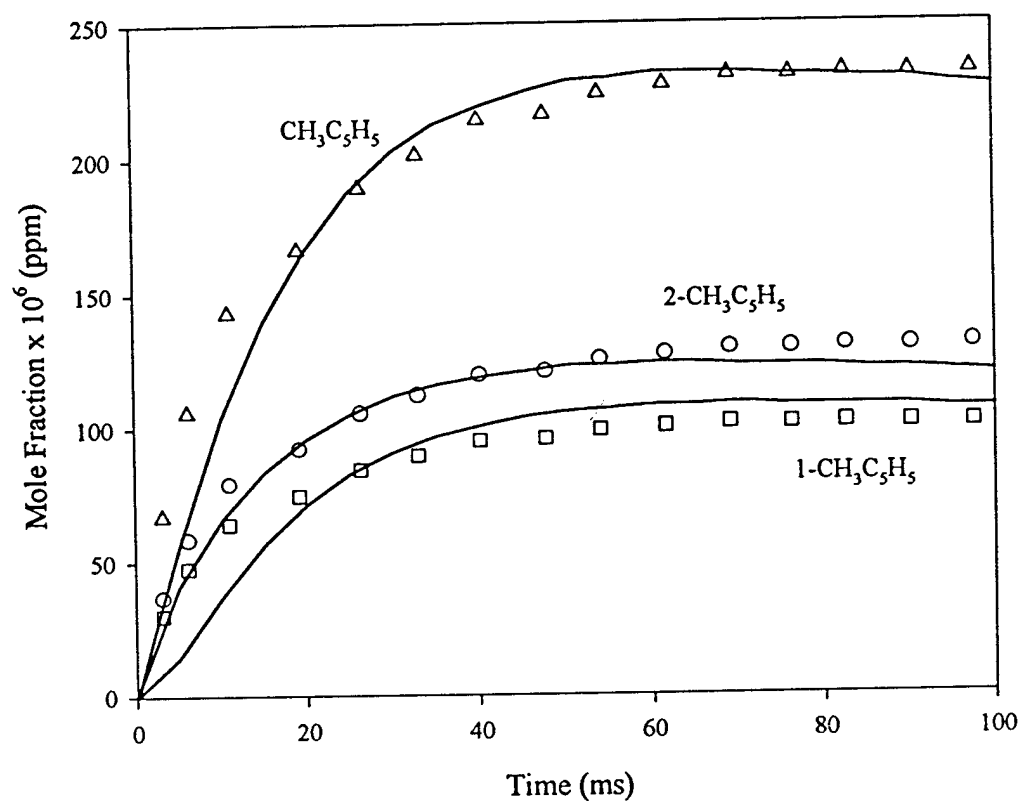


Figure 4.5: Comparison of anisole pyrolysis data ( $T=1003$  K) with model predictions of methylcyclopentadiene. Symbols represent experimental data; solid lines are model predictions.

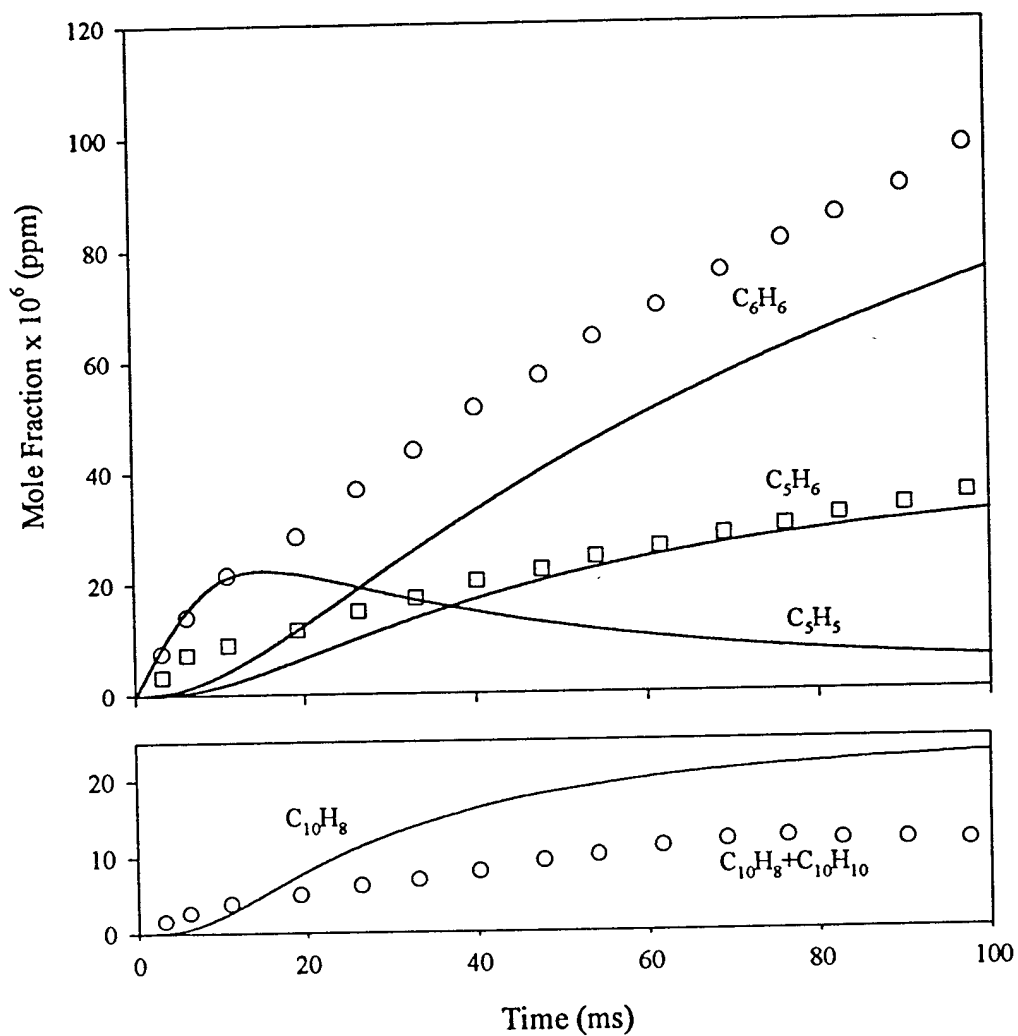


Figure 4.6: Comparison of anisole pyrolysis data ( $T=1003$  K) with model predictions of benzene, cyclopentadiene, cyclopentadienyl radical, and naphthalene. Symbols represent experimental data; solid lines are model predictions.

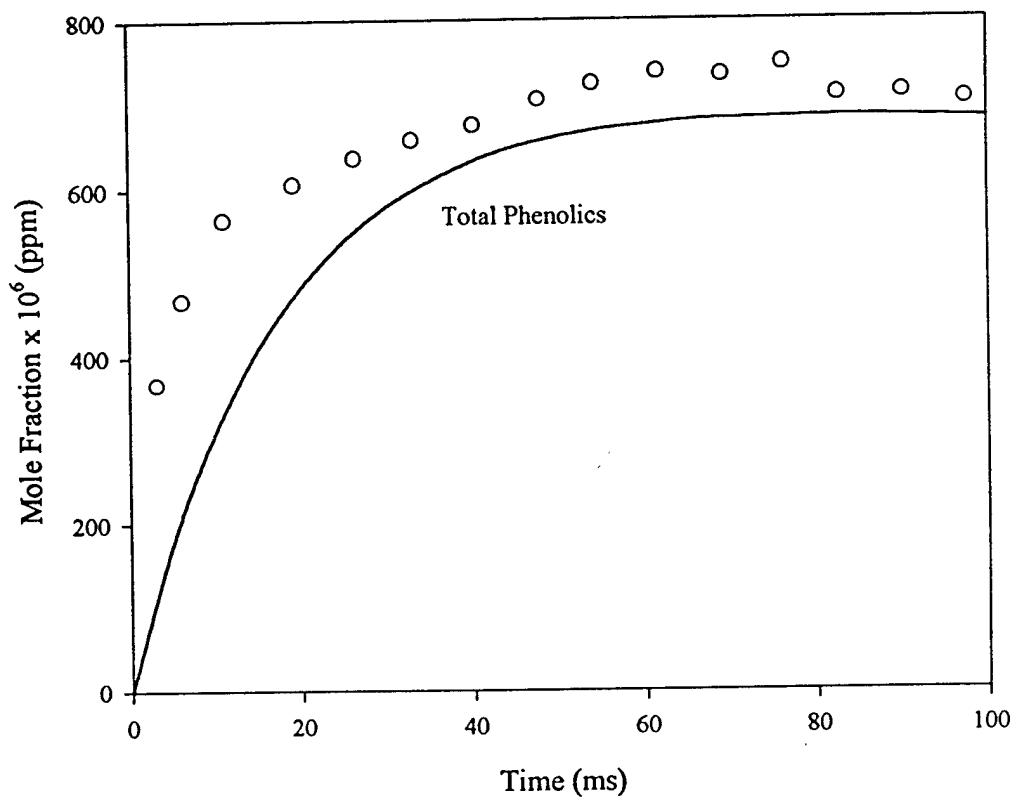


Figure 4.7: Comparison of anisole pyrolysis data ( $T=1003$  K) with model predictions of total phenolics ( $C_6H_5OH + CH_3C_6H_4OH$ ). Symbols represent experimental data; solid lines are model predictions.

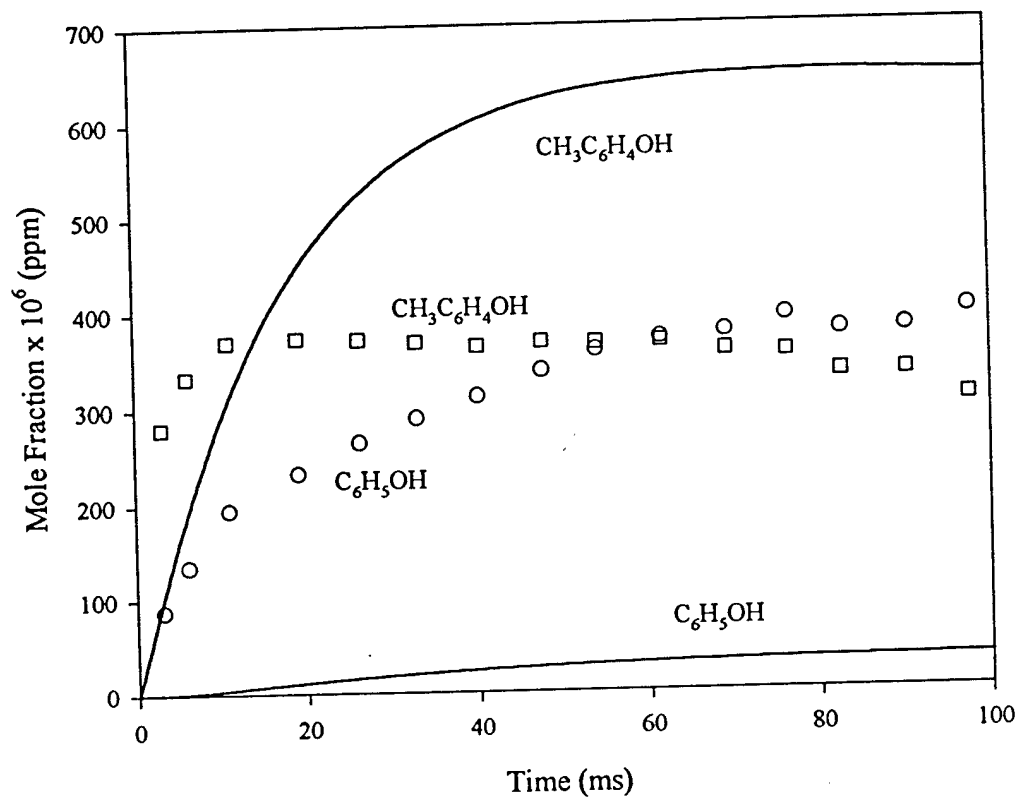


Figure 4.8: Comparison of anisole pyrolysis data ( $T=1003$  K) with model predictions of phenol and cresols. Symbols represent experimental data; solid lines are model predictions.

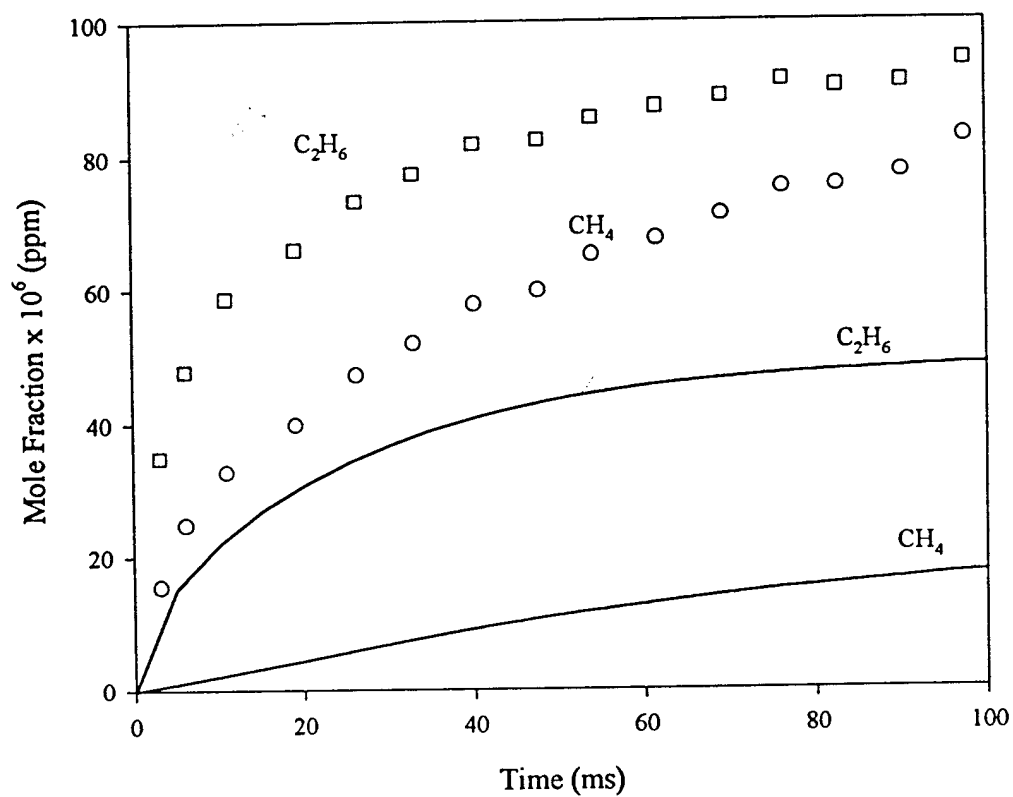


Figure 4.9: Comparison of anisole pyrolysis data ( $T=1003$  K) with model predictions of methane and ethane. Symbols represent experimental data; solid lines are model predictions.

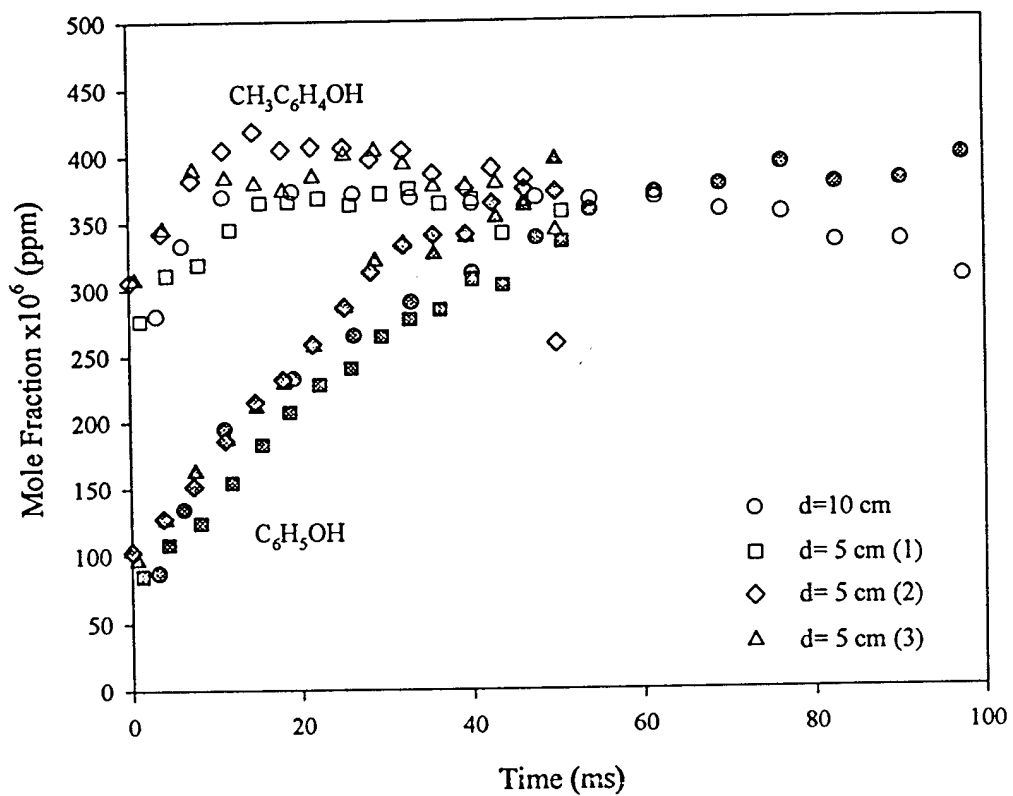


Figure 4.10: Comparison of species profiles from anisole pyrolysis in 5 and 10 cm diameter test sections. Nominal temperature=1000 K.

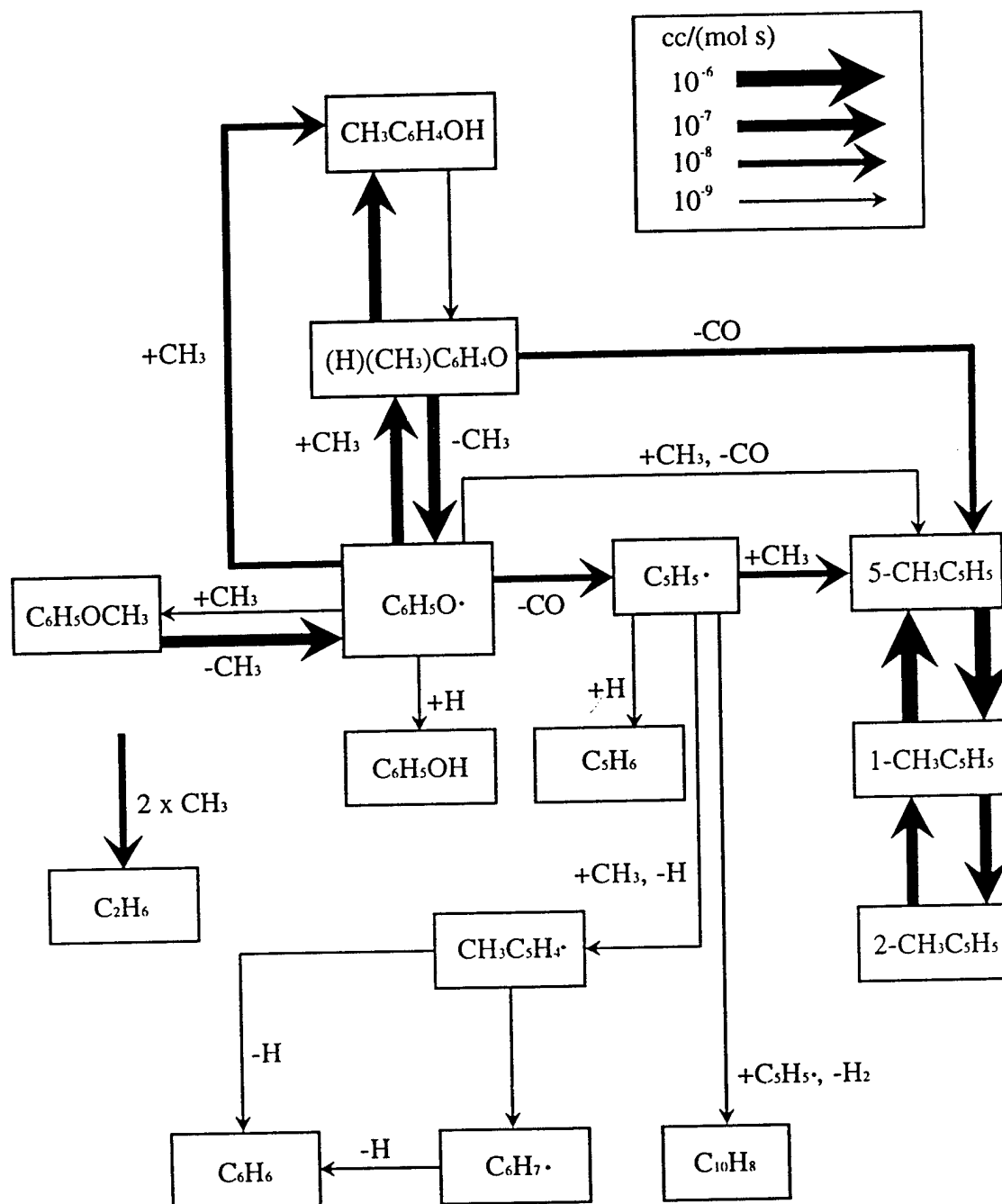


Figure 4.11: Flux diagram at 15 ms for anisole pyrolysis model (Table 4.1).

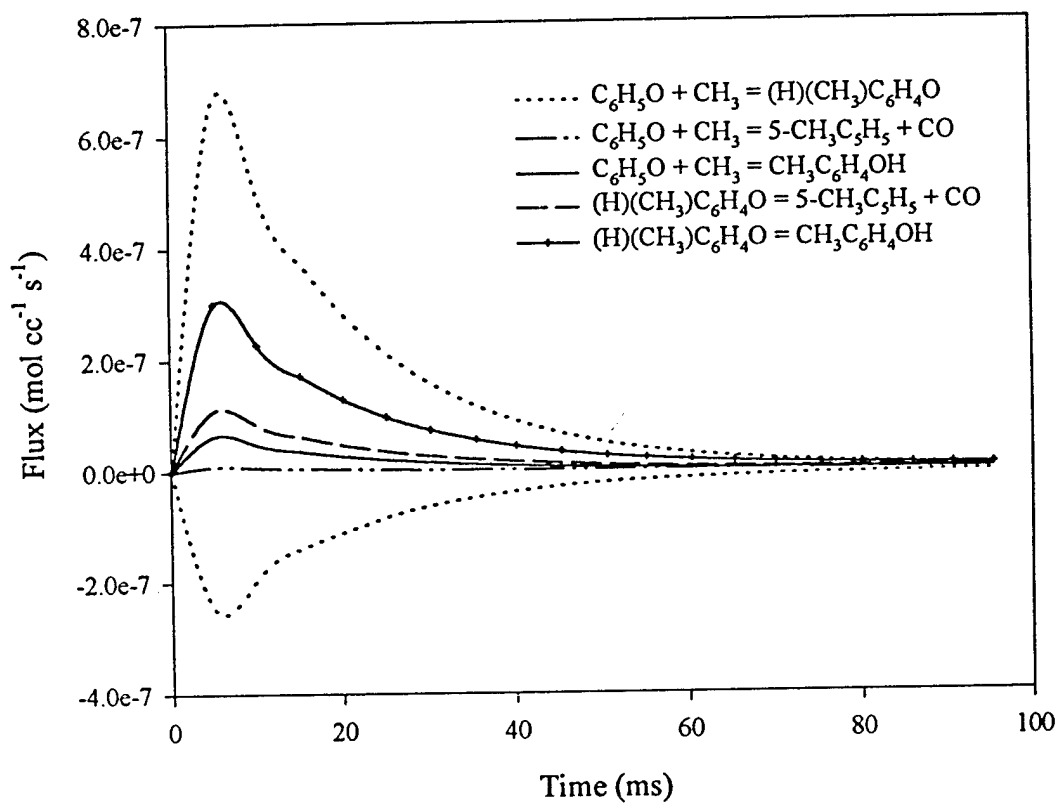


Figure 4.12: Comparison of reaction fluxes for direct and indirect formation of cresol and methylcyclopentadiene. Negative flux indicates the reverse of the reaction as written.



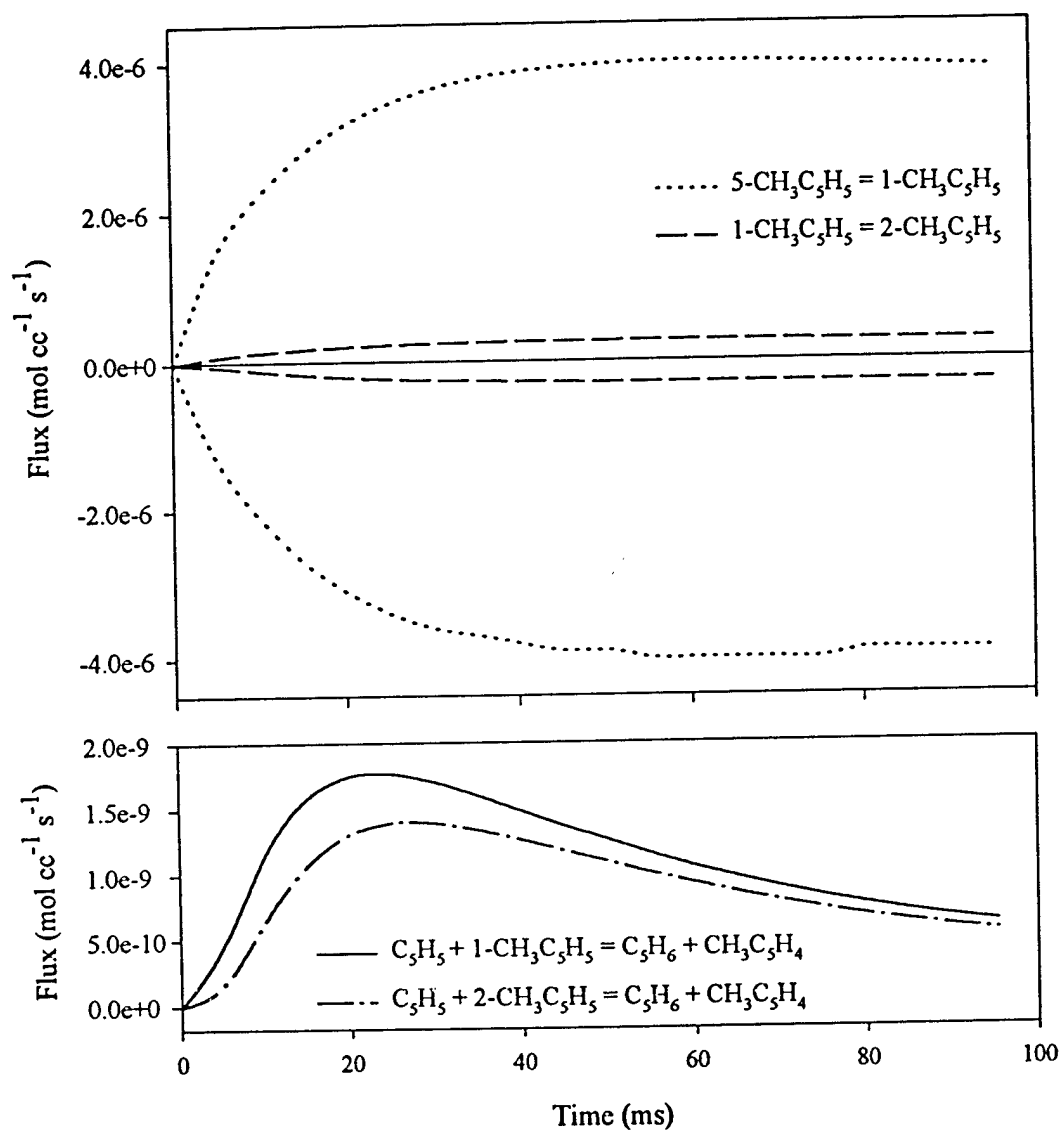


Figure 4.13: Flux of 1- and 2-methylcyclopentadiene through isomerization and abstraction reactions. Negative flux indicates reverse of reaction as written.

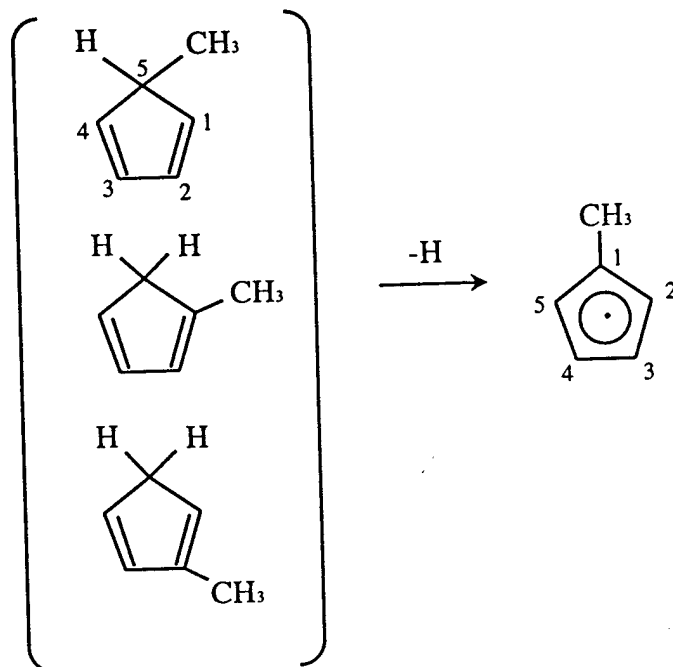


Figure 4.14: Formation of  $\text{CH}_3\text{C}_5\text{H}_4$  radical from 5-, 1-, or 2- $\text{CH}_3\text{C}_5\text{H}_5$ .

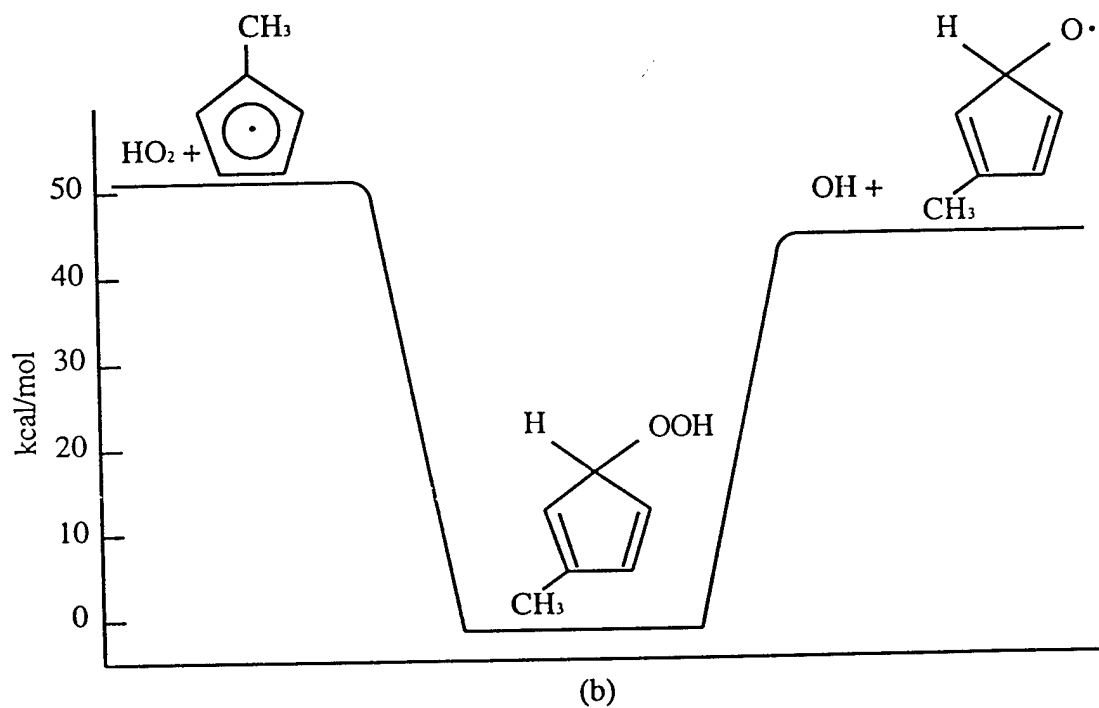
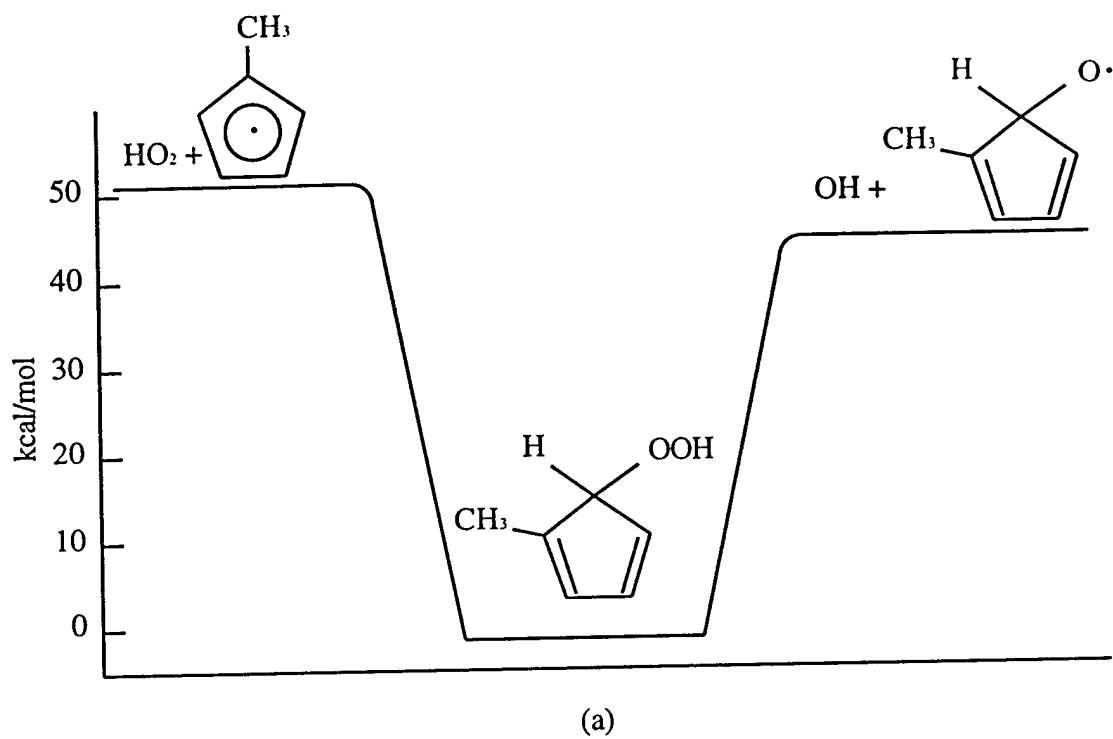


Figure 4.15: Addition of  $\text{HO}_2$  to  $\text{CH}_3\text{C}_5\text{H}_7$  at the (a) 2 and (b) 3 sites. Energies are approximate.

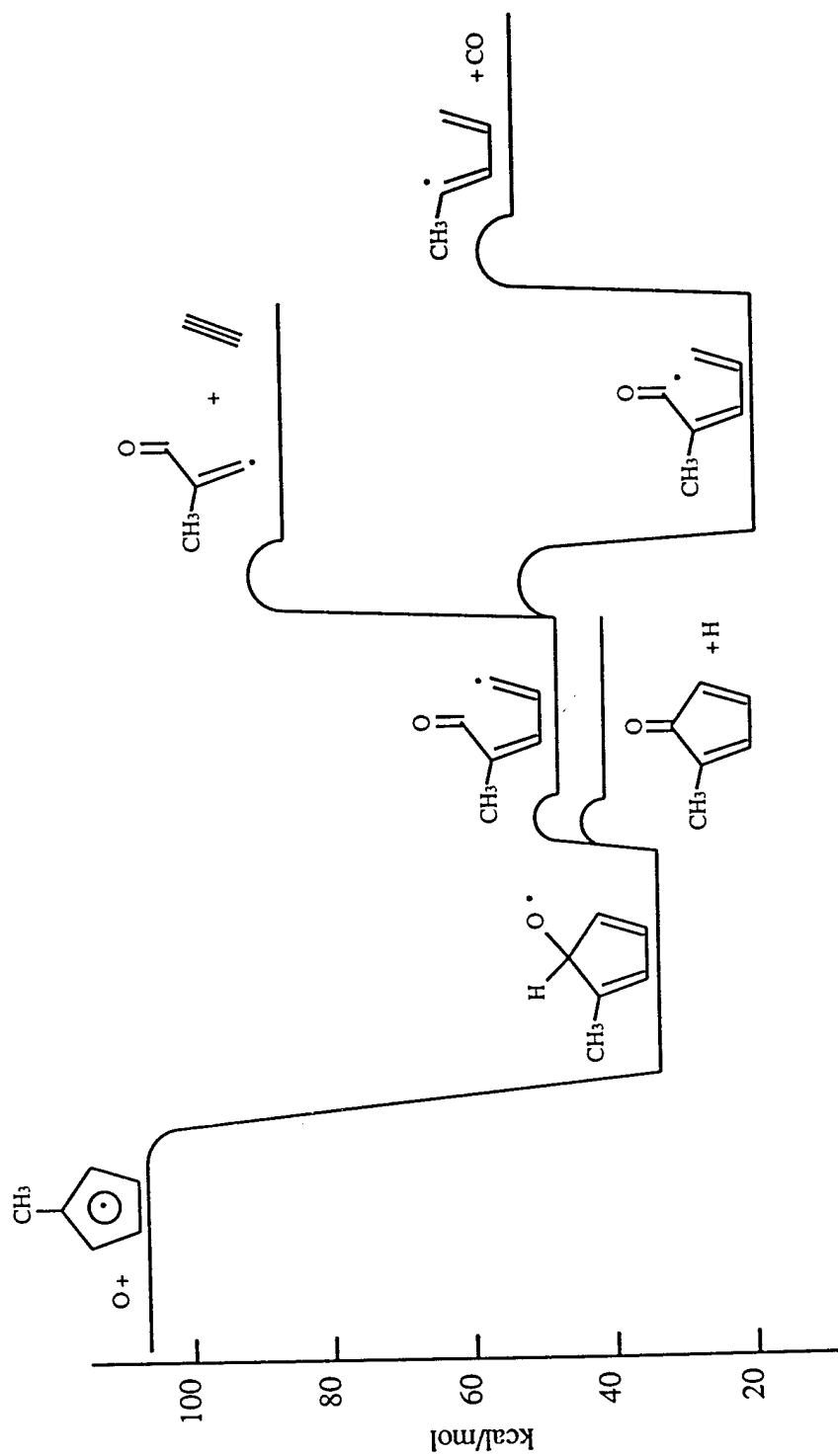


Figure 4.16a: Addition of O to  $\text{CH}_3\text{C}_3\text{H}_4$  at the 2 site. Energies are approximate.

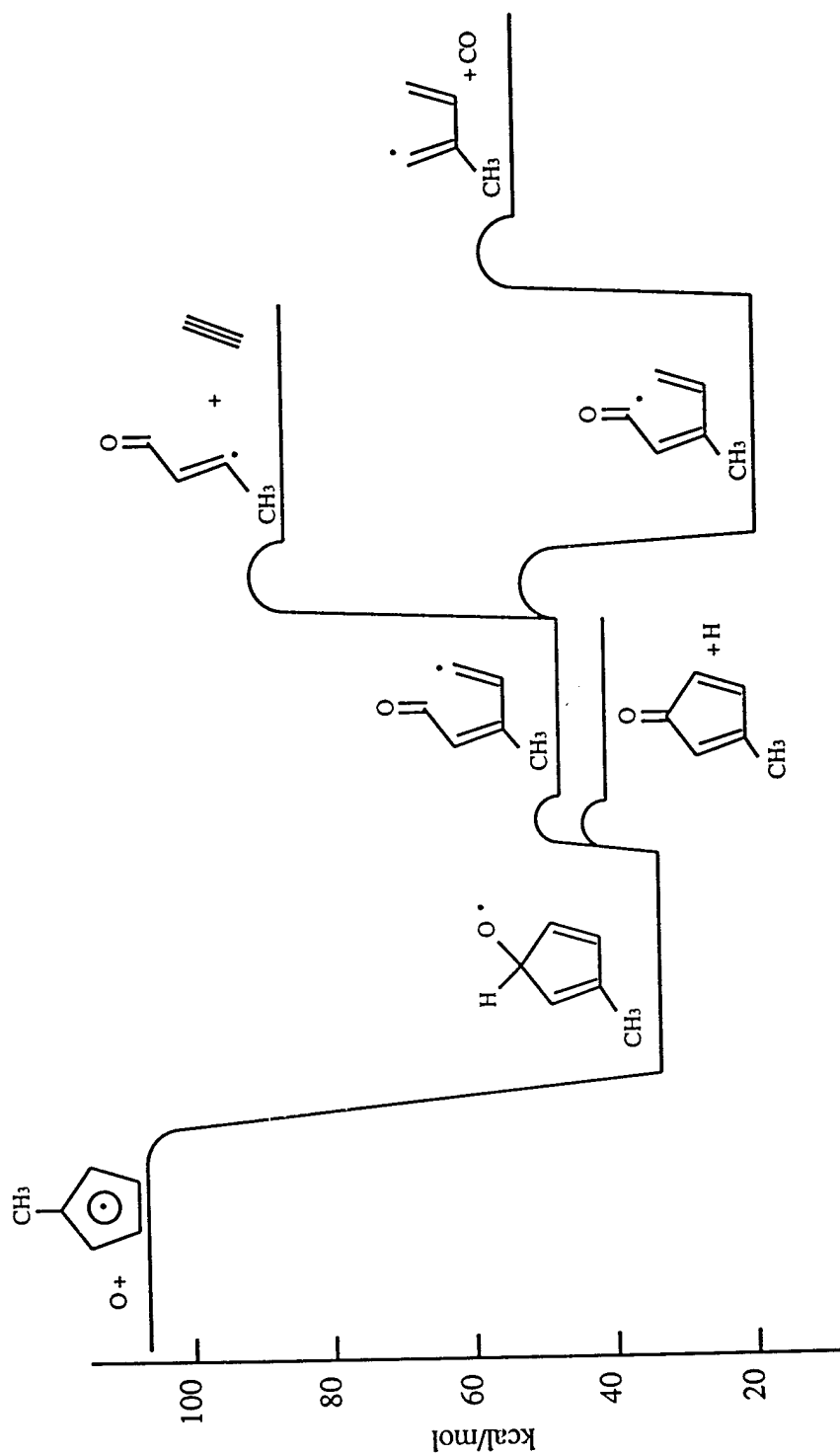


Figure 4.16b: Addition of O to CH<sub>3</sub>C<sub>3</sub>H<sub>4</sub> at the 3 site. Energies are approximate.

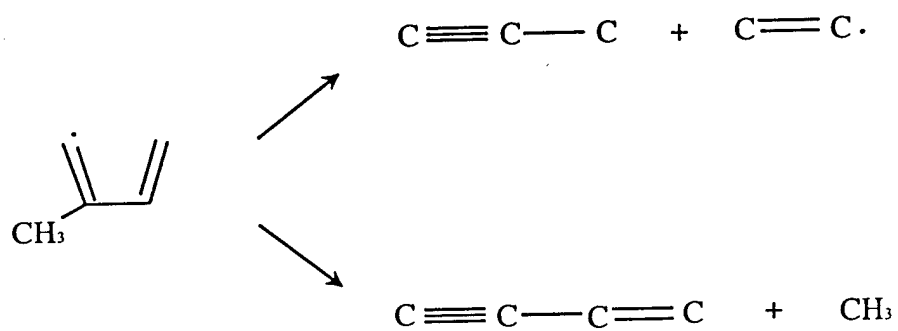
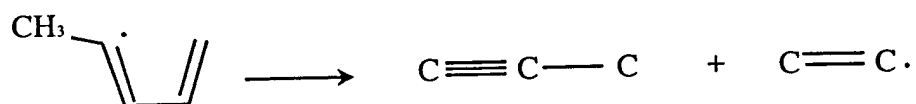
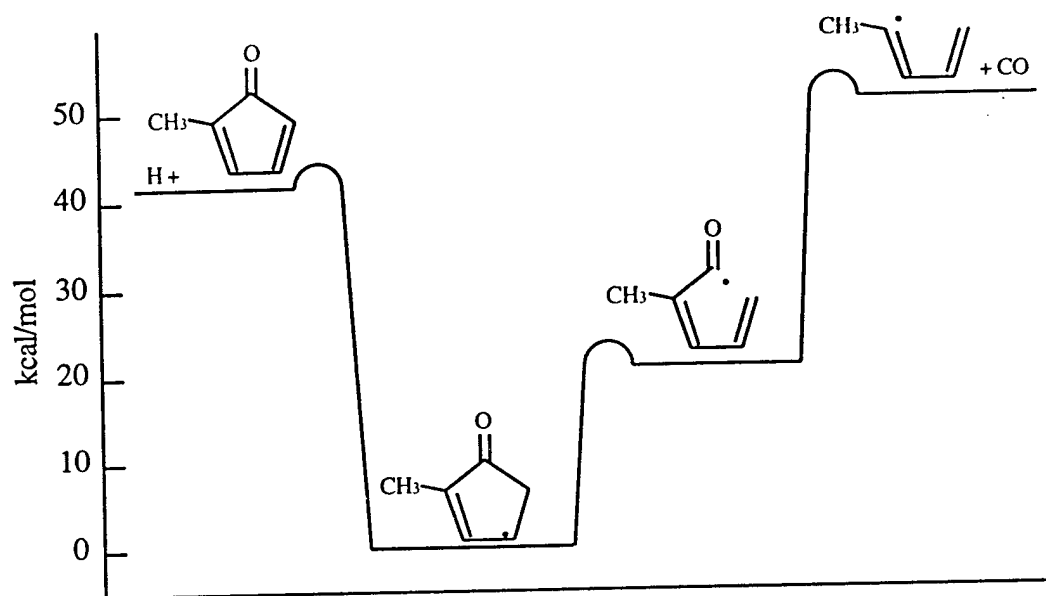
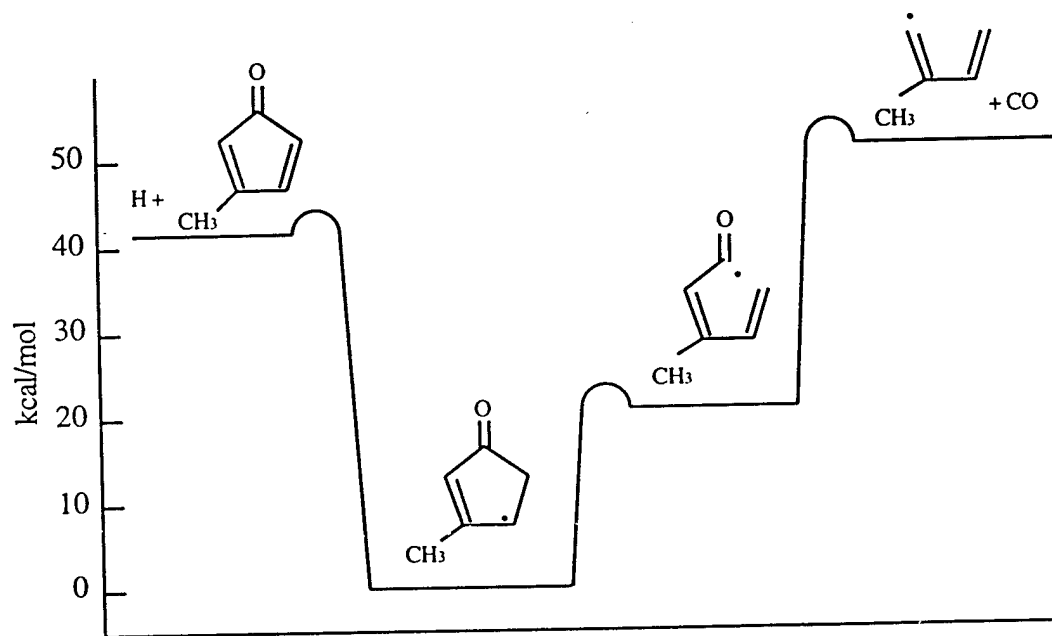


Figure 4.17: Subsequent reactions of the 1,3-pentadien-4-yl and 2-methyl-1,3-butadien-1-yl radicals.



(a)



(b)

Figure 4.19: Addition of H to (a) 1- and (b) 2-methylcyclopentadien-1-one. Energies are approximate.

## CHAPTER 5. PHENOL PYROLYSIS AND OXIDATION

---

Phenol is a major reaction intermediate in the combustion of aromatic hydrocarbons [Bittner and Howard, 1981; Venkat et al., 1982; Emdee et al., 1992] and therefore the development of a comprehensive model of aromatics chemistry requires an understanding of phenol oxidation. Nonetheless, few high-temperature phenol studies have been reported [Cypres and Bettens, 1974, 1975a; He et al., 1988; Lovell et al., 1989; Manion and Louw, 1989] and no gas-phase oxidation data are available in the archival literature. Therefore, the primary intent of the present phenol study was the acquisition of experimental data over a range of stoichiometries. Reaction intermediate data obtained from flow reactor experiments near 1170 K are presented in this chapter. In addition, reactions which are expected to be important in kinetic modeling (in particular, reactions of phenol itself) will be discussed.

The set of experimental conditions is given in Table 5.1.

Table 5.1: Experimental conditions for phenol experiments.

Equivalence Ratio, $\phi$	Temperature (K)	Residence Time (ms)	Fuel Loading (ppm)
pyrolysis	1173	131	1004
1.73	1169	126	533
1.03	1169	127	538
0.64	1169	126	533



## 5.1 PYROLYSIS

As expected in view of prior studies [Cypres and Bettens, 1975a; Colussi et al., 1977; Lovell, 1989; Butler, 1992], major reaction intermediates found in the phenol pyrolysis experiments were carbon monoxide and cyclopentadiene. Minor species observed included benzene, acetylene, naphthalene, methane, and methylcyclopentadiene.

### C<sub>6</sub>H<sub>5</sub>OH Consumption

The phenol decay profile is shown in Figure 5.1. The destruction of phenol will occur initially via the thermal decomposition:



A rate constant for the reverse reaction was determined by He et al. [1988] to be  $2.5 \times 10^{14} \text{ cc}\cdot\text{mol}^{-1}\cdot\text{s}^{-1}$ . This value is consistent with earlier observations [Tsang, 1986] that rates of recombinations involving resonance stabilized radicals seem to be especially large.

Following initiation, phenol consumption will proceed also via reactions with H atom:



He et al. [1988] determined the rate constants  $k_{(1.17)} = 1.15 \times 10^{14} \exp(-6240/T) \text{ cc}\cdot\text{mol}^{-1}\cdot\text{s}^{-1}$  and  $k_{(1.18)} = 2.21 \times 10^{13} \exp(-3990/T) \text{ cc}\cdot\text{mol}^{-1}\cdot\text{s}^{-1}$ . Their results indicate that displacement is favored over abstraction for  $T \leq 1360 \text{ K}$ . This finding has important implications for aromatics oxidation. Overall reaction progress is hindered since displacement results in the unoxidized product benzene [ibid.]. OH produced in the displacement reaction will abstract H from phenol to form water:



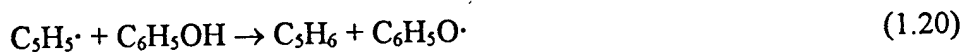
He et al. [ibid.] found the rate constant for reaction of OH with phenol to be  $6 \times 10^{12} \text{ cc}\cdot\text{mol}^{-1}\cdot\text{s}^{-1}$  at 1032 K. The authors concluded that this result must correspond to abstraction of the phenolic H since the previously determined [Tully et al., 1981; Perry et al., 1977] rate constant for attack on the ring is a factor of 10 smaller.

#### CO and C<sub>5</sub>H<sub>6</sub>

As discussed in previous chapters, the phenoxy radical decomposes unimolecularly to CO and cyclopentadienyl radical:



The parent species cyclopentadiene is derived via reaction of the radical C<sub>5</sub>H<sub>5</sub>· with a hydrogen donor, e.g. the initial fuel:



Carbon monoxide and cyclopentadiene profiles are shown in Figure 5.2. Both the CO and C<sub>5</sub>H<sub>6</sub> profiles are linear in time. Also, the CO yield exceeds the C<sub>5</sub>H<sub>6</sub> yield by a factor of roughly 1.4. These observations are consistent with those of Lovell [1989] who found that, over a range of experimental conditions, the rate of CO formation was always significantly greater than that of C<sub>5</sub>H<sub>6</sub>. However, the above six reactions taken alone predict nearly equal rates of formation for CO and cyclopentadiene. Lovell suggested the occurrence of a reaction which would remove C<sub>5</sub> species from the system without an equivalent restriction of CO production. Naphthalene and indene, presumably derived from two cyclopentadienyl radicals, were observed by Lovell but their yields were too small to constitute a major sink for C<sub>5</sub>H<sub>5</sub>·. Thermal decomposition of C<sub>5</sub> species was ruled

out since the expected  $C_3H_3\cdot$  pyrolysis products (methane,  $C_3$ 's, and  $C_4$ 's) were not observed. Ultimately, the addition reaction:



was proposed to explain the imbalance of CO and  $C_3H_6$ . It was postulated that the  $C_6H_5OC_3H_3$  product would go unobserved since large, oxygenated aromatics (with low vapor pressures and high boiling points) are difficult to detect by sample trapping and batch analysis.

On the basis of present experimental results which are not entirely consistent with those of Lovell, an alternative analysis is given below.

#### $C_5H_6$ Decomposition

As mentioned above, it was concluded in Lovell's study that the decomposition of  $C_5$  species did not occur. Acetylene, an expected product of cyclopentadiene pyrolysis [Butler, 1992], was reportedly observed. But Lovell's conclusion was based upon the absence of methane and  $C_{3,4}$  species. In the present study, however, both acetylene and methane were observed (Figure 5.3).

Acetylene and allyl radical may be derived via H addition to cyclopentadiene followed by ring opening and decomposition of the resultant linear  $C_5H_7\cdot$  radical [Bozzelli et al., 1990]:



Subsequent reaction of allyl may yield acetylene and methyl radical [Dean, 1990]:

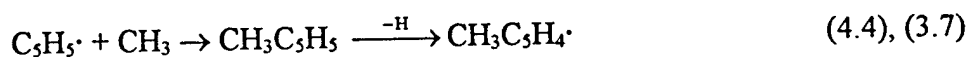


which reacts in part to form methane.

### C<sub>6</sub>H<sub>6</sub>

Benzene yield is shown in Figure 5.2. Consistent with the observations of Lovell, the profile is linear in time. As stated earlier, benzene may be formed directly from phenol via displacement of OH by H atom. But trace methylcyclopentadiene (<2 ppm) observed in the present study suggests an additional benzene formation route.

Methylcyclopentadiene and its radical are likely formed by reactions of C<sub>3</sub>H<sub>5</sub>· and CH<sub>3</sub>:



As discussed in Chapter 4, benzene is evolved from the methylcyclopentadienyl radical [Ritter et al., 1990; Moskaleva et al., 1996]:



Therefore, some fraction of the observed benzene may in fact be derived via C<sub>3</sub>H<sub>5</sub>· rather than from phenol directly. This is consistent with the observations of Butler [1992] who found benzene to be a major product in the pyrolysis of cyclopentadiene at similar temperatures.

### CO/C<sub>3</sub>H<sub>5</sub> Balance

The above discussion implies a balance between CO the sum of C<sub>3</sub>H<sub>5</sub>· derivatives. Derivatives of C<sub>3</sub>H<sub>5</sub>· include C<sub>3</sub>H<sub>6</sub>, CH<sub>3</sub>C<sub>3</sub>H<sub>5</sub>, naphthalene, acetylene, and some fraction of the total benzene. Naphthalene, derived from two C<sub>3</sub>H<sub>5</sub>· radicals, is counted twice in the

tally. Acetylene is weighted by a factor of one half since the thermal decomposition of a single C<sub>5</sub> ring will yield two C<sub>2</sub>H<sub>2</sub> molecules.

The CO/C<sub>3</sub>H<sub>5</sub> comparison is illustrated in Figure 5.4. Near perfect agreement between the CO and C<sub>3</sub>H<sub>5</sub> curves is obtained if all of the observed benzene is assumed to be formed via CH<sub>3</sub>C<sub>3</sub>H<sub>4</sub><sup>•</sup>. Detailed reaction modeling must be undertaken in order to establish whether or not this is a valid assumption for the conditions of the present study.

## 5.2 OXIDATION

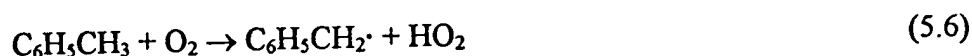
Species profiles obtained from the oxidation of phenol near 1170 K are shown in Figures 5.5–13. While no prior high-temperature phenol oxidation studies have been reported, the oxidation of cyclopentadiene [Butler, 1992] has been investigated in the Princeton APFR. Reaction intermediates observed in the phenol experiments were consistent with the findings of the cyclopentadiene study. Major species included carbon monoxide, carbon dioxide, acetylene, cyclopentadiene, benzene, 1,3-butadiene, ethene, and methane. Minor species were allene, methylacetylene, propene, ethane, methylcyclopentadiene, and naphthalene.

### C<sub>6</sub>H<sub>5</sub>OH Consumption

Phenol decay profiles for a range of equivalence ratios are shown in Figure 5.5. In addition to the phenol consumption reactions discussed above, the reaction of phenol with molecular oxygen:



must be considered. No measured rate for this reaction has been reported. However, a rate may be estimated by analogy with the reaction:



since the phenolic O–H bond and the benzylic C–H bond are roughly equal in strength. Emdee et al. [1992] determined that the toluene profile predicted by their model was most sensitive to reaction 5.6. At that time, no direct determination of its rate was available in the literature. Therefore, the rate was initially estimated and then adjusted for a better fit to the experimental data to yield  $A=3.00 \times 10^{14} \text{ cc}\cdot\text{mol}^{-1}\cdot\text{s}^{-1}$  and  $E_a=41.4 \text{ kcal/mol}$ . To model the oxidation of phenol in supercritical water, Gopalan and Savage [1995] estimated the rate of reaction 5.5 using Emdee's A factor for reaction 5.6. The activation energy was estimated from the heat of reaction plus a barrier of 1.31 kcal/mol ( $E_a$  for  $\text{HO}_2 + \text{allyl radical} \rightarrow \text{propene} + \text{O}_2$ ). A recent study [Ingham et al., 1994], however, suggests that the preexponential of reaction 5.6 is actually a factor of 100 smaller,  $\approx 2 \times 10^{12}$ .

As explained in Chapter 1,  $\text{HO}_2$  chemistry should be considered in kinetic modeling of experiments performed at the conditions of the present study (1 atm,  $T \sim 1170 \text{ K}$ ). Thus the reaction of phenol with  $\text{HO}_2$ :



is mentioned here. Gopalan and Savage estimated  $k=1.0 \times 10^{12} \exp(-10000 \text{ cal}\cdot\text{mol}^{-1}/RT)$  based on the rate constant for abstraction of the aldehydic H from acetaldehyde ( $\text{CH}_3\text{CHO} + \text{HO}_2$ ).

### C<sub>5</sub>H<sub>6</sub> Oxidation

Cyclopentadiene profiles are shown in Figure 5.6. The profiles exhibit the expected  $\phi$ -dependence with the most significant consumption of C<sub>5</sub>H<sub>6</sub> observed at the leanest condition. Cyclopentadiene oxidation products including acetylene, 1,3-butadiene, methane, and C<sub>3</sub> species are shown in Figures 5.7–10. Yields of these species increase with decreasing equivalence ratio. With the exception of 1,3-C<sub>4</sub>H<sub>6</sub>, the observed cyclopentadiene oxidation products do not undergo subsequent conversion on the time scale of these experiments.

The decomposition of C<sub>5</sub>H<sub>6</sub> via H addition and subsequent ring opening was described above. In an oxidation system, addition of O and OH must be considered as well. Radical recombination reactions of C<sub>5</sub>H<sub>5</sub>· with O and HO<sub>2</sub> are also expected to play a role in the conversion of the C<sub>5</sub> ring to non-cyclic products. These reactions are detailed by Bozzelli et al. [1990] and Butler [1992], and the analogous reactions of methylcyclopentadiene are discussed in Chapter 4 of this thesis.

### C<sub>6</sub>H<sub>6</sub>

In the absence of oxygen, the benzene profile was found to be linear in time. As shown in Figure 5.11, the benzene profile is also linear under oxidation conditions; the slope (i.e. the rate of benzene production) increases with decreasing equivalence ratio. Trace methylcyclopentadiene was observed, suggestive of the formation of benzene via CH<sub>3</sub>C<sub>5</sub>H<sub>4</sub>·.

## CO and CO<sub>2</sub>

CO and CO<sub>2</sub> profiles are shown in Figure 5.12. The CO<sub>2</sub> profiles are characterized by a rapid, early growth (i.e. prior to the first sampling point) followed by a period of near-zero growth which persists over most of the 126–127 ms reaction time. This is indicative of a rapid, early production of CO<sub>2</sub> (i.e. in the diffuser section) which is terminated prior to the first sampling point.

The present data suggest that the chemistry in the diffuser is more rapid than would be expected for a uniform, zero-dimensional, chemically evolving mixture. As discussed in Chapter 2, these results are a consequence of flow non-idealities in the diffuser section and similar results have been found by other investigators [Emdee, 1991; Held, 1993]. The prevailing effect of the diffuser chemistry is merely a shortening of the chemical induction time; modeling results [Held, 1993] indicate that the post-induction chemistry is unaffected. Therefore, comparison of zero-dimensional model predictions with the present data may be made; a shift in time of the calculated species profiles will likely be required.

## 5.3 SUMMARY

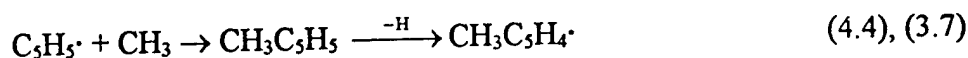
The pyrolysis of phenol, previously studied in this laboratory [Lovell et al., 1989], has been re-investigated. CO, cyclopentadiene, and benzene were major reaction intermediates, consistent with prior findings. And, CO yield was once again found to exceed that of C<sub>3</sub>H<sub>6</sub>. However, trace species not detected in the earlier study were observed and are suggestive of kinetic pathways not considered by Lovell.



Lovell reported the formation of benzene by the displacement reaction:



Detection of trace methylcyclopentadiene in the present study suggests an additional mechanism for the formation of benzene:



The presence of the required methyl radicals is inferred from detection of the parent species  $\text{CH}_4$ , also not observed by Lovell.

In accordance with the discussion above, some fraction of the observed benzene is expected to be derived via  $\text{C}_5\text{H}_5\cdot$  rather than from phenol directly. Therefore, benzene production may explain in part the discrepancy between the CO and  $\text{C}_5\text{H}_6$  profiles (Figure 5.2). Lovell proposed the reaction:



in order to account for the inconsistency in his CO/ $\text{C}_5\text{H}_6$  data. The present data (Figure 5.4), however, do not suggest that this recombination is a significant reaction path.

High-temperature phenol oxidation data have been acquired and, to the author's knowledge, are the first and only data of their kind. In accordance with earlier studies of phenol pyrolysis, cyclopentadiene is a major reaction intermediate. Cyclopentadiene is derived from its radical, formed via unimolecular decomposition of the phenoxy radical. Other reaction intermediates observed in the phenol experiments were consistent with the findings of a cyclopentadiene oxidation study [Butler, 1992] also performed in this

laboratory. Major species included carbon monoxide, carbon dioxide, acetylene, benzene, 1,3-butadiene, ethene, and methane. Minor species were allene, methylacetylene, propene, ethane, methylcyclopentadiene, and naphthalene.

It is expected that these data will be instrumental in the validation of benzene oxidation models and will prove contributive to our understanding of the whole of aromatics chemistry.

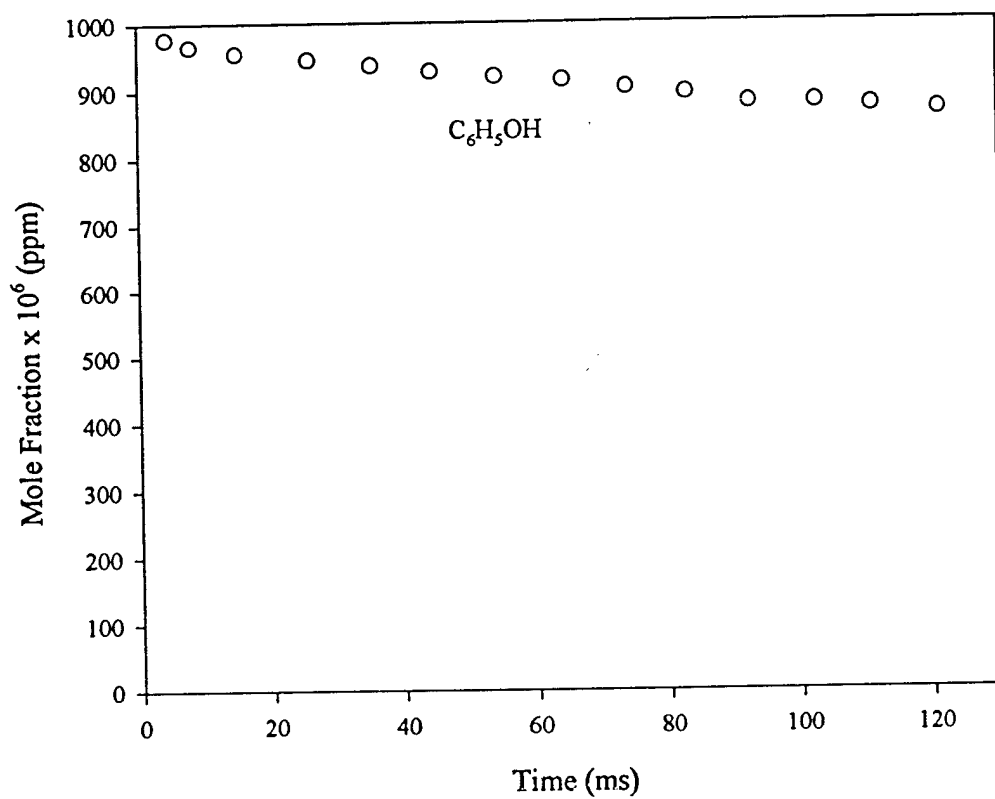


Figure 5.1: Fuel decay profile from the pyrolysis of phenol at 1173 K. Profile reconstructed by method described in Chapter 2.

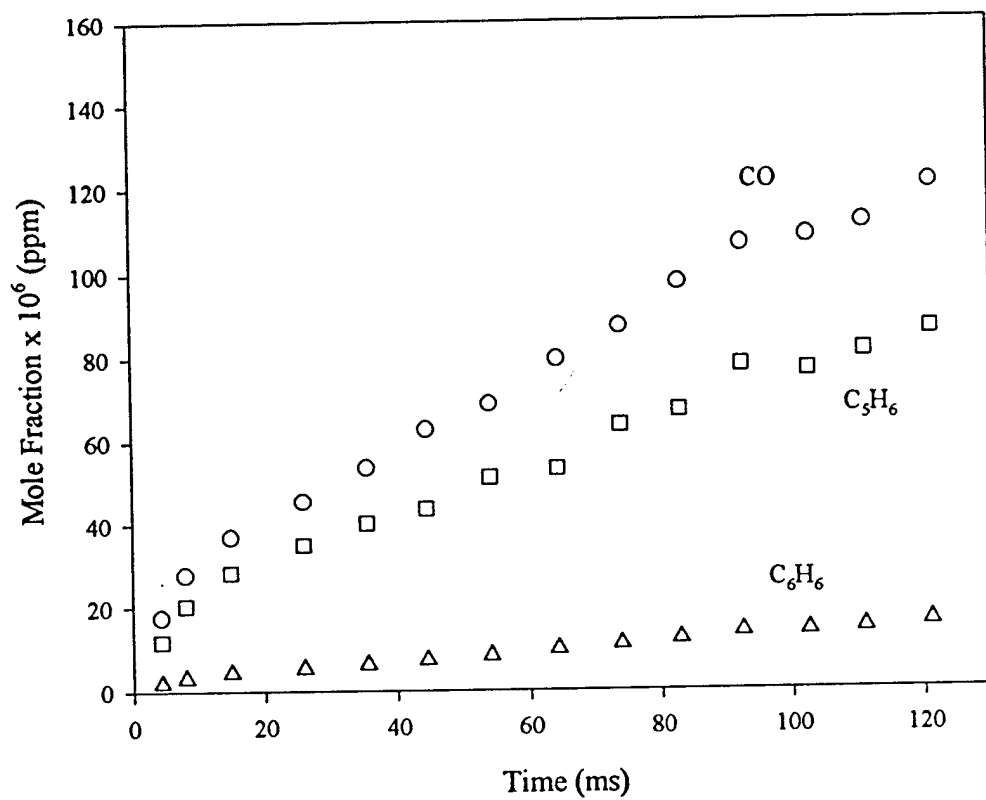


Figure 5.2: Carbon monoxide, cyclopentadiene, and benzene profiles from the pyrolysis of phenol at 1173 K.

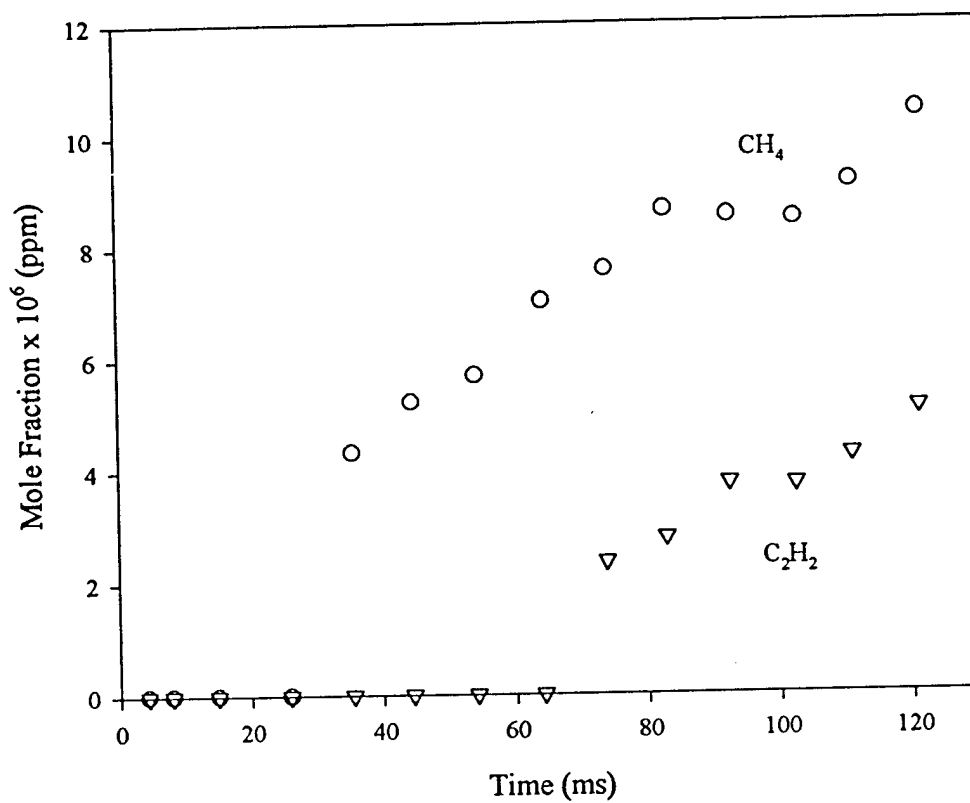


Figure 5.3: Methane and acetylene profiles from the pyrolysis of phenol at 1173 K.

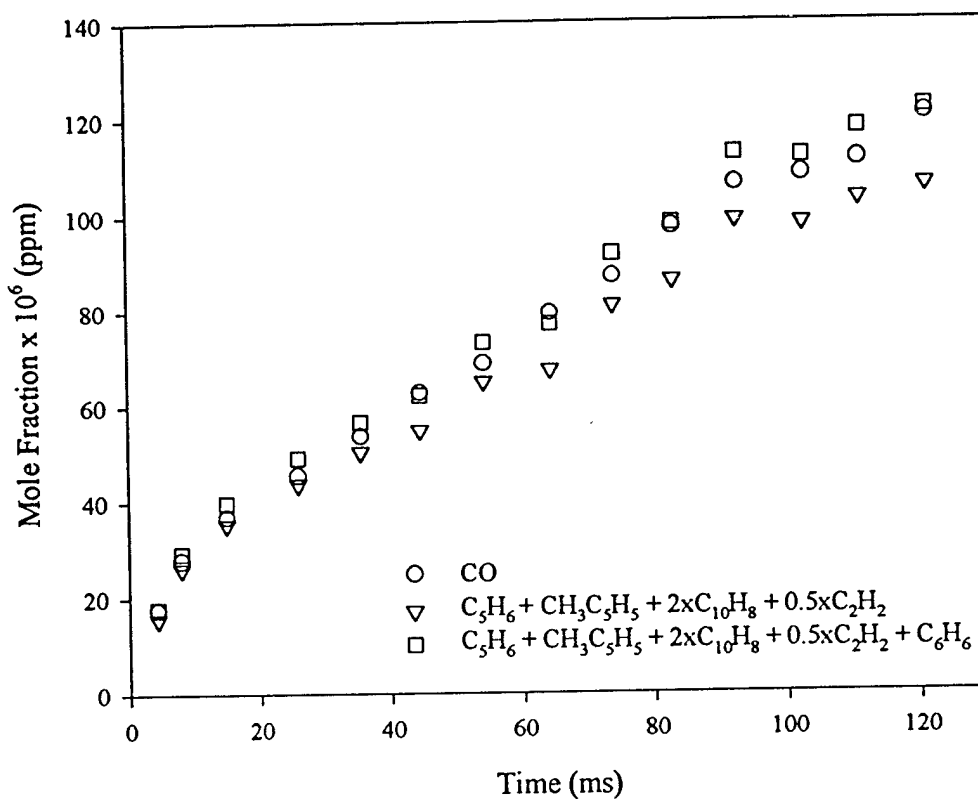


Figure 5.4: Comparison of carbon monoxide and sum of  $C_5H_5$  derivatives from the pyrolysis of phenol at 1173 K.

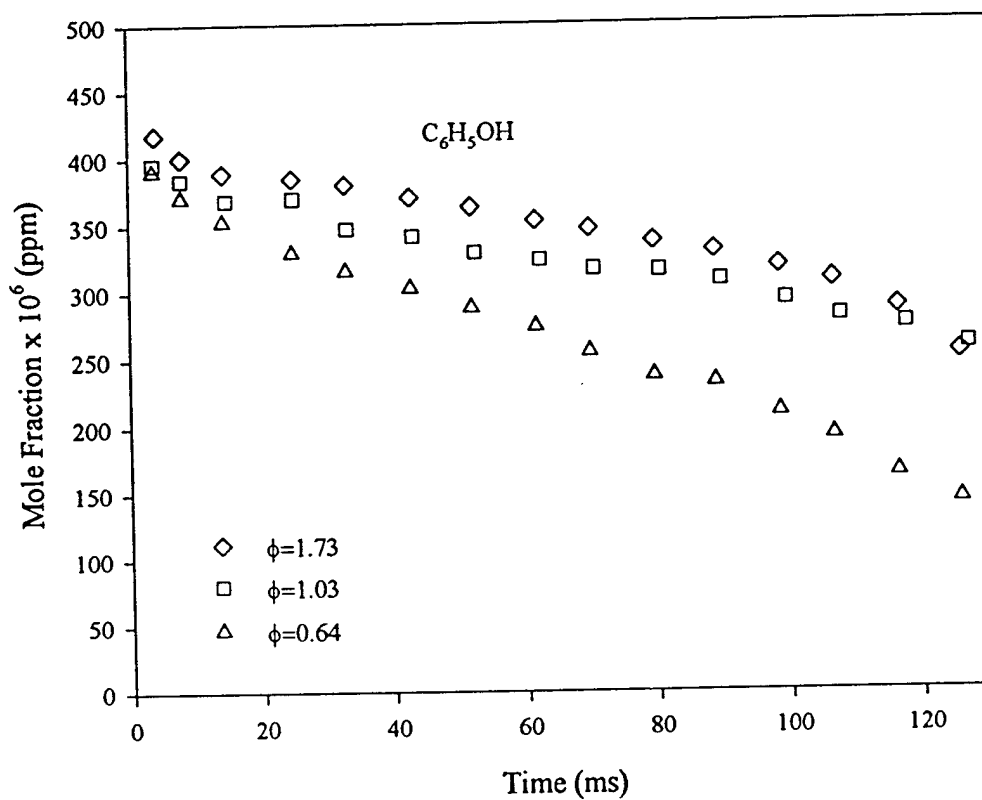


Figure 5.5: Fuel decay profiles from the oxidation of phenol at 1169 K. Profiles were reconstructed by method described in Chapter 2.

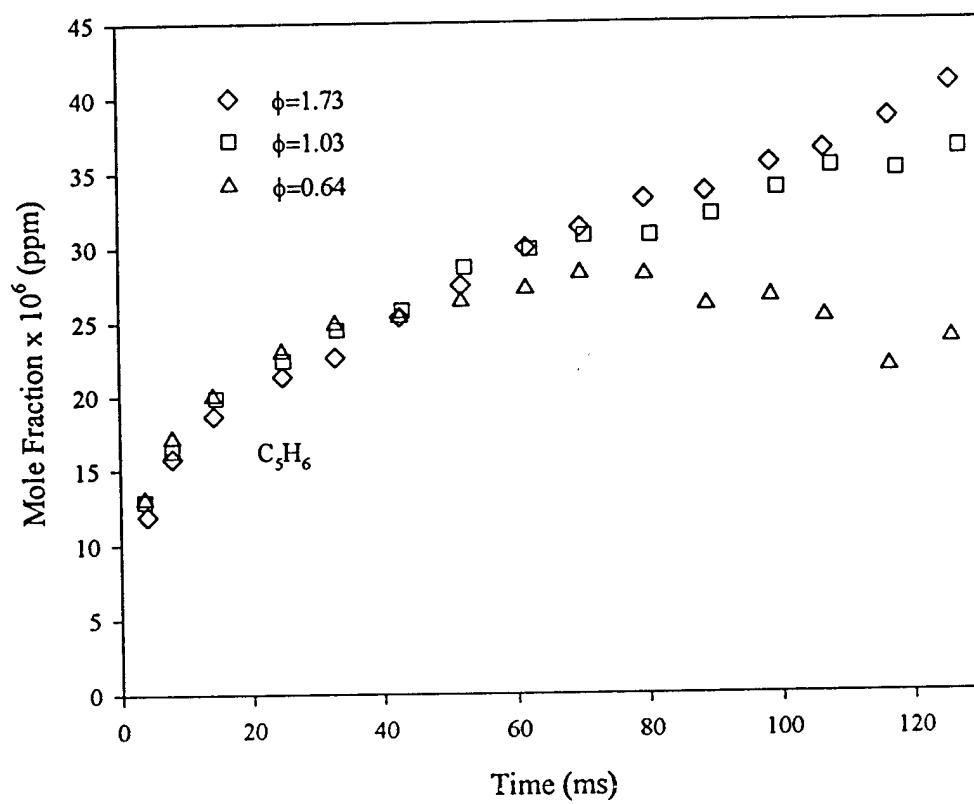


Figure 5.6: Cyclopentadiene profiles from the oxidation of phenol at 1169 K.



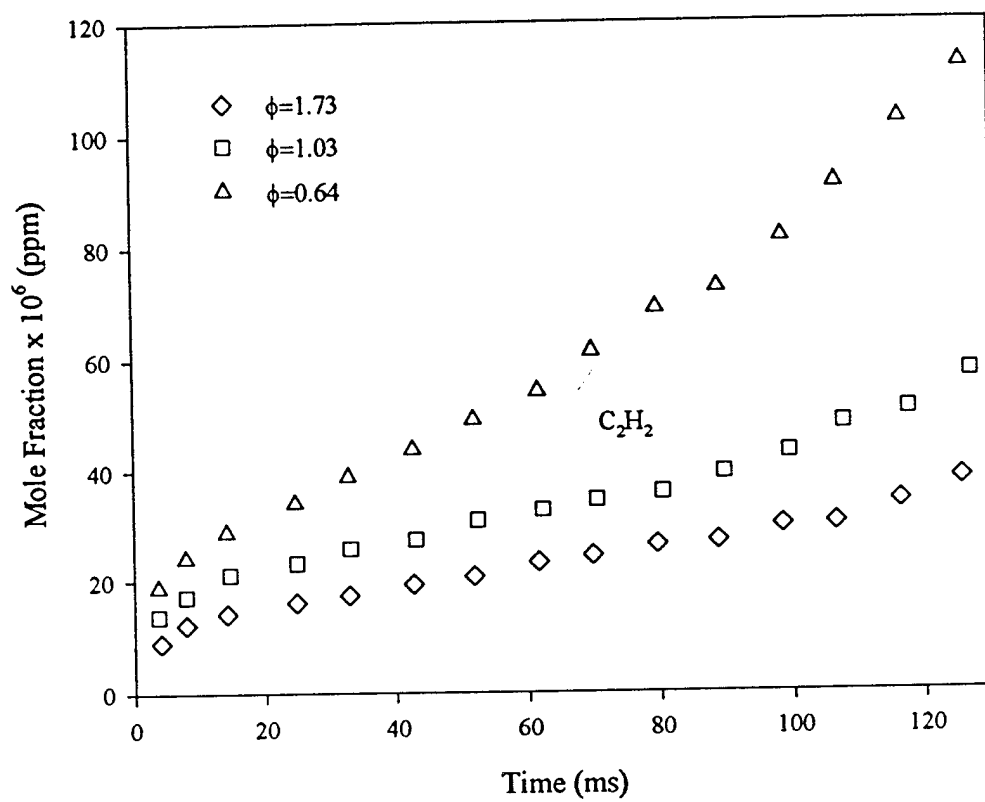


Figure 5.7: Acetylene profiles from the oxidation of phenol at 1169 K.

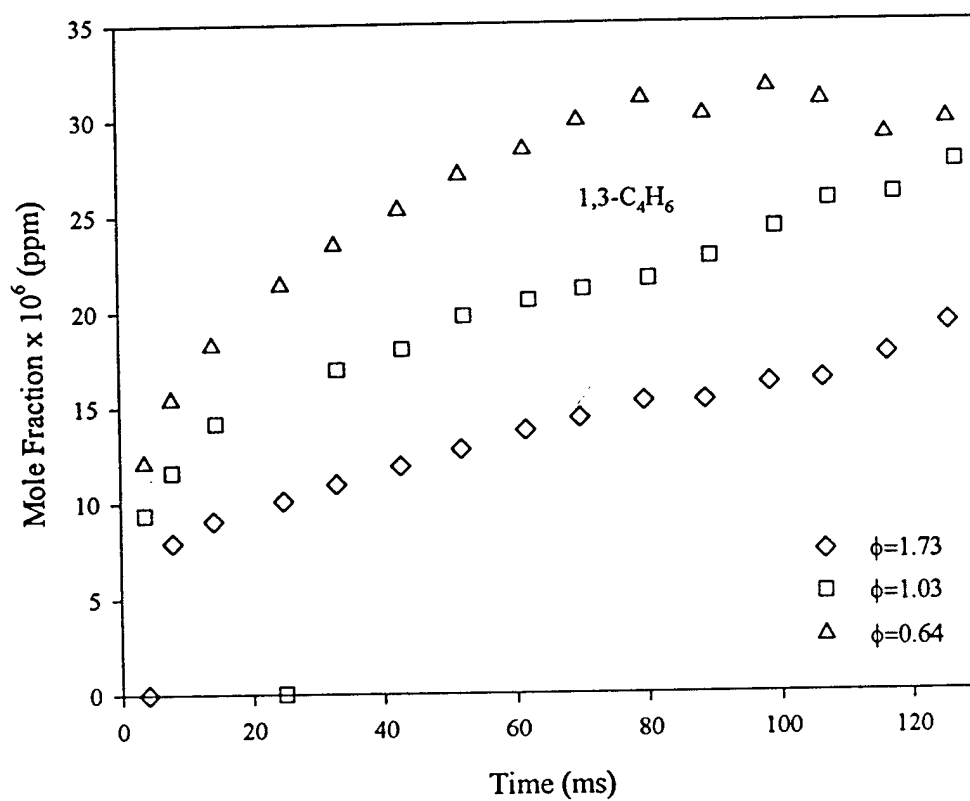


Figure 5.8: 1,3-Butadiene profiles from the oxidation of phenol at 1169 K.

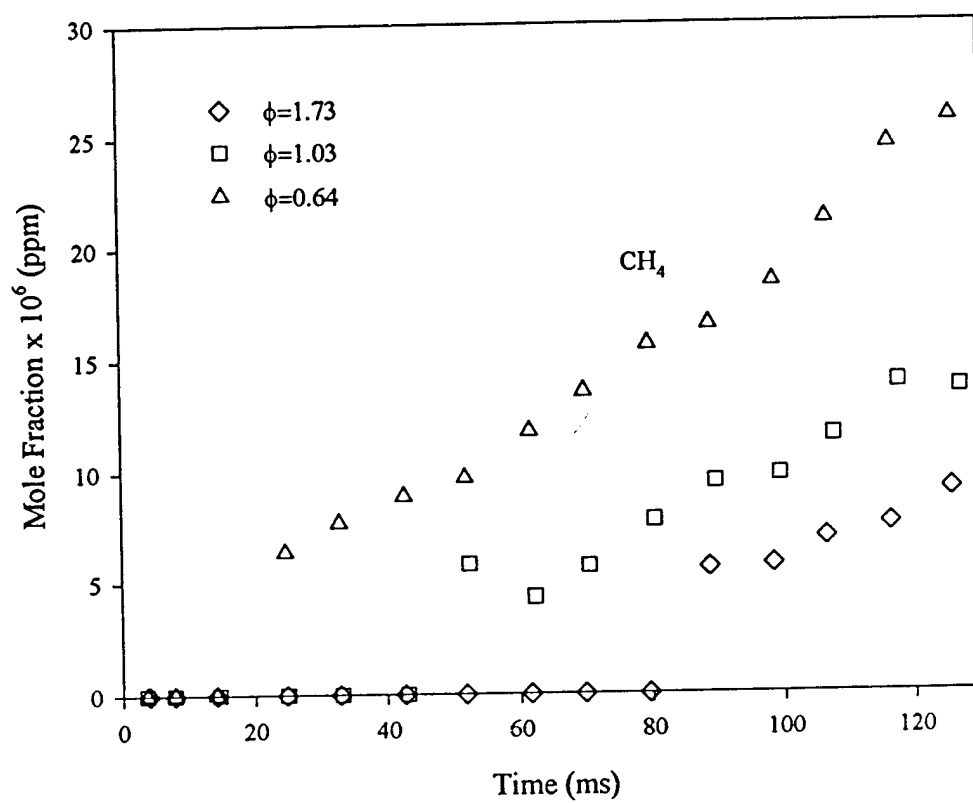


Figure 5.9: Methane profiles from the oxidation of phenol at 1169 K.

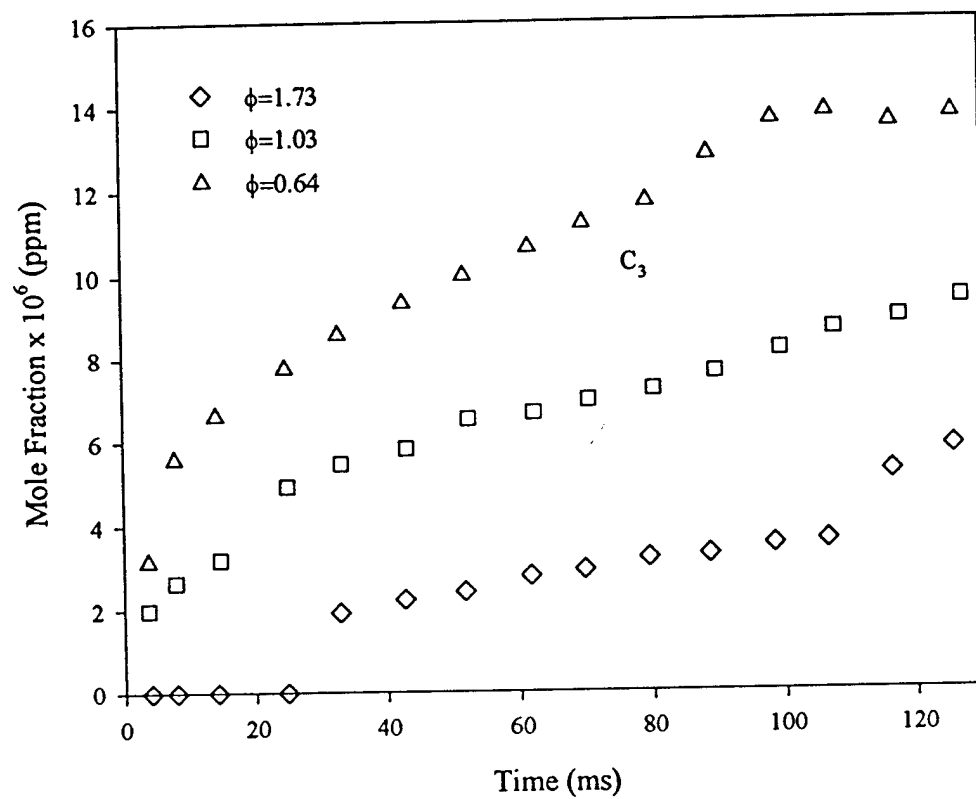


Figure 5.10:  $C_3$  profiles from the oxidation of phenol at 1169 K.  $C_3$  = propene + allene + methylacetylene.

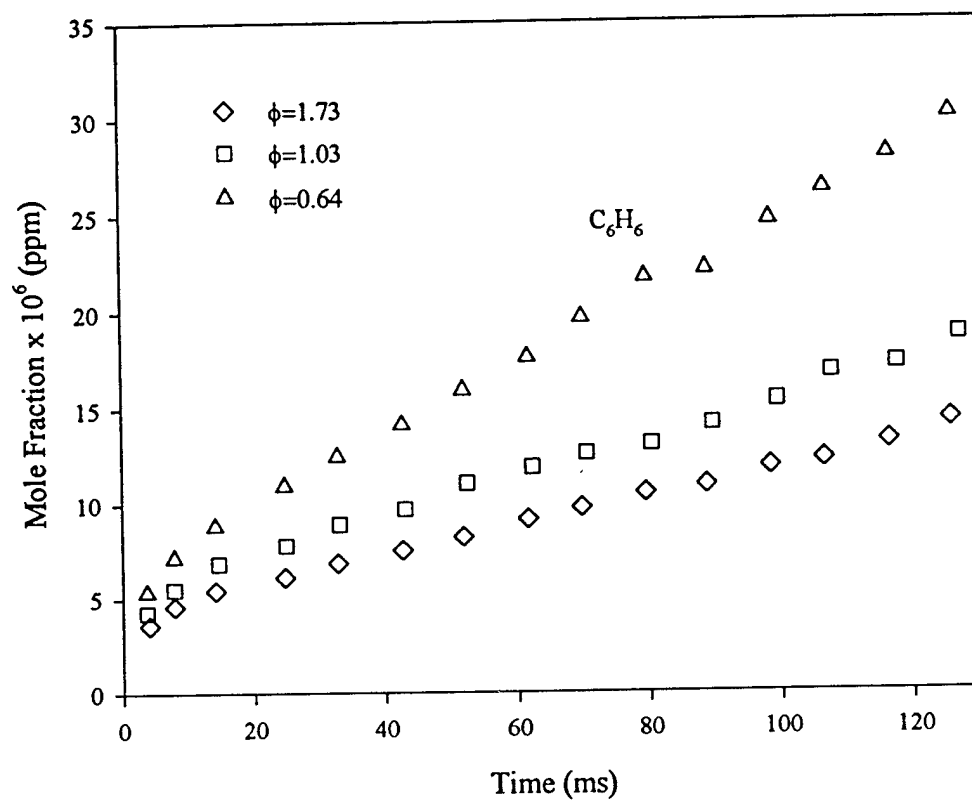


Figure 5.11: Benzene profiles from the oxidation of phenol at 1169 K.

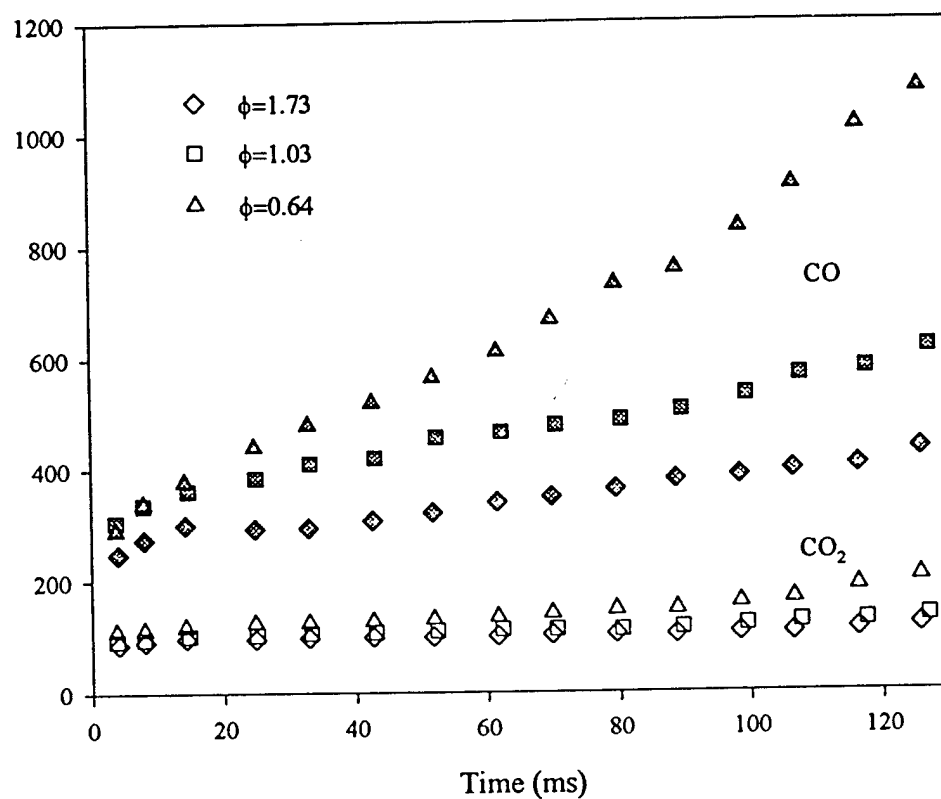


Figure 5.12: Carbon monoxide and carbon dioxide profiles from the oxidation of phenol at 1169 K.

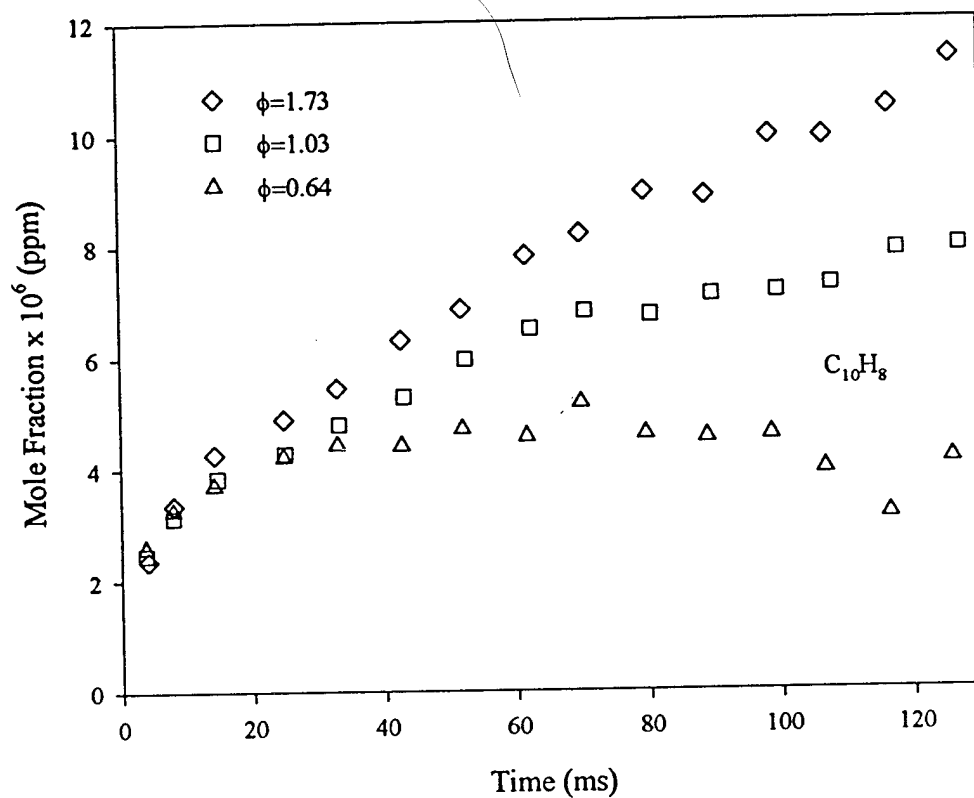


Figure 5.13: Naphthalene profiles from the oxidation of phenol at 1169 K.

## CHAPTER 6. SUMMARY AND RECOMMENDATIONS

---

Phenol and its radical phenoxy have long been recognized as important reaction intermediates in the combustion of aromatic species. Reported phenol data are scarce, presumably by virtue of the difficulties incumbent in the use of a room-temperature solid reactant which is also corrosive. Instead, phenyl alkyl ethers like anisole have been used as chemical sources of the phenoxy radical at high temperature. Prior investigations of anisole and phenol have been limited to pyrolysis experiments performed in either inert or hydrogen atmospheres. For the first time, the high-temperature chemistry of anisole and phenol have been studied under oxidizing conditions.

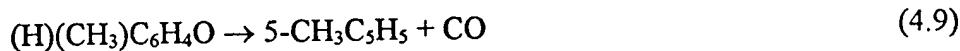
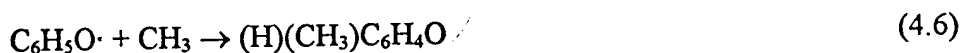
### 6.1 THE PYROLYSIS AND OXIDATION OF ANISOLE

The distribution of reaction intermediates observed in anisole pyrolysis and oxidation experiments near 1000 K was virtually independent of equivalence ratio. Phenol, cresols, methylcyclopentadiene, and carbon monoxide were the major species detected. It was inferred that, following O-CH<sub>3</sub> bond homolysis, reactions of phenoxy with methyl (loosely termed "pyrolytic") dominate the system chemistry even in the presence of oxygen. Oxidation was found to occur exclusively through intermediate methylcyclopentadiene. It has been proposed that oxidation of methylcyclopentadiene



proceeds 1) via H abstraction followed by radical recombination with HO<sub>2</sub> or O, and 2) by addition of radicals (i.e. H, O, and OH) to unsaturated bonds of the parent molecule. Ring opening and subsequent decomposition reactions yield CO and non-cyclic hydrocarbon molecules and radicals. Methylcyclopentadiene conversion was accompanied by the production of CO and C<sub>2</sub>–C<sub>4</sub> hydrocarbons including acetylene, ethene, allene, propene, methylacetylene, and 1,3-butadiene.

A set of 66 reversible reactions involving 31 species was developed to model the pyrolysis of anisole. The recombination of phenoxy and methyl was treated by QRRK chemical activation principles. Stabilization of the energized C<sub>6</sub>H<sub>5</sub>O–CH<sub>3</sub> complex followed by decomposition/isomerization to methylcyclopentadiene + CO or cresol:



were found to be the dominant reaction paths. Distinction among the three isomers of methylcyclopentadiene was found to be critical to successful model prediction of the CH<sub>3</sub>C<sub>5</sub>H<sub>5</sub> data. 5-CH<sub>3</sub>C<sub>5</sub>H<sub>5</sub> is formed initially, and the more stable 1- and 2- forms are derived via sigmatropic rearrangement(s):



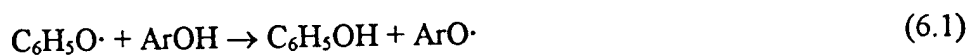
The anisole pyrolysis model produces excellent agreement between experimental data and predictions of fuel decay, methylcyclopentadiene, carbon monoxide, and total phenolics.

The model's primary shortcoming is its inability to predict correctly the relative distribution of phenol and cresols.

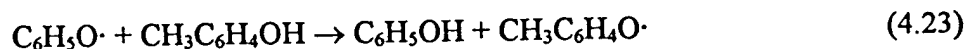
Reaction path analysis revealed that the recombination:



is the primary phenol production reaction, but the concentration of atomic H is rate limiting. Abstraction reactions were investigated as a potentially significant source of phenol. Optimization of rate parameters—within the range of values currently understood to be physically realistic for these reactions—did not improve sufficiently prediction of the experimental phenol data. A recent report [Foti et al., 1994] suggests, however, that the rates of phenolic H abstraction by phenoxy from phenols are surprisingly high. Rate constants for reactions of the type:



(where Ar=an aryl radical) were measured in nonpolar solvents. In general, the thermochemistry for H abstraction by  $\text{C}_6\text{H}_5\text{O}\cdot$  is similar to the thermochemistry for the same H abstraction by  $\text{HO}_2$ . However, the phenoxy rate constants were found to be 100–300 times greater than the already well-known peroxy rate constants. In light of these findings, the reaction of phenoxy with cresol:



may play an unexpectedly significant role in the production of phenol. This possibility deserves further exploration.

## 6.2 THE PYROLYSIS AND OXIDATION OF PHENOL

The pyrolysis of phenol was re-investigated for comparison with the findings of Lovell et al. [1989] and to acquire bench mark data for comparison with oxidation experiments. The distribution of major reaction intermediates was consistent with that reported by Lovell. CO, cyclopentadiene, and benzene were major species, and CO yield was found to exceed that of C<sub>5</sub>H<sub>6</sub>. However, trace methane and methylcyclopentadiene not detected in the earlier study were observed and are suggestive of kinetic pathways not considered by Lovell.

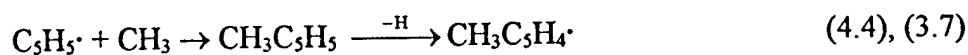
CO and C<sub>5</sub>H<sub>5</sub>· are produced concomitantly via the unimolecular decomposition of the phenoxy radical:



Lovell proposed the reaction:



in order to account for the disparity in his CO and C<sub>5</sub>H<sub>6</sub> data. The present data, however, do not suggest that this recombination is a significant reaction path. Rather, some fraction of the C<sub>5</sub>H<sub>5</sub>· formed is expected to be converted to benzene:



The presence of the required methyl radicals is inferred from detection of the parent species CH<sub>4</sub>. Such reaction steps seem to resolve Lovell's CO/C<sub>5</sub>H<sub>6</sub> inconsistency and,

furthermore, have implications regarding the formation of soot from cyclic  $C_5$  species as suggested by Glassman [1988].

High-temperature phenol oxidation data, the first of their kind, were acquired over a range of equivalence ratios. Cyclopentadiene was found to be a major reaction intermediate, consistent with the pyrolysis results. Other reaction intermediates observed in the phenol experiments were consistent with the findings of an earlier cyclopentadiene oxidation study [Butler, 1992]. Major species included carbon monoxide, carbon dioxide, acetylene, benzene, 1,3-butadiene, ethene, and methane. Minor species were allene, methylacetylene, propene, ethane, methylcyclopentadiene, and naphthalene.

Phenol consumption was proposed to proceed via 1) loss of the phenolic H (either by homolysis or abstraction) followed by unimolecular decomposition of the phenoxy radical, and 2) displacement of the hydroxyl group by H to yield benzene. The OH displacement reaction is a hindrance to oxidation since the benzene product is less easily oxidized than the  $C_5H_5\cdot$  produced via the H loss route. In order to determine the relative importance of the various phenol consumption reactions, a detailed oxidation model must be developed. It is expected that accurate characterization of the phenol chemistry will be instrumental in remedying our models of benzene oxidation.

### 6.3 RECOMMENDATIONS

#### Anisole

While the anisole pyrolysis model predicts very well the sum of phenolic species observed in the present experiments, the individual phenol and cresol profiles are not well-

predicted. Other investigators [Mackie et al., 1989] have suggested that phenol is derived from cresol. And, there is evidence [Foti et al., 1994] which suggests that phenolic H abstraction from cresol by phenoxy will be unusually fast. Therefore, a pyrolysis experiment in which some amount of cresol is added to the anisole fuel (a so-called "spiking experiment") may be useful in assessing the importance of reaction 6.2. At 1000 K, thermal decomposition of cresol is slow; alternative reaction pathways (i.e. C-CH<sub>3</sub> bond homolysis, unimolecular loss of benzylic or phenolic H) are not expected to contribute significantly to the production of phenol. Thus a resultant shift in the phenol profile should be attributable to the abstraction reaction.

The anisole oxidation experiments revealed that oxidation occurs exclusively through intermediate methylcyclopentadiene. A series of methylcyclopentadiene oxidation experiments will provide a more practical data base for the development of a detailed model. Furthermore, these experiments would complement nicely the cyclopentadiene oxidation data of Butler [1992, 1996].

### Phenol

The phenol oxidation data reported here represent the (until now, missing) link between the cyclopentadiene [Butler, 1996] and benzene [Lovell, 1989] oxidation data also collected in this laboratory. With the three sets of data, an improved model for benzene oxidation may be developed stepwise, from cyclopentadiene up. Advances in our understanding of the cyclopentadiene chemistry are currently being made [Butler, 1996]. These are expected to aid in the development of a detailed kinetic model which predicts the newly acquired phenol oxidation data. Ultimately, the oxidation of benzene should be

revisited. It is hoped that, with insights gained from the recent cyclopentadiene and phenol studies, predictions of these species and their radicals will be improved.

#### **6.4 FINAL REMARKS**

Environmental concerns have stimulated considerable interest in developing the ability to model the chemistry of fuels. Advanced computing capacity is widespread and detailed kinetic modeling is common practice. But while our predictive capabilities are continually improving, kinetic models will never supplant experiment entirely in the development of practical combustion devices. Rather, the understanding gained through modeling will guide the design process permitting the more efficient, less costly evolution of cleaner technologies.

## REFERENCES

---

- Ackermann, L., Hippler, H., Pagsberg, P., Reihs, C. and Troe, J. (1990). Pulse Radiolysis, Flash Photolysis and Shock Wave Study of the Recombination  $\text{H} + \text{Benzyl} \rightarrow \text{Toluene}$  at 300 and 1300–1650 K. *J. Phys. Chem.* **94**, 5247.
- Arends, I. W. C. E., Louw, R. and Mulder, P. (1993). Kinetic Study of the Thermolysis of Anisole in a Hydrogen Atmosphere. *J. Phys. Chem.* **97**, 7914.
- Barnard, J. A. and Ibberson, V. J. (1965). The Gaseous Oxidation of Toluene II: The Analytical Results. *Combust. Flame* **9**, 149.
- Benson, S. W. (1965). Effects of resonance and structure on the thermochemistry of organic peroxy radicals and the kinetics of combustion reactions. *J. Am. Chem. Soc.* **87**, 972.
- Benson, S. W. (1968). *Thermochemical Kinetics*; John Wiley & Sons: New York.
- Benson, S. W. (1982). Cool Flames and Oxidation: Mechanism, Thermochemistry, and Kinetics. *Oxid. Commun.* **2**, 169.
- Bittker, D. A. (1991). Detailed Mechanism for Oxidation of Benzene. *Combust. Sci. and Tech.* **79**, 49.
- Bittner, J. D. and Howard, J. B. (1981). Composition Profiles and Reaction Mechanisms in a Near-Sooting Premixed Benzene-Oxygen-Argon Flame. *Eighteenth Symposium (International) on Combustion*, The Combustion Institute, p 1105.
- Bowman, C. T., Hanson, R. K., Davidson, D. F., Gardiner, Jr., W. C., Lissianski, V., Smith, G. P., Golden, D. M., Frenklach, M. and Goldenberg, M.  
[http://www.me.berkeley.edu/gri\\_mech/](http://www.me.berkeley.edu/gri_mech/).
- Bozzelli, J. W., Desai, V. and Ritter, E. R. (1990). Mechanistic Considerations for Cyclopentadienyl Radical Conversion During Benzene Oxidation. The Spring Meeting of the Central States Section of the Combustion Institute, Paper No. 19.

Brezinsky, K. (1986). The High-Temperature Oxidation of Aromatic Hydrocarbons. *Prog. Energy Combust. Sci.* **12**, 1.

Burcat, A. and McBride, B. (1993). 1994 Ideal Gas Thermodynamic Data for Combustion and Air-Pollution Use. Technion, Haifa, T.A.E. 697.

Butler, R. G. (1992). A Flow Reactor Study of the Oxidation of 1,3-Cyclopentadiene. M.S.E. Thesis, Department of Mechanical and Aerospace Engineering, Princeton University, Princeton, NJ.

Butler, R. G. (1996). Work in progress.

Chang, E. (1989). Characterization of the Flow Field of the Flow Reactor. Undergraduate Independent Work, Final Report, Department of Mechanical and Aerospace Engineering, Princeton University.

Chang, R. (1988). *Chemistry*; Random House: New York; p 387-388.

Colussi, A. J., Zabel, F. and Benson, S. W. (1977). The Very Low-Pressure Pyrolysis of Phenyl Ethyl Ether, Phenyl Allyl Ether, and Benzyl Methyl Ether and the Enthalpy of Formation of the Phenoxy Radical. *Int. J. Chem. Kin.* **9**, 161.

Crocco, I., Glassman, I. and Smith, I. E. (1957). A Flow Reactor for High Temperature Reaction Kinetics. *Jet Propulsion* **27**, 1266.

Crocco, I., Glassman, I. and Smith, I. E. (1959). Kinetics and Mechanism of Ethylene Oxide Decomposition at High Temperatures. *J. Chem. Phys.* **31**, 506.

Cypres, R. and Bettens, B. (1974). Mecanismes de Fragmentation Pyrolytique du Phenol et des Cresols. *Tetrahedron* **30**, 1253.

Cypres, R. and Bettens, B. (1975a). La Formation de la Plupart des Composes Aromatiques Produits Lors de la Pyrolyse du Phenol, Ne Fait Pas Intervenir le Carbone Porteur de la Fonction Hydroxyle. *Tetrahedron* **31**, 359.

Cypres, R. and Bettens, B. (1975b). Pyrolyse Thermique des [ $^{14}\text{C}$ ] et [ $^3\text{H}$ ] Ortho et Para-Cresols. *Tetrahedron* **31**, 353.

Davis, S. G., Wang, H., Brezinsky, K. and Law, C. K. (1996). Laminar Flame Speeds and Oxidation Kinetics of Benzene/Air and Toluene/Air Flames. *Twenty-Sixth Symposium (International) on Combustion*, The Combustion Institute, in press.

Dean, A. M. (1985). Predictions of Pressure and Temperature Effects upon Radical Addition and Recombination Reactions. *J. Phys. Chem.* **89**, 4600.



- Dean, A. M. (1990). Detailed Kinetic Modeling of Autocatalysis in Methane Pyrolysis. *J. Phys. Chem.* **94**, 1436.
- Dean, A. M., Bozzelli, J. W. and Ritter, E. R. (1991). CHEMACT: A Computer Code to Estimate Rate Constants for Chemically-Activated Reactions. *Combust. Sci. and Tech.* **80**, 63.
- Dewar, M. J. S. (1992). The Semiempirical Approach to Chemistry. *Int. J. Quantum Chem.* **44**, 427.
- Dryer, F. L. (1972). High Temperature Oxidation of Carbon Monoxide and Methane in a Turbulent Flow Reactor. Ph.D. Thesis, Department of Mechanical and Aerospace Engineering, Princeton University, Princeton, NJ.
- Dryer, F. L. (1991). In *Fossil Fuel Combustion: A Source Book*, Bartok, W. and Sarofim, A. F., Eds.; John Wiley and Sons: New York; pp 121-213.
- Emdee, J. L. (1991). An Experimental and Modeling Study of the High Temperature Oxidation of the Xylenes. Ph.D. Thesis, Department of Mechanical and Aerospace Engineering, Princeton University, Princeton, NJ.
- Emdee, J. L., Brezinsky, K. and Glassman, I. (1990). Oxidation of *o*-Xylene. *Twenty-Third Symposium (International) on Combustion*, The Combustion Institute, p 77.
- Emdee, J. L., Brezinsky, K. and Glassman, I. (1991). High-Temperature Oxidation Mechanisms of *m*- and *p*-Xylene. *J. Phys. Chem.* **95**, 1626.
- Emdee, J. L., Brezinsky, K. and Glassman, I. (1992). A Kinetic Model for the Oxidation of Toluene near 1200 K. *J. Phys. Chem.* **96**, 2151.
- Euchner, J. A., Venkat, C., Brezinsky, K. and Glassman, I. (1981). Preliminary Studies on the Oxidation of Aromatics at High Temperatures. *First (International) Specialists Meeting of the Combustion Institute*.
- Fahr, A. and Stein, S. E. (1988). Gas Phase Reactions of Phenyl Radicals with Aromatic Molecules. *J. Phys. Chem.* **92**, 4951.
- Foti, M., Ingold, K. U. and Luszyk, J. (1994) The Surprisingly High Reactivity of Phenoxy Radicals. *J. Am. Chem. Soc.* **116**, 9440.
- Frank, P., Herzler, J., Just, T. and Wahl, C. (1994). High-Temperature Reactions of Phenyl Oxidation. *Twenty-Fifth Symposium (International) on Combustion*, The Combustion Institute, p 833.

- Frenklach, M. and Warnatz, J. (1987). Detailed Modeling of PAH Profiles in a Sooting Low-Pressure Acetylene Flame. *Combust. Sci. Technol.* **51**, 265.
- Frenklach, M., Clary, D. W., Gardiner, W. C. and Stein, S. E. (1988). Effect of Fuel Structure on Pathways to Soot. *Twenty-First Symposium (International) on Combustion*, The Combustion Institute, p 1067.
- Frenklach, M. and Wang, H. (1991). Aromatics Growth Beyond the First Ring and the Nucleation of Soot Particles. *ACS Preprints, Division of Fuel Chemistry* **36**, 1509.
- Gardiner, W. C., Jr. and Troe, J. (1984). In *Combustion Chemistry*, Gardiner, W. C., Jr., Ed.; Springer-Verlag: New York; pp 173-196.
- Glassman, I. and Eberstein, I. J. (1963). Turbulence Effects in Chemical Reactions Kinetics Measurements. *AIAA J.* **1**, 1424.
- Glassman, I. (1996). *Combustion*; Academic Press: San Diego; pp 139-146.
- Glassman, I. (1988). Soot Formation in Combustion Processes. *Twenty-Second Symposium (International) on Combustion*, The Combustion Institute, p 295.
- Goodger, E. M. (1995). Jet fuels development and alternatives. *Proc. Instn. Mech. Engrs.* **209**, 147.
- Gopalan, S. and Savage, P. E. (1995). In *Innovations in Supercritical Fluids*; Hutchenson, K. W., Ed.; American Chemical Society: Washington, DC, Chapter 14.
- Graham, S. C., Homer, J. B. and Rosenfeld, J. L. J. (1975). The formation and coagulation of soot aerosols generated by the pyrolysis of aromatic hydrocarbons. *Proc. R. Soc. Lond. A.* **344**, 259.
- Held, T. J. (1993). The Oxidation of Methanol, Isobutene and Methyl tertiary-Butyl Ether. Ph.D. Thesis, Department of Mechanical and Aerospace Engineering, Princeton University, Princeton, NJ.
- Harris, S. J., Weiner, A. M. and Blint, R. J. (1988). Formation of Small Aromatic Molecules in a Sooting Ethylene Flame. *Combust. Flame* **72**, 91.
- Hart, H. (1979). Simple Enols. *Chem. Rev.* **79**, 515.
- Hausmann, M., Hebgén, P. and Homann, K-H. (1992). Radicals in Flames: Analysis via Scavenging Reaction. *Twenty-Fourth Symposium (International) on Combustion*, The Combustion Institute, p 793.

He, Y. Z., Mallard, W. G. and Tsang, W. (1988). Kinetics of Hydrogen and Hydroxyl Radical Attack on Phenol at High Temperatures. *J. Phys. Chem.* **92**, 2196.

Heywood, J. B. (1988). *Internal Combustion Engine Fundamentals*; McGraw-Hill: New York; p 475.

Hochgreb, S. (1991). An Experimental and Numerical Study on the Oxidation of Formaldehyde. Ph.D. Thesis, Department of Mechanical and Aerospace Engineering, Princeton University, Princeton, NJ.

Ingham, T., Walker, R. W. and Woolford, R. E. (1994). Kinetic Parameters for the Initiation Reaction  $\text{RH} + \text{O}_2 \rightarrow \text{R} + \text{HO}_2$ . *Twenty-Fifth Symposium (International) on Combustion*, The Combustion Institute, p 767.

Kee, R. J., Warnatz, J. and Miller, J. A. (1983). A Fortran Computer Code Package for the Evaluation of Gas-Phase Viscosities, Conductivities, and Diffusion Coefficients. Sandia National Laboratories, SAND83-8209.

Kee, R. J., Rupley, F. M. and Miller, J. A. (1987). The CHEMKIN Thermodynamic Data Base. Sandia National Laboratories, SAND87-8215.

Kerr, J. A., O'Grady, B. V. and Trotman-Dickenson, A. F. (1967). The Reaction of Methylene with Hydroxyl Groups. *J. Chem. Soc. (A)* **6**, 897.

Kerr, J. A. and Parsonage, M. J. (1976). *Evaluated Kinetic Data on Gas Phase Hydrogen Transfer Reactions of Methyl Radicals*; Butterworths: London.

Kiefer, J. H., Mizerka, L., Patel, M. R. and Wei, H.-C. (1985). A Shock Tube Investigation of Major Pathways in the High-Temperature Pyrolysis of Benzene. *J. Phys. Chem.* **89**, 2013.

Klinkenberg, W. and Louw, R. Thermal Hydrogenolysis of Cyclopentadiene: Rates, Products and Thermochemistry (1987). C.C.E. Special Report Series; Leiden University: Leiden; No. 87-01.

Kopinke, F.-D., Remmler, M., Mensing, H. and Higo, P. (1994). Relative Reactivities of Some C-H Bonds in Hydrogen Abstraction by Methyl Radicals at 950 K. *J. Phys. Chem.* **98**, 1171.

Laidler, K. J. (1987). *Chemical Kinetics*; Harper & Row: New York; pp 157-163.

Lin, C.-Y. and Lin, M. C. (1985). Unimolecular Decomposition of the Phenoxy Radical in Shock Waves. *Int. J. Chem. Kin.* **17**, 1025.

- Lin, C.-Y. and Lin, M. C. (1986a). Thermal Decomposition of Methyl Phenyl Ether in Shock Waves: The Kinetics of Phenoxy Radical Reactions. *J. Phys. Chem.* **90**, 431.
- Lin, C.-Y. and Lin, M. C. (1986b). The Combination Reaction of  $\text{CH}_3$  and  $\text{C}_6\text{H}_5\text{O}$ . *Aust. J. Chem.* **39**, 723.
- Lindstedt, R. P. and Skevis, G. (1994). Detailed Kinetic Modeling of Premixed Benzene Flames. *Combust. Flame* **99**, 551.
- Litzinger, T. A. (1985). The High Temperature Oxidation of Alkylated Aromatic Hydrocarbons. Ph.D. Thesis, Department of Mechanical and Aerospace Engineering, Princeton University, Princeton, NJ.
- Liu, R., Morokuma, K., Mebel, A. M. and Lin, M. C. (1996). *Ab Initio* Study of the Mechanism for the Thermal Decomposition of the Phenoxy Radical. *J. Phys. Chem.* **100**, 9314.
- Lovell, A. B., Brezinsky, K. and Glassman, I. (1988). Benzene Oxidation Perturbed by  $\text{NO}_2$  Addition. *Twenty-Second Symposium (International) on Combustion*, The Combustion Institute, p 1063.
- Lovell, A. B., Brezinsky, K. and Glassman, I. (1989). The Gas Phase Pyrolysis of Pure Phenol. *Int. J. Chem. Kin.* **21**, 547.
- Lovell, A. B. (1989). Role of Phenoxy Formation in the Oxidation of Aromatic Hydrocarbons. Ph.D. Thesis, Department of Mechanical and Aerospace Engineering, Princeton University, Princeton, NJ.
- Lowry, T. H. and Richardson, K. S. (1987). *Mechanism and Theory in Organic Chemistry*; Harper Collins: New York; p 161-162.
- Lutz, A. E., Kee, R. J. and Miller, J. A. (1987). SENKIN: A Fortran Program for Predicting Homogeneous Gas Phase Chemical Kinetics with Sensitivity Analysis. Sandia National Laboratories, SAND87-8248.
- Mackie, J. C., Doolan, K. R. and Nelson, P. F. (1989). Kinetics of the Thermal Decomposition of Methoxybenzene (Anisole). *J. Phys. Chem.* **93**, 664.
- Manion, J. A. and Louw, R. (1989). Rates, Products, and Mechanisms in the Gas-Phase Hydrogenolysis of Phenol between 922 and 1175 K. *J. Phys. Chem.* **93**, 3563.
- Mayotte, S. C., Venkatesh, R., Lindhjem, C. E. and Sklar, M. S. Reformulated Gasoline Effects on Exhaust Emissions: Phase II: Continued Investigation of the Effects of Fuel Oxygenate Content, Oxygenate Type, Volatility, Sulfur, Olefins and Distillation Parameters. *Journal of Fuels and Lubricants* **103**, 1331.

- McLean, S. and Haynes, P. (1965). Substitution in the Cyclopentadienide Anion Series: Methylation of the Cyclopentadienide and Methylcyclopentadienide Anions. *Tetrahedron* **21**, 2313.
- Melius, C. F., Colvin, M. E., Marinov, N. M. and Pitz, W. (1996). Reaction Mechanisms in Aromatic Hydrocarbon Formation Involving the C<sub>5</sub>H<sub>5</sub> Cyclopentadienyl Moiety. *Twenty-Sixth Symposium (International) on Combustion*, The Combustion Institute, in press.
- Moreno, M. and Miller, W. H. (1990). On the tautomerization reaction 2-pyridone $\leftrightarrow$ 2-hydroxypyridine: an ab initio study. *Chem. Phys. Lett.* **171**, 475.
- Moskaleva, L. V., Mebel, A. M. and Lin, M. C. (1996). The CH<sub>3</sub> + C<sub>5</sub>H<sub>5</sub> Reaction: A Potential Source of Benzene at High Temperatures. *Twenty-Sixth Symposium (International) on Combustion*, The Combustion Institute, in press.
- Mulcahy, M. F. R. and Williams, D. J. (1963). Reaction of Phenoxy Radicals with Methyl Radicals in the Gaseous Phase. *Nature* **199**, 761.
- Mulcahy, M. F. R. and Williams, D. J. (1965). Reactions of Free Radicals with Aromatic Compounds in the Gaseous Phase. *Aust. J. Chem.* **18**, 20.
- Nelson, P. F. and Quigley, S. M. (1984). The Hydrocarbon Composition of Exhaust Emitted From Gasoline Fuelled Vehicles. *Atmospheric Environment* **18**, 79.
- Norrish, R. G. W. and Taylor, G. W. (1956). The oxidation of benzene. *Proc. R. Soc.* **A234**, 160.
- Norton, T.S. (1990). The Combustion Chemistry of Simple Alcohol Fuels. Ph.D. Thesis, Department of Mechanical and Aerospace Engineering, Princeton University, Princeton, NJ.
- O'Brien, M. J. (1985). In *Modern Practice of Gas Chromatography*, 2nd ed.; Grob, R. L., Ed.; John Wiley & Sons: New York; Chapter 6.
- Olivella, S., Solé, A. and García-Raso, A. (1995). *Ab Initio* Calculations of the Potential Surface for the Thermal Decomposition of the Phenoxy Radical. *J. Phys. Chem.* **99**, 10549.
- Pallix, J. B. and Copeland, R. A. (1996). Measurement of Catalytic Recombination Coefficients on Quartz using Laser-Induced Fluorescence. *Journal of Thermophysics and Heat Transfer* **10**, 224.

- Paul, S. and Back, M. H. (1975). A Kinetic Determination of the Dissociation Energy of the C-O Bond in Anisole. *Can. J. Chem.* **53**, 3330.
- Perry, R. L., Atkinson, R. and Pitts, J. N. (1977). Kinetics and Mechanism of the Gas Phase Reaction of OH Radicals with Aromatic Hydrocarbons Over the Temperature Range 296-473 K. *J. Phys. Chem.* **81**, 296.
- Pitz, W. J., Westbrook, C. K., Proscia, W. M. and Dryer, F. L. (1984). A Comprehensive Chemical Kinetic Reaction Mechanism for the Oxidation of *n*-Butane. *Twentieth Symposium (International) on Combustion*, The Combustion Institute, p 831.
- Rao, V. S. and Skinner, G. B. (1989). Formation of H and D Atoms in the Pyrolysis of Toluene-*d*<sub>8</sub> and Toluene- $\alpha,\alpha,\alpha$ -*d*<sub>3</sub> behind Shock Waves. *J. Phys. Chem.* **93**, 1864.
- Reid, R. C., Prausnitz, J. M. and Poling, B. E (1987). *Properties of Gases and Liquids*, 4th ed.; McGraw Hill: New York.
- Ritter, E. R. and Bozzelli, J. W. (1987). THERM: Thermodynamic Property Estimation for Radicals and Molecules; computer code, New Jersey Institute of Technology.
- Ritter, E. R., Bozzelli, J. W. and Dean, A. M. (1990). Kinetic Study on Thermal Decomposition of Chlorobenzene Diluted in H<sub>2</sub>. *J. Phys. Chem.* **94**, 2493.
- Roesler, John (1992). Laboratory memo.
- Scully, D. B. and Davies, R. A. (1965). Carbon Formation from Aromatic Hydrocarbons. *Combust. Flame* **9**, 185.
- Shaddix, C. R. (1993). An Experimental Study of the High Temperature Oxidation of 1-Methylnaphthalene. Ph.D. Thesis, Department of Mechanical and Aerospace Engineering, Princeton University, Princeton, NJ.
- Somorjai, G. A. (1994). *Introduction to Surface Chemistry and Catalysis*; John Wiley & Sons: New York; p 12.
- Spangler, C. W. (1976). Thermal [1,*j*] Sigmatropic Rearrangements. *Chem. Rev.* **76**, 187.
- Stewart, J. J. P. (1989). A semiempirical molecular orbital program. *J. Computer Aided Molecular Design* **4**, 1.
- Suryan, M. M., Kafafi, S. A. and Stein, S. E. (1989). The Thermal Decomposition of Hydroxy- and Methoxy-Substituted Anisoles. *J. Am. Chem. Soc.* **111**, 1423.
- Troe, J. (1979). Predictive Possibilities of Unimolecular Rate Theory. *J. Phys. Chem.* **83**, 114.

Tully, F. P., Ravishankara, A. R., Thompson, R. L., Nicovich, J. M., Shah, R. H., Kreutter, N. M. and Wine, P. H. (1981). Kinetics of the Reaction of Hydroxyl Radical with Benzene and Toluene. *J. Phys. Chem.* **85**, 2262.

US Environmental Protection Agency (1977). *Control Techniques for Lead Air Emissions*, EPA-450/2-77-012.

US Environmental Protection Agency (1981). *Second Annual Report on Carcinogens*, NTP 81-43, p 47-50.

Venkat, C., Brezinsky, K. and Glassman, I. (1982). High Temperature Oxidation of Aromatic Hydrocarbons. *Nineteenth Symposium (International) on Combustion*, The Combustion Institute, p 143.

Weast, R. C. and Astle, M. J., Eds. (1980). *CRC Handbook of Chemistry and Physics*; CRC Press: Boca Raton; pp C-1-45.

Weckman, E., Brezinsky, K., DeMay, J. and Glassman, I. (1983). The Pyrolysis of Phenol. Meeting of the Eastern States Section of the Combustion Institute, Paper No. 35.

Westmoreland, P. R., Longwell, J. P. and Dean, A. M. (1986). Prediction of Rate Constants for Combustion and Pyrolysis Reactions by Bimolecular QRRK. *AIChE Journal* **32**, 1971.

Wu, C. H. and Kern, R. D. (1987). Shock-Tube Study of Allene Pyrolysis. *J. Phys. Chem.* **91**, 6291.

Yetter, R. A. (1985). An Experimental/Numerical Study of Carbon Monoxide-Hydrogen-Oxygen Kinetics with Applications of Gradient Sensitivity Analysis. Ph.D. Thesis, Department of Mechanical and Aerospace Engineering, Princeton University, Princeton, NJ.

Yetter, R. A., Dryer, F. L. and Rabitz, H. (1990). A Comprehensive Reaction Mechanism for the Carbon Monoxide/Hydrogen/Oxygen Kinetics. *Combust. Sci. Technol.* **79**, 97.